

VENTURI FLOWMETER PERFORMANCE INSTALLED DOWNSTREAM OF THE
BRANCH OF A TEE JUNCTION

by

Benjamin G. Sandberg

A thesis submitted in partial fulfillment
of the requirements for the degree

of

MASTER OF SCIENCE

in

Civil and Environmental Engineering

Approved:

Michael C. Johnson, Ph.D., P.E.
Major Professor

Zachary B. Sharp, Ph.D., P.E.
Committee Member

Bethany Neilson, Ph.D.
Committee Member

Richard S. Inouye, Ph.D.
Vice Provost of Graduate Studies

UTAH STATE UNIVERSITY
Logan, Utah

2020

Copyright © Benjamin G. Sandberg 2020

All Rights Reserved

ABSTRACT

Venturi Flowmeter Performance Installed Downstream of the
Branch of a Tee Junction

by

Benjamin G. Sandberg, Master of Science

Utah State University, 2020

Major Professor: Dr. Michael C. Johnson
Department: Civil and Environmental Engineering

The purpose of this research was to evaluate the influence of a tee junction on flow rate measurement of a Venturi flowmeter installed downstream of the branch of a tee. Accuracy in flow measurement is important to organizations where miscalculated flow rates can add up to be millions of dollars in either lost revenue, overcharges to the client, or improper system operation. A Venturi can function in many different and difficult installations. For example, installations where the Venturi is placed at a location relatively close to the branch of a tee. To get the most accurate flow reading from a Venturi in this installation, a laboratory calibration is necessary. However, calibration adds cost to a project, may not be feasible and in some circumstances, the Venturi has already been installed and cannot be taken out for calibration.

This research used Computational Fluid Dynamics (CFD) to determine ratios by which the manufacturer's straight-line calibrated C_d (discharge coefficient) can be adjusted to improve the accuracy of the flow measurement when the Venturi is installed on the branch of a tee.

Physical laboratory data was obtained for a 6-in. Venturi in a straight-line, followed by installation on the branch of a tee at zero pipe diameters and five pipe diameters downstream. CFD modeling was then used as it was impractical to simulate all the possibilities of flow and physical location in the laboratory. The 6-in. physical laboratory data were used to calibrate and verify the chosen CFD physics models. The CFD modeling was then done for a different Venturi geometry, pipe size, tee junction corner, beta ratio, flow splits entering the tee, and distances from the tee.

Results show the flow rate measurement was less affected when all flow was entering the tee branch and more affected when less flow was entering the tee branch. While physical laboratory calibration is still the best way to get the most accurate flow measurement performance for a Venturi, using CFD to create contour plots of C_d ratios to adjust manufacturer given C_d s over a range of Reynolds numbers and flow splits entering the tee could be an option.

(140 pages)

PUBLIC ABSTRACT

Venturi Flowmeter Performance Installed on the
Branch of a Tee Junction
Benjamin G. Sandberg

The purpose of this research was to evaluate the influence of a tee junction on flow rate measurement of a Venturi flowmeter installed downstream of the branch of a tee. Accuracy in flow measurement is important to organizations where miscalculated flow rates can add up to be millions of dollars in either lost revenue, overcharges to the client, or improper system operation. This research used Computational Fluid Dynamics (CFD) to determine ratios by which the manufacturer's straight-line calibrated C_d (discharge coefficient) can be adjusted to improve the accuracy of the flow measurement when the Venturi is installed on the branch of a tee. Physical laboratory data was obtained for a 6-in. Venturi in a straight-line, followed by installation on the branch of a tee at zero pipe diameters and five pipe diameters downstream. CFD modeling was then used.

Results show the flow rate measurement was less affected when all flow was entering the tee branch and more affected when less flow was entering the tee branch. While physical laboratory calibration is still the best way to get the most accurate flow measurement performance for a Venturi, using CFD to create contour plots of C_d ratios to adjust manufacturer given C_d s over a range of Reynolds numbers and flow splits entering the tee could be an option.

ACKNOWLEDGMENTS

I would like to thank Dr. Michael Johnson for providing me the opportunity to research and work under his supervision at the Utah Water Research Laboratory. His knowledge of hydraulics and flow metering has been most instructive and valuable. His support was most needed in conducting this research.

I would also like to thank the rest of my committee, Dr. Zac Sharp and Dr. Bethany Neilson, for their support and comments to help improve the presentation of this research. Dr. Sharp was also instrumental in providing guidance for the computational fluid dynamics simulations.

Finally, no acknowledgment would be complete without thanking my wife, Jessica. On top of helping grammatically edit this paper, she has been very supportive as I have finished this research.

Benjamin G. Sandberg

CONTENTS

	Page
ABSTRACT	iii
PUBLIC ABSTRACT	v
ACKNOWLEDGMENTS	vi
LIST OF TABLES	ix
LIST OF FIGURES	x
LIST OF EQUATIONS	xvii
NOTATION	xviii
CHAPTER	
I. INTRODUCTION	1
Venturi Review	1
The Problem.....	2
II. LITERATURE REVIEW	5
Objectives	7
III. EXPERIMENTAL METHODS	9
Methods Overview	9
Physical Laboratory Data Collection	11
CFD Modeling Methods	15
Contour Plots	21
IV. RESULTS AND DISCUSSION	23
6-in. Physical Laboratory Data and CFD Modeling Results	23
24-in. 0.6 Beta Ratio CFD Model Results	33
24-in. 0.7 Beta Ratio CFD Model Results	36
Additional 6-in. 0.7 Beta Ratio CFD Model Results	40
Using the Results	43
V. CONCLUSIONS	47
REFERENCES	52
APPENDICES	54

A. SIMULATION TABLE AND CONTOUR PLOTS55

B. METHOD FOR DETERMINING GRID INDEPENDENCE102

C. METHOD FOR CONTOUR PLOT CREATION.....118

LIST OF TABLES

Table	Page
1 Physical laboratory data collected.....	15
2 CFD modeled installations and approximate Reynolds numbers entering the tee.	18
A1 Parameters used for the CFD 6-in. and 24-in. 0.6 beta ratio GCI simulations.	55
C1 SQLite Query “Where” Statement Variables.....	120

LIST OF FIGURES

Figure	Page
1 Classical Venturi basic geometry layout.	1
2 Geometry of a Universal Venturi Tube (UVT).	2
3 General installation of flow entering a tee junction for the research.	4
4 Defined locations of Tap Sets 1-4 for the straight-line and tee installations. ..	10
5 The UVT in the straight-line installation.	13
6 UVT on the branch of the tee junction at zero diameters.	14
7 UVT on the branch of the tee junction at five diameters.	14
8 Screenshot showing some of the mesh scene for the 0.6 beta ratio 24-in. 2D installation.	16
9 Lengths and diameters used for the 6-in. UVT installation in CFD. All values are in inches.	19
10 Lengths and diameters used for the 24-in. 0.6 beta Classical installation in CFD. All values are in inches.	20
11 Plot of discharge coefficient, C_d , versus Reynolds number for the physical laboratory data and CFD straight-line UVT installation. Tap Set 1 is typical of Tap Set 2, 3, and 4 for the straight-line UVT installation.	23
12 Percent deviation from straight versus Reynolds number entering the UVT for the 0D installation at the three Reynolds numbers entering the tee tested in the UWRL.	24
13 Tap Set 1 all three main Reynolds numbers tested/modeled plotted together as percent deviation versus Reynolds number ratio, with the exception of the 0.2 Reynolds number ratio data due to higher deviations from straight than 40%.	26
14 Tap Set 2 all three main Reynolds numbers tested/modeled plotted together as percent deviation versus Reynolds number ratio, with the exception of one CFD 0.2 Reynolds number ratio data point which had a deviation from straight higher than 40%.	26

Figure	Page
15 Screenshots of the velocity vector scene for the 82% and 45% flow splits entering the UVT. On top is the 82% split screenshot and on the bottom is the 45% split screenshot. In both screenshots, flow is coming from the bottom moving to the top and right.	28
16 Percent deviation from straight versus Reynolds number entering the UVT for the 5D installation at the three Reynolds numbers entering the tee tested in the UWRL.	30
17 Tap Set 1 all three main Reynolds numbers tested/modeled plotted together as percent deviation versus Reynolds number ratio.	31
18 Tap Set 2 all three main Reynolds numbers tested/modeled plotted together as percent deviation versus Reynolds number ratio.	32
19 CFD calibrated discharge coefficient curves in a straight-line installation for the 0.6 beta 24-in. classical Venturi.	34
20 All five CFD modeled main Reynolds numbers for Tap Sets 1-4 of the 0.6 beta 24-in Classical Venturi in the 2D installation plotted together as percent deviation versus Reynolds number ratio. Note that the y-axis is between -5% and 40%.	34
21 All five CFD modeled main Reynolds numbers for Tap Sets 1-4 of the 0.6 beta 24-in Classical Venturi in the 5D installation plotted together as percent deviation versus Reynolds number ratio. Note that the y-axis is between -2% and 5%.	35
22 All five CFD modeled main Reynolds numbers for Tap Sets 1-4 of the 0.6 beta 24-in Classical Venturi in the 10D installation plotted together as percent deviation versus Reynolds number ratio. Note the y-axis is between -2% and 2%.	36
23 All five CFD modeled main Reynolds numbers for Tap Sets 1-4 of the 0.7 beta 24-in Classical Venturi in the 0D installation plotted together as percent deviation versus Reynolds number ratio. Note that the y-axis is between -5% and 40%.	37
24 All three CFD modeled main Reynolds numbers for Tap Sets 1-4 of the 0.7 beta 24-in Classical Venturi in the 2D installation plotted together as percent deviation versus Reynolds number ratio. Note that the y-axis is between -5% and 40%.	38

Figure	Page
25 All five CFD modeled main Reynolds numbers for Tap Sets 1-4 of the 0.7 beta 24-in Classical Venturi in the 5D installation plotted together as percent deviation versus Reynolds number ratio. Note that the y-axis is between -5% and 15%.....	39
26 All three CFD modeled main Reynolds numbers for Tap Sets 1-4 of the 0.7 beta 24-in Classical Venturi in the 10D installation plotted together as percent deviation versus Reynolds number ratio. Note that the y-axis is between -2% and 2%.....	40
27 CFD model results for Tap Set 1 of a 6-in. UVT in the 5D installation downstream of a sharp cornered tee at a Reynolds number of 760,000 entering the tee.	41
28 CFD model results for Tap Set 2 of a 6-in. UVT in the 5D installation downstream of a sharp cornered tee at a Reynolds number of 760,000 entering the tee.	42
29 CFD model results for Tap Set 1 of a 6-in. classical Venturi in the 5D installation downstream of a round-cornered tee at a Reynolds number of 760,000 entering the tee.	42
30 CFD model results for Tap Set 2 of a 6-in. classical Venturi in the 5D installation downstream of a round-cornered tee at a Reynolds number of 760,000 entering the tee.	43
31 Contour plot for Tap Set 1 of the 24-in. 0.6 beta ratio Classical Venturi. The plot has lines and arrows identifying the Venturi Reynolds number and flow split for the example problem. The red circle identifies where the lines cross and the $C_d/C_{d_straight}$ ratio is read.....	45
A1 Contour plot for Tap Set 2 of the CFD 6-in. 0.7 beta ratio 0D installation.....	59
A2 Contour plot for Tap Set 2 of the CFD 6-in. 0.7 beta ratio 0D installation without 20% flow split data.....	60
A3 Contour plot for Tap Set 2 of the physical 6-in. 0.7 beta ratio 0D installation.	61
A4 Contour plot for Tap Set 2 of the physical 6-in. 0.7 beta ratio 0D installation without 20% flow split data.....	62
A5 Contour plot for Tap Set 1 of the CFD 6-in. 0.7 beta ratio 0D installation without 20% flow split data.....	63

Figure	Page
A6 Contour plot for Tap Set 1 of the physical 6-in. 0.7 beta ratio 0D installation.	64
A7 Contour plot for Tap Set 1 of the physical 6-in. 0.7 beta ratio 0D installation without 20% flow split data.....	65
A8 Contour plot for Tap Set 3 of the CFD 6-in. 0.7 beta ratio 0D installation without 20% flow split data.....	66
A9 Contour plot for Tap Set 4 of the CFD 6-in. 0.7 beta ratio 0D installation without 20% flow split data.....	67
A10 Contour plot for Tap Set 1 of the CFD 6-in. 0.7 beta ratio 5D installation...	68
A11 Contour plot for Tap Set 1 of the Physical 6-in. 0.7 beta ratio 5D installation.	69
A12 Contour plot for Tap Set 2 of the CFD 6-in. 0.7 beta ratio 5D installation...	70
A13 Contour plot for Tap Set 2 of the Physical 6-in. 0.7 beta ratio 5D installation.	71
A14 Contour plot for Tap Set 3 of the CFD 6-in. 0.7 beta ratio 5D installation...	72
A15 Contour plot for Tap Set 4 of the CFD 6-in. 0.7 beta ratio 5D installation...	73
A16 Contour plot for Tap Set 1 of the CFD 24-in. 0.6 beta ratio 2D installation.	74
A17 Contour plot for Tap Set 2 of the CFD 24-in. 0.6 beta ratio 2D installation.	75
A18 Contour plot for Tap Set 3 of the CFD 24-in. 0.6 beta ratio 2D installation.	76
A19 Contour plot for Tap Set 4 of the CFD 24-in. 0.6 beta ratio 2D installation.	77
A20 Contour plot for Tap Set 1 of the CFD 24-in. 0.6 beta ratio 5D installation.	78
A21 Contour plot for Tap Set 2 of the CFD 24-in. 0.6 beta ratio 5D installation.	79

Figure	Page
A22 Contour plot for Tap Set 3 of the CFD 24-in. 0.6 beta ratio 5D installation.	80
A23 Contour plot for Tap Set 4 of the CFD 24-in. 0.6 beta ratio 5D installation.	81
A24 Contour plot for Tap Set 1 of the CFD 24-in. 0.6 beta ratio 10D installation.	82
A25 Contour plot for Tap Set 2 of the CFD 24-in. 0.6 beta ratio 10D installation.	83
A26 Contour plot for Tap Set 3 of the CFD 24-in. 0.6 beta ratio 10D installation.	84
A27 Contour plot for Tap Set 4 of the CFD 24-in. 0.6 beta ratio 10D installation.	85
A28 Contour plot for Tap Set 1 of the CFD 24-in. 0.7 beta ratio 0D installation without 40% or 20% flow split data.	86
A29 Contour plot for Tap Set 2 of the CFD 24-in. 0.7 beta ratio 0D installation without 40% or 20% flow split data.	87
A30 Contour plot for Tap Set 3 of the CFD 24-in. 0.7 beta ratio 0D installation without 40% or 20% flow split data.	88
A31 Contour plot for Tap Set 4 of the CFD 24-in. 0.7 beta ratio 0D installation without 40% or 20% flow split data.	89
A32 Contour plot for Tap Set 1 of the CFD 24-in. 0.7 beta ratio 2D installation without 20% flow split data.	90
A33 Contour plot for Tap Set 2 of the CFD 24-in. 0.7 beta ratio 2D installation without 20% flow split data.	91
A34 Contour plot for Tap Set 3 of the CFD 24-in. 0.7 beta ratio 2D installation without 20% flow split data.	92
A35 Contour plot for Tap Set 4 of the CFD 24-in. 0.7 beta ratio 2D installation without 20% flow split data.	93
A36 Contour plot for Tap Set 1 of the CFD 24-in. 0.7 beta ratio 5D installation.	94

Figure	Page
A37 Contour plot for Tap Set 2 of the CFD 24-in. 0.7 beta ratio 5D installation.	95
A38 Contour plot for Tap Set 3 of the CFD 24-in. 0.7 beta ratio 5D installation.	96
A39 Contour plot for Tap Set 4 of the CFD 24-in. 0.7 beta ratio 5D installation.	97
A40 Contour plot for Tap Set 1 of the CFD 24-in. 0.7 beta ratio 10D installation.	98
A41 Contour plot for Tap Set 2 of the CFD 24-in. 0.7 beta ratio 10D installation.	99
A42 Contour plot for Tap Set 3 of the CFD 24-in. 0.7 beta ratio 10D installation.	100
A43 Contour plot for Tap Set 4 of the CFD 24-in. 0.7 beta ratio 10D installation.	101
B1 Histogram for the percent difference in the discharge coefficient for the 24-in. 0.6 beta ratio, 2 diameter tee junction installation.	104
B2 Histogram for the percent difference in the discharge coefficient without the 40% and 20% flow split differences for the 24-in. 0.6 beta ratio, 2D tee junction installation.	105
B3 Histogram for Tap Sets 1 and 2 of the percent difference in discharge coefficient between the base size of 2 in. and the base size of 0.8 in. for the 24-in. 0.6 beta ratio, straight-line installation.....	106
B4 Histogram for Tap Sets 3 and 4 of the percent difference in discharge coefficient between the base size of 2 in. and the base size of 0.8 in. for the 24-in. 0.6 beta ratio, straight-line installation.....	107
B5 Histogram for Tap Sets 3 and 4 of the percent difference in discharge coefficient between the base size of 2 in. and the base size of 0.8 in. for the 24-in. 0.6 beta ratio, 2D tee junction installation.	108
B6 Histogram for Tap Sets 3 and 4 of the percent difference in discharge coefficient between the base size of 2 in. and the base size of 0.8 in. for the 24-in. 0.6 beta ratio, 2D tee junction installation, without the 40% and 20% flow split data.....	109

Figure	Page
B7 Histogram for Tap Sets 1 and 2 of the percent difference in discharge coefficient between the base size of 2 in. and the base size of 0.8 in. for the 24-in. 0.6 beta ratio, 5D tee junction installation.	110
B8 Histogram for Tap Sets 1 and 2 of the percent difference in discharge coefficient between the base size of 2 in. and the base size of 0.8 in. for the 24-in. 0.6 beta ratio, 5D tee junction installation, without the 20% flow split data.	111
B9 Histogram for Tap Sets 3 and 4 of the percent difference in discharge coefficient between the base size of 2 in. and the base size of 0.8 in. for the 24-in. 0.6 beta ratio, 5D tee junction installation.	112
B10 Histogram for Tap Sets 3 and 4 of the percent difference in discharge coefficient between the base size of 2 in. and the base size of 0.8 in. for the 24-in. 0.6 beta ratio, 5D tee junction installation, without the 20% flow split data.	113
B11 Histogram for Tap Sets 1 and 2 of the percent difference in discharge coefficient between the base size of 2 in. and the base size of 0.8 in. for the 24-in. 0.6 beta ratio, 10D tee junction installation.	114
B12 Histogram for Tap Sets 1 and 2 of the percent difference in discharge coefficient between the base size of 2 in. and the base size of 0.8 in. for the 24-in. 0.6 beta ratio, 10D tee junction installation, without the 20% flow split data.	115
B13 Histogram for Tap Sets 3 and 4 of the percent difference in discharge coefficient between the base size of 2 in. and the base size of 0.8 in. for the 24-in. 0.6 beta ratio, 10D tee junction installation.	116
B14 Histogram for Tap Sets 3 and 4 of the percent difference in discharge coefficient between the base size of 2 in. and the base size of 0.8 in. for the 24-in. 0.6 beta ratio, 10D tee junction installation, without the 20% flow split data.	117

LIST OF EQUATIONS

Equation	Page
1 Theoretical Venturi Discharge	6
2 Discharge Coefficient	6
3 Venturi Discharge in lb/s	6
4 Venturi Discharge in cfs	7

NOTATION

Definition

Beta = The ratio of throat diameter to the inlet diameter of the Venturi

CFD = Computational Fluid Dynamics

GCI = Grid Convergence Index

RANS = Reynolds Averaged-Navier Stokes turbulence model

Tap Set 1 = The tap set on the left side of the Venturi when standing upstream looking downstream at the Venturi when the Venturi is in the straight-line condition. Or the tap set in line with the inside curve of the tee junction when in the tee set up

Tap Set 2 = The tap set on the right side of the Venturi when standing upstream looking downstream at the Venturi when the Venturi is in the straight-line condition. Or the tap set in line with the outside curve of the tee junction when in the tee set up

Tap Set 3 = The tap set in line with the top of the pipe

Tap Set 4 = The tap set in line with the invert of the pipe

UVT = Universal Venturi Tube

UWRL = Utah Water Research Laboratory in Logan, Utah

0D = The Venturi is located zero diameters downstream of the tee junction

2D = The Venturi is located two diameters downstream of the tee junction

5D = The Venturi is located five diameters downstream of the tee junction

10D = The Venturi is located ten diameters downstream of the tee junction

Variables

A_t = The area of the throat of the Venturi

C_d = Discharge coefficient for a Venturi in a closed conduit system

$C_{d_straight}$ = The discharge coefficient without any upstream obstructions, or in other words a straight-line condition

$C_d/C_{d_straight}$ = The ratio of discharge coefficient to the straight-line discharge coefficient

d_t = Diameter of the Venturi throat

g_c = Dimensional conversion constant 32.17405 pounds mass multiplied by feet and all divided by the multiplication of pounds-force and seconds squared

P = Variable calculated and then used to calculate a GCI in the GCI method

$(q_{PPS})_{theo}$ = Theoretical discharge measurement in pounds mass per second

Q = Flow rate or discharge rate

Q_b/Q_t = Ratio of flow rate entering the branch of the tee to the total flow rate entering the tee

β = The ratio of throat diameter to the inlet diameter of the Venturi

ΔP = Differential pressure between the upstream and downstream pressure taps

ϵ_{21} = The difference between φ_2 and φ_1

ϵ_{32} = The difference between φ_3 and φ_2

ρ_f = Fluid density at flowing conditions in pounds mass per cubic foot

φ_1 = The desired simulation answer for the finest mesh size of the three needed for the GCI method

ϕ_2 = The desired simulation answer for the second finest mesh size of the three needed for the GCI method

ϕ_3 = The desired simulation answer for the coarsest mesh size of the three needed for the GCI method

CHAPTER I
INTRODUCTION

Venturi Review

The Venturi tube, investigated by Giovanni B. Venturi in about 1791, consists of a converging tube and a diverging tube (Finnemore and Franzini 2002). The Venturi tube creates a pressure differential related to the rate of flow, which, when the Venturi tube is used for flow metering, is called a Venturi meter (Finnemore and Franzini 2002).

Throughout the remainder of this text, the Venturi tube will be talked about in terms of metering; therefore, the geometry will be referred to exclusively as a Venturi.

In 1887, Clemens Herschel “applied Venturi principle to the water flow measurement and modified the original Venturi design of the converging-diverging cones incorporating a contoured throat and thus created what is now called the classical [also called Herschel] Venturi (Cascetta 1995)” (see Figure 1).

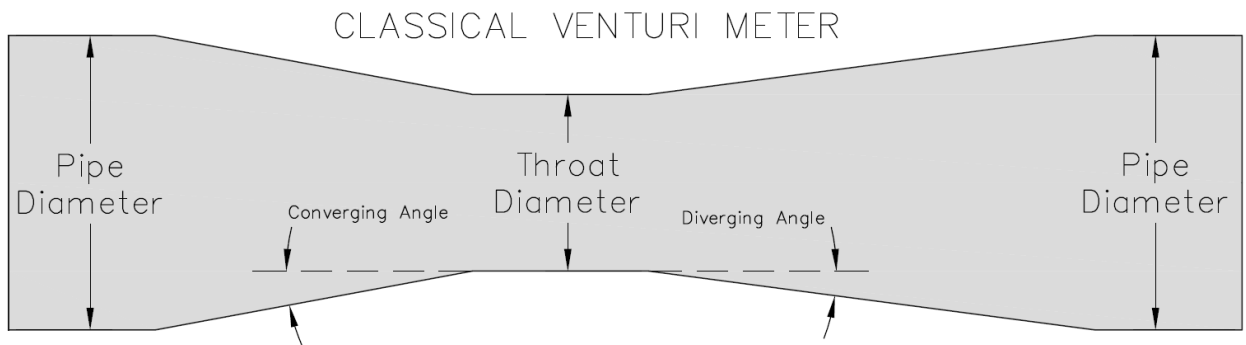


Figure 1. Classical Venturi basic geometry layout.

Since the development of the classical Venturi, there have been other modifications to the design. For example, the Universal Venturi Tube (UVT) (see Figure 2) “was designed to reduce overall lay-in length but retain the pressure recovery and coefficient constancy of the classical Venturi (Miller 1996a).” There are several other

proprietary short form Venturi designs, including low loss tubes like the Halmi Venturi Tube, Lo-Loss flow tube, Dall Tube, Froster flow tube (Gentile Tube), and Twin Throat Venturi tube (Miller 1996a). While these are all viable flowmeters, only the classical Venturi and UVT were considered within the scope of this research because of the availability of a 6-in. UVT for laboratory experiments.

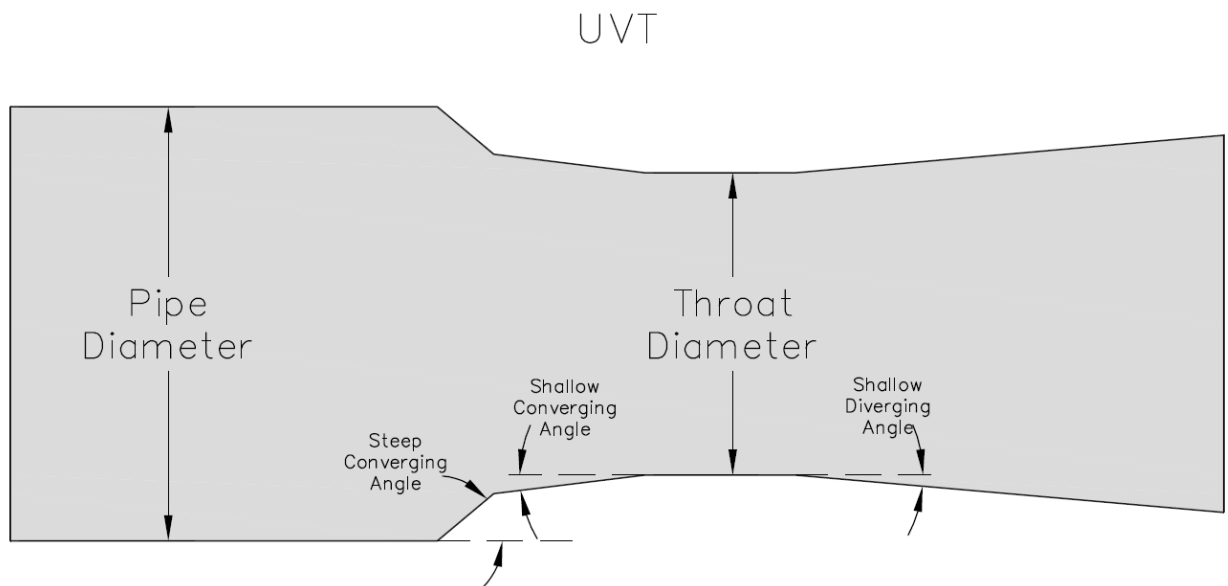


Figure 2. Geometry of a Universal Venturi Tube (UVT).

The Problem

Accuracy in flow measurement is important to organizations where miscalculated flow rates can add up to be millions or billions of dollars in either lost revenue, overcharges to the client, or improper system operation. Standards are available to help reduce error and increase accuracy however, not all meter types or installations are covered by standards. In 2008, the American Society of Mechanical Engineers (ASME) published the minimum number of upstream pipe diameters a classical Venturi needs to be downstream of a single 90-degree bend for good performance. They provided a range

between 8 and 16 diameters, dependent on the Venturi's beta ratio (ASME 2008b). The beta ratio is defined as the ratio of throat diameter to the inlet diameter of the Venturi. This standard only covers the classical meter design and does not indicate the minimum diameters needed for a short-form Venturi.

In practice, however, there are times when these minimum downstream distance requirements, which may be specified by code or manufacturers, cannot be met due to space requirements or other design constraints. When this situation occurs, the discharge coefficient provided by the manufacturer for the Venturi may not be suitable to accurately measure the flow entering the Venturi. To accurately measure flow, the Venturi would need to be calibrated in a laboratory with the same installation configuration as it will be in the field. Such calibration may not be feasible and depends on the Venturi size and piping arrangement.

One such undesirable installation is a Venturi placed 0 to 5 diameters downstream of a tee junction on the branch of the tee. The branch exits 90-degrees from the through-flow of the tee. Such cases justify the need for the investigation of flow entering in one end of the tee junction and splitting between the branch and the run. The run is the straight-through flow of the junction and does not change direction (Figure 3).

Because of the frequency of this type of installation and the potential for significant metering errors associated with it, this research was commissioned. It is expected that the results of this study will be beneficial to those interested in Venturi performance in such applications.

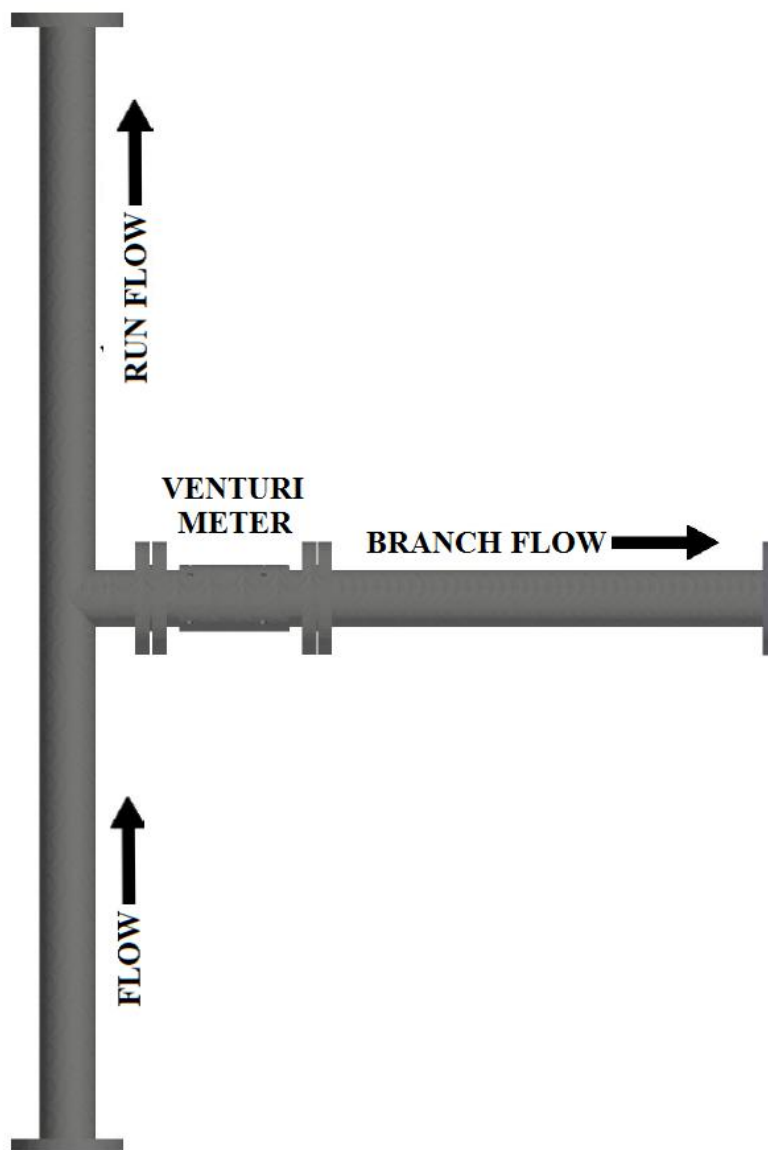


Figure 3. General installation of flow entering a tee junction for the research.

CHAPTER II

LITERATURE REVIEW

From the literature reviewed, much of the work done with single-phase fluid flow entering tee junctions has focused on pressure losses across the tee junction (Abdulwahhab et al. 2013; Costa et al. 2006). In one study, rounded- versus sharp-corners in a tee junction and the effects on pressure loss in the junction was investigated (Costa et al. 2006).

Some published works have considered close obstructions upstream of a flowmeter. One considered the close installation of an ultrasonic flowmeter (Stoker et al. 2012). Another looked at increasing the number of pressure taps on a Venturi installed close to an obstruction to measure a hydraulically averaged differential pressure to use for calculation of flow rate (Stauffer 2019). However, neither of these or any other work reviewed, investigated how the Venturi placed close to a tee junction is influenced or how to correct for the proximity; particularly when the flow is split between the run and branch. A search of the literature has shown no publicly available work examining the proximity of a Venturi at a tee junction. Furthermore, because of the dearth of information available, even one of the largest Venturi manufacturers in the U.S. often requests calibrations at the Utah Water Research Lab (UWRL) for performance information on difficult installations. Consequently, the concept of this research was conceived.

Some of the literature reviewed was on Venturi meters and the equations for calculating flow measurement and the discharge coefficient. In Miller's "Flow

Measurement Engineering Handbook” the theoretical equation for calculating mass flow in a “differential producer” is provided (Miller 1996b). A Venturi falls under that classification and the theoretical incompressible flow entering such a flowmeter can be calculated by Equation 1.

$$(q_{PPS})_{theo} = \frac{\pi}{4} * d_t^2 * \sqrt{\frac{2 * g_c * \Delta P * \rho_f}{1 - \beta^4}} \quad (1)$$

Where $(q_{PPS})_{theo}$ is the theoretical discharge measurement in pounds mass per second, d_t is the diameter of the throat in feet, g_c is a dimensional conversion constant 32.17405 pounds mass multiplied by feet and all divided by the multiplication of pounds-force and seconds squared, ΔP is the differential pressure between the inlet pressure tap and the throat pressure tap in pounds-force per foot squared, ρ_f is the fluid density at flowing conditions in pounds mass per cubic foot, and β is a dimensionless ratio of throat diameter to inlet diameter.

A discharge coefficient, C_d , is added to Equation 1 to calculate the true flow rate. The discharge coefficient is determined by laboratory calibration, where the true flow rate is measured and then divided by the theoretical flow rate as shown in Equation 2 (Miller 1996b).

$$C_d = \frac{\text{true flow rate}}{\text{theoretical flow rate}} \quad (2)$$

Therefore, the true flow rate, q_{pps} , Venturi equation for incompressible flow becomes:

$$q_{PPS} = C_d * \frac{\pi}{4} * d_t^2 * \sqrt{\frac{2 * g_c * \Delta P * \rho_f}{1 - \beta^4}} \quad (3)$$

By dividing both sides of Equation 3 by ρ_f the Venturi equation then solves for flow rate in the English units of cubic feet per second (cfs). Equation 4 shows this form of the equation.

$$Q = C_d * A_t * \sqrt{\frac{2 * g_c * \Delta P}{(1 - \beta^4) * \rho_f}} \quad (4)$$

Where throat area, A_t , is in square feet. Dependent on the Venturi installation, C_d maybe different at different tap sets on the Venturi.

Objectives

Due to the lack of research on the flow measurement characteristics of a Venturi downstream of a tee junction, the purpose of this research was to evaluate the effect this challenging installation has on the flow measurement accuracy of the Venturi. The following objectives were established:

- 1) Collect physical data from the laboratory
- 2) Validate Computational Fluid Dynamics (CFD) as a viable engineering tool for understanding fluid flow in a piping situation.
- 3) Understand the effect of different flow rates, or Reynolds numbers, entering the tee junction on flow measurement in the Venturi.
- 4) Understand how varying the flow split entering the branch of the tee junction effects the Venturi flow measurement.
- 5) Understand how the distance downstream from the tee junction effects the Venturi flow measurement reading.

- 6) Understand the effect of different beta ratios on flow measurement in the discussed installation.

CHAPTER III

EXPERIMENTAL METHODS

Methods Overview

Reproducibility is an important part of any study. To make this work reproducible details are provided for how the physical laboratory data and CFD model results were collected and how the contour plots, used as a way of showing the data, were created. As part of detailing the physical laboratory data, the test installations, instrumentation used, data collected, and test uncertainty are explained. In connection with the details for the CFD model results, the different physics models used, grid convergence, and model geometry are discussed. The contour plot section discusses how a database and Python code were created to generate the plots.

To quickly outline the purpose of the items discussed in this chapter, a simple example is presented here. A more in-depth example is given at the end of Chapter IV. Physical laboratory data has been collected and CFD model results have been verified by comparing them with the laboratory data. The CFD model is then modified to represent a Venturi previously installed. The CFD model is run at a range of flow splits and Reynolds numbers. Using the CFD model results, a range of discharge coefficient ratios are calculated. The ratios are then plotted on a contour plot by flow split versus Reynolds number. The contour plot allows an individual to look up any flow split and Reynolds number within the range modeled and get a ratio to adjust the given discharge coefficient and then calculate flow rate using Equation 4.

For both physical laboratory and CFD data, the Venturi installations are referred to in the same way. In each tee junction installation for this paper, the Venturi is always located some distance downstream of the tee junction on the branch of the tee. Commonly, distances in pipeline flow are defined as a number of pipe diameters. Consistent with this, the different installation distances downstream of the tee junction will be referred to in diameters. To further simplify how the tee installations are referred to as the installation will be defined by the number of diameters followed by a “D” for diameters. All the tee junction Venturi installations are 0D, 2D, 5D, and 10D. The other installation referred to is the straight-line. The straight-line installation is where the Venturi has enough straight pipe upstream of the Venturi inlet to have a fully developed flow profile at the Venturi inlet.

Throughout this work, a Tap Set will refer to one high-pressure tap and one low-pressure tap in line with each other on the Venturi. The Tap Set numbering has reference to where on the Venturi the tap set is located. Tap Sets 1, 2, 3, and 4 are defined in Figure 4.

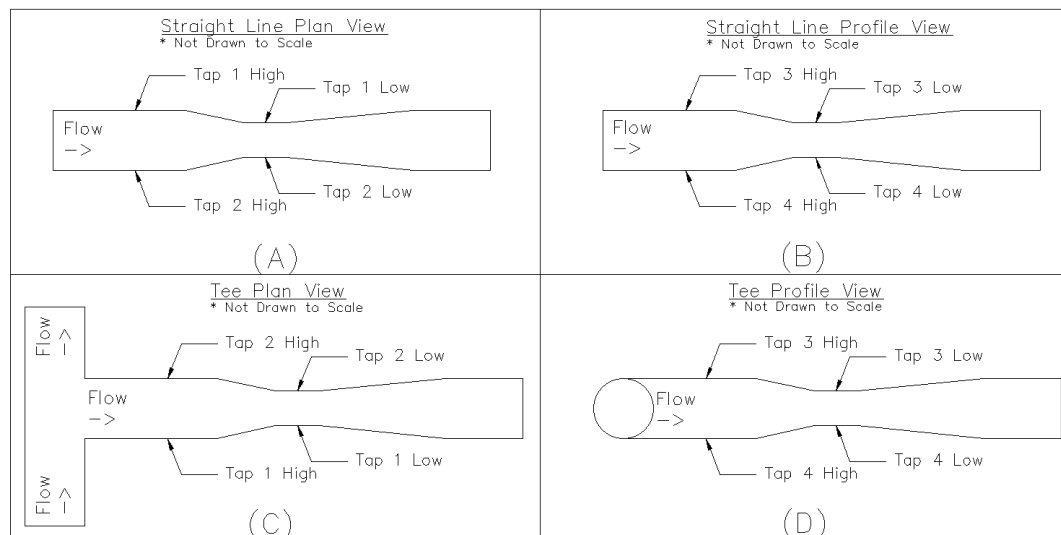


Figure 4. Defined locations of Tap Sets 1-4 for the straight-line and tee installations.

The main variables collected for both physical laboratory testing and CFD simulations were differential pressure and flow rate. Two flow rate measurements were obtained when the Venturi was in any tee installation, one for the total flow entering the tee and another for flow rate entering the Venturi. How these variables were specifically collected from the physical laboratory tests and the CFD simulations will be discussed in the following sections.

Physical Laboratory Data Collection

The physical laboratory data for this Venturi problem was obtained at the UWRL. A 6-in. 0.696 beta ratio UVT was used, though the UWRL has the capability to test “flowmeter sizes from 1/8-inch to 78-inches in diameter (UWRL 2019).” The 6-in. UVT was used for the physical testing instead of other sizes and Venturi designs because of the availability of the UVT and simpler test installation. At the time of testing, the UWRL had a 6-in. UVT, a 6-in. rounded corner tee junction, and the correct length of 6-in. pipe for a 5D installation available.

To measure the differential pressure in the laboratory, differential pressure (DP) transmitters, which measure the change in pressure between two pressure taps, were used. The reading from the DP transmitters was then sent to a multimeter unit, which displays the reading as a voltage. The voltage is recorded and converted to a differential pressure reading of inches of H₂O in a spreadsheet software. The same multimeters and pressure transmitters were used to collect data for all the physical laboratory test installations.

The flow rate for the straight-line installation was measured by using a weighing tank filled for a given amount of time. Then, using Equation 4, the discharge coefficient,

C_d , for each tap set was calculated. While running the straight-line installation, the 6-in. electromagnetic (Mag) meter upstream of the Venturi was compared against the weighing tank measurements of flow to verify the Mag meter was accurately measuring flow. The Mag meter measures flow and then sends the reading to a multimeter that reports the flow in hertz, which is converted in the spreadsheet to gallons per minute.

It was important to verify the Mag meter because in the tee configurations the weighing tank was needed to know the flow rate exiting the run of the tee so the correct flow rate entering the branch could be determined. It was determined by subtracting the run flow rate from the total flow rate entering the tee measured by the Mag meter. Once the correct flow rate entering the branch of the tee junction was known then Equation 4 could be used to solve for the discharge coefficient, C_d .

As the weighing tank was an important part of calculating flow in the laboratory the process to collect one data point using the 25,000 lb weighing tank is explained in the following steps:

- Start filling the weighing tank
- Start the stopwatch and note the start weight
- Start the multimeters averaging the voltage for differential pressure at each tap set
- Start the multimeter averaging the hertz for flow entering the Mag meter
- Record water temperature
- Stop stopwatch and note end weight
- Record averages from multimeters

The process to collect one data point using the 250,000 lb weighing tank is the same except the stopwatch is not used, because the tank system’s “divert” option only fills for a user-specified number of seconds.

Temperature was collected from a temperature probe in the pipe for the physical laboratory testing. The temperature measurements taken throughout the different flow rates in a particular installation were averaged to determine temperature-dependent water properties, like the unit weight of water.

The UVT was tested in the straight-line installation, or in other words calibrated before the UVT was tested in the 0D and 5D installations. In the straight-line installation, the UVT was placed 14 feet downstream of any obstructions (Figure 5). Having more than 18 diameters of straight pipe upstream helped to establish a fully developed flow profile at the UVT inlet, reducing any upstream disturbance errors.

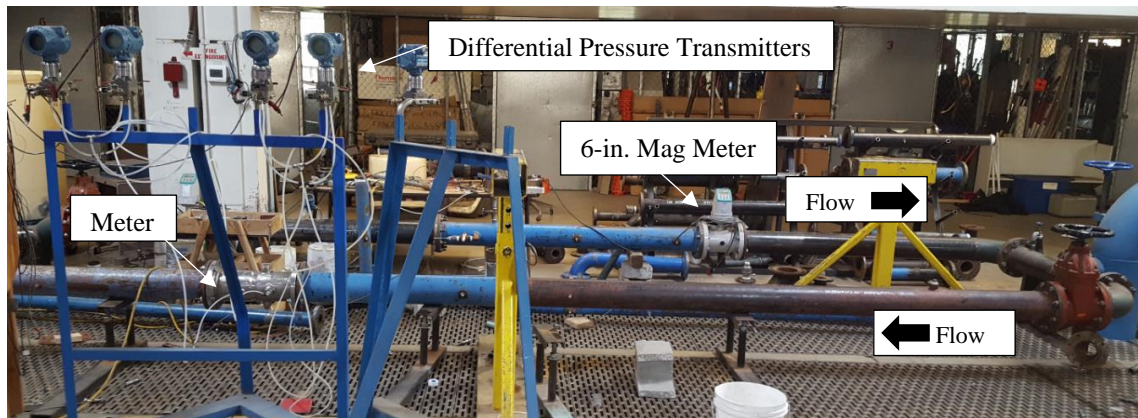


Figure 5. The UVT in the straight-line installation.

The 0D installation (Figure 6) featured the UVT bolted directly to the tee junction. The 5D installation (Figure 7) was the same as the 0D with the exception that the UVT was placed 30 inches downstream of the tee junction.

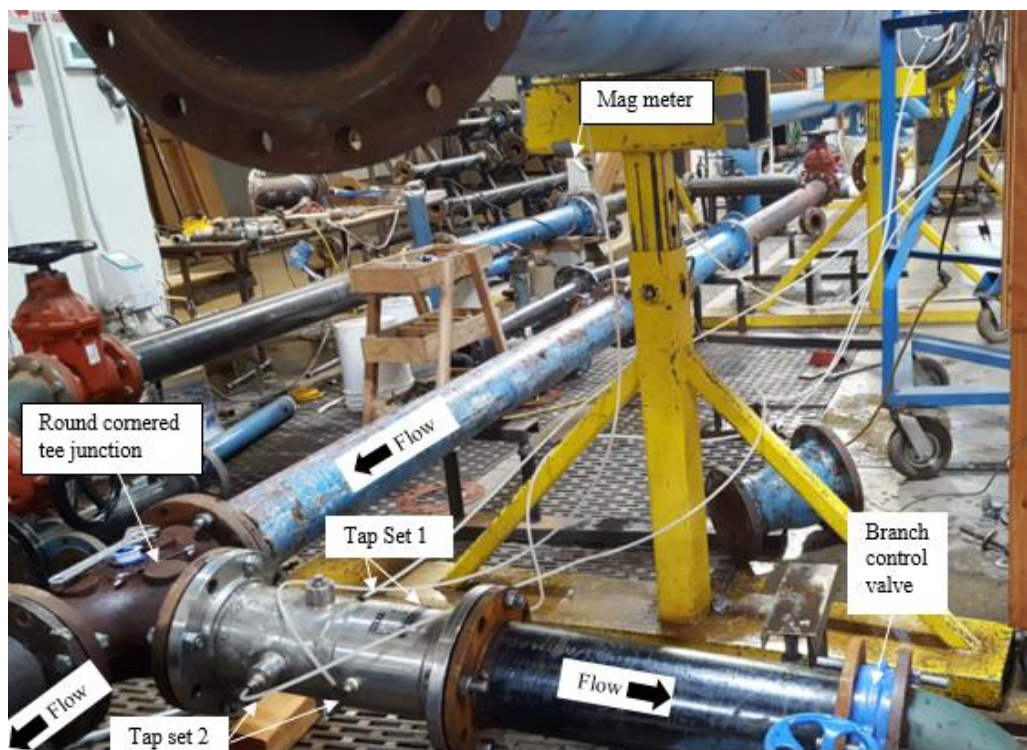


Figure 6. UVT on the branch of the tee junction at zero diameters.

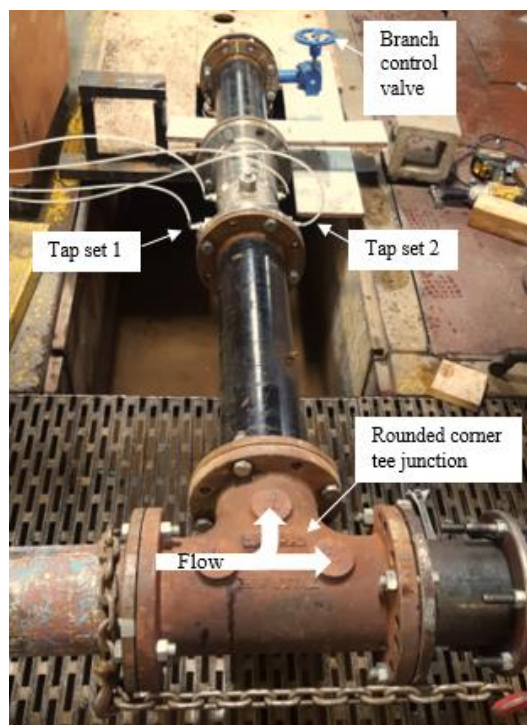


Figure 7. UVT on the branch of the tee junction at five diameters.

All physical laboratory data uncertainty was determined using the ASME PTC 19.1 2005 test uncertainty national standard. The standard documents how to calculate the uncertainty of a result at the 95% confidence level (ASME 2006). The physical data of this research had a maximum uncertainty of 0.25% at the 95% confidence level. Table 1 provides a summary of the UVT installations run in the laboratory.

Table 1. Physical laboratory data collected.

	Flow Splits Run for the Different Reynolds Numbers Entering the Tee			
	~760,000	~730,000	~380,000	~190,000
6-in. 0.7 beta UVT at 0D		100.0%	100.0%	100.0%
		82.6%	82.1%	82.4%
		63.2%	62.9%	64.4%
		45.5%	45.4%	44.9%
		30.7%	31.5%	24.3%
6-in. 0.7 beta UVT at 5D	100.0%		100.0%	100.0%
	79.6%		80.8%	79.9%
	63.5%		65.5%	65.1%
	37.1%		38.2%	34.9%
	20.3%		20.2%	20.7%

CFD Modeling Methods

Computational Fluid Dynamics (CFD) makes simulations of various configurations cost-effective and provides a way to test different Venturi sizes, geometries, and beta ratios. The CFD software used for this research was STAR-CCM+, a Siemens product.

The same physics models were used for all the CFD simulations completed. The following physics models were used: constant density, exact wall distance, gradients, K-Epsilon turbulence, liquid, realizable K-Epsilon two-layer, Reynolds-Averaged Navier-Stokes (RANS), segregated flow, steady-state, three dimensional, turbulent, and two-

layer all y^+ wall treatment. For more information on RANS or any of the physics models listed see Simcenter STAR-CCM+ documentation (Siemens 2020). Run specific parameters for some of the 6-in. and 24-in. models are presented in Table A1.

For all the CFD model results, care was taken to ensure the model results were mesh, or grid, independent. The procedure used to determine grid independence is outlined in Appendix B. A typical mesh for the 6-in. CFD models was about one million cells and for the 24-in. was approximately half-a-million cells. Figure 8 shows an example mesh scene from the CFD models.

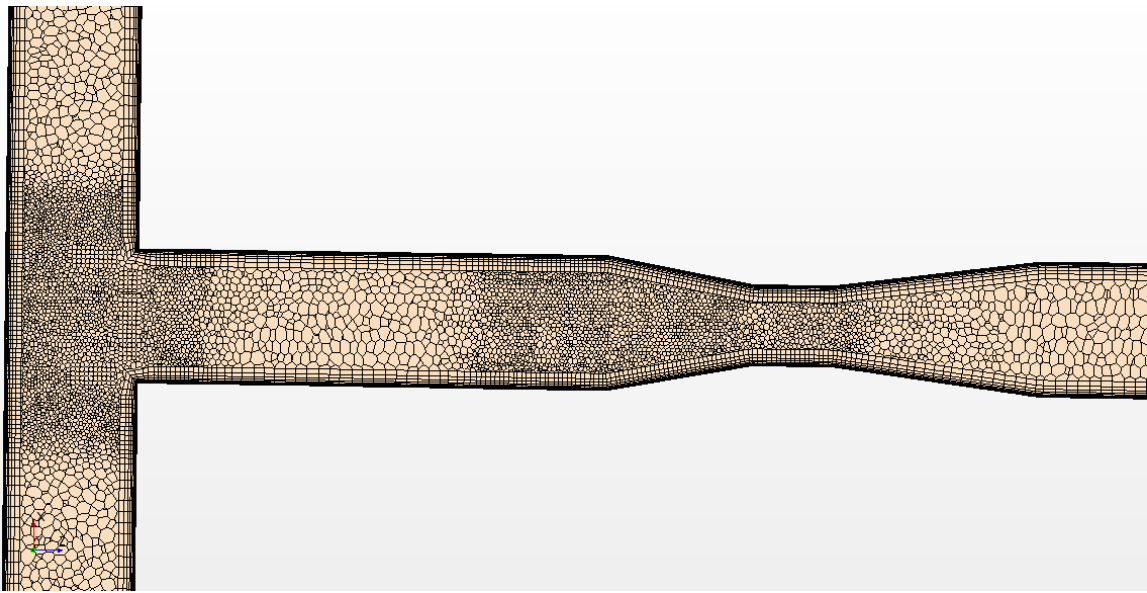


Figure 8. Screenshot showing some of the mesh scene for the 0.6 beta ratio 24-in. 2D installation.

Using probes and planes, the differential pressure in psi, the mass flow rate in lb/s, and the mesh area of the Venturi inlet and throat were obtained from the model results. The values were placed in a spreadsheet that made the appropriate unit

conversions and calculations for information such as flow split, percent deviation from straight-line discharge coefficient, and Reynolds number entering the Venturi.

It is important to verify that CFD can adequately model the physical laboratory test installations before modeling other installations not tested on the laboratory floor. In this way, the CFD approach may be validated and extended to other related problems. Each physical laboratory installation was recreated in STAR-CCM+ using the STAR-CCM+ 3-D CAD capabilities. The UVT was drawn in accordance with the provided flowmeter geometry. To reduce areas that could create unnecessary meshing problems, the upstream and downstream pipes were meshed to the same diameter as the UVT inlet. Examples include the 3/64 of an inch difference between the UVT inlet and the tee inner diameter, as well as, the smaller difference between the upstream pipe and UVT inlet diameters.

It would be ideal to have the CFD model get the same discharge coefficient as the physical laboratory tests. However, this is often not the case with CFD. Therefore, an adequate agreement between the CFD and physical laboratory data is when CFD models the general trend in physical laboratory data. If the trend is repeatable for the CFD model results, then the difference (or bias) of the CFD results relative to the physical laboratory data can be corrected for.

Once the CFD model showed adequate agreement with the physical laboratory data, the 24-in. classical Venturi was numerically modeled. The geometry used for the classical Venturi came from ASME (ASME 2008b). The converging cone angle used was 21 degrees and the diverging cone angle used was 15 degrees. Sharp et al. (2018) showed

that CFD can closely match the trends of laboratory data for different sizes of the ASME classical Venturi design. Because of Sharp et al. (2018), physical laboratory data was not performed for the 24-in. classical Venturi, considering the physics models calibrated for the 6-in. UVT to be adequate physics models for the 24-in. classical Venturi.

Table 2 outlines all the modeled installations, not including the straight-line model results. Each installation presented in Table 2 modeled five flow splits entering the tee. The straight-line was run for a range of Reynolds numbers, from a little less than the smallest to a little more than the largest Reynolds number entering the Venturi.

Table 2. CFD modeled installations and approximate Reynolds numbers entering the tee.

Approximate Reynolds Numbers Entering the Tee at the Different Tee Installations				
	0D	2D	5D	10D
6-in. 0.7 beta UVT, round-cornered tee	730,000		760,000	
	380,000		380,000	
	190,000		190,000	
6-in. 0.7 beta UVT, sharp-cornered tee			760,000	
6-in. 0.7 beta Classical Venturi, round-cornered tee			760,000	
24-in. 0.6 beta Classical Venturi, sharp-cornered tee	2,000,000	2,000,000	2,000,000	2,000,000
	1,300,000	1,300,000	1,300,000	1,300,000
	700,000	700,000	700,000	700,000
	300,000	300,000	300,000	300,000
	100,000	100,000	100,000	100,000
24-in. 0.7 beta Classical Venturi, sharp-cornered tee	2,000,000	2,000,000	2,000,000	2,000,000
	1,300,000	1,300,000	1,300,000	1,300,000
	700,000	700,000	700,000	700,000
	300,000	300,000	300,000	300,000
	100,000	100,000	100,000	100,000

Figure 9 and Figure 10 show the lengths and diameters used for the CFD geometry of the 6-in. pipe and 24-in. pipe CAD drawings. Figure 9 shows the pipe centerlines and the

curve used to sweep the pipe diameter along to get the rounded tee. The triangular divot left by sweeping the circles was filled to match the physical tee junction. The line perpendicular to the pipe walls is used to represent, or distinguish, the different pipeline parts (e.g., the tee junction and Venturi). In Figure 9, the half-line perpendicular to the pipe walls in the tee junction shows where the tee junction begins and ends curving. The curving is 2.25 inches in from each opening in the tee junction. The geometry is changed to the other Venturi installations by simply adjusting the pipe length between the branch of the tee junction and the inlet to the Venturi. For example, in Figure 9 changing the 30 inches to 0 inches gives the 0D installation for the 6-in. installation or in Figure 10 changing 48 inches to 120 inches gives the 5D installation for the 24-in. Venturi.

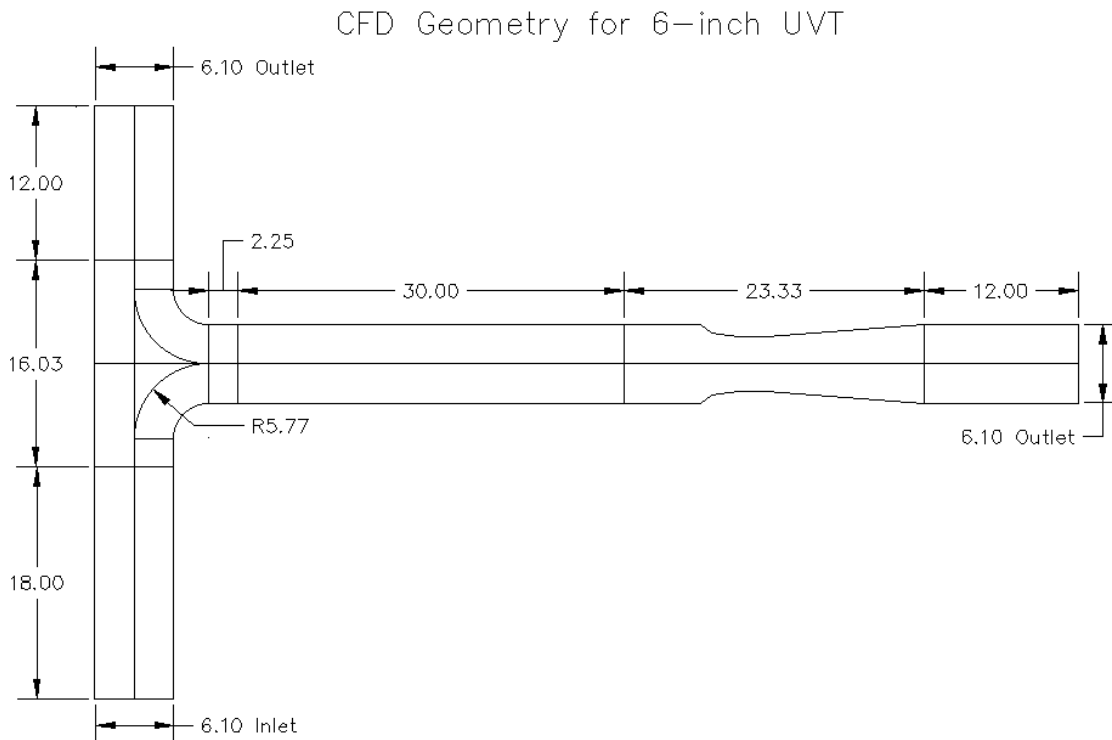


Figure 9. Lengths and diameters used for the 6-in. UVT installation in CFD. All values are in inches.

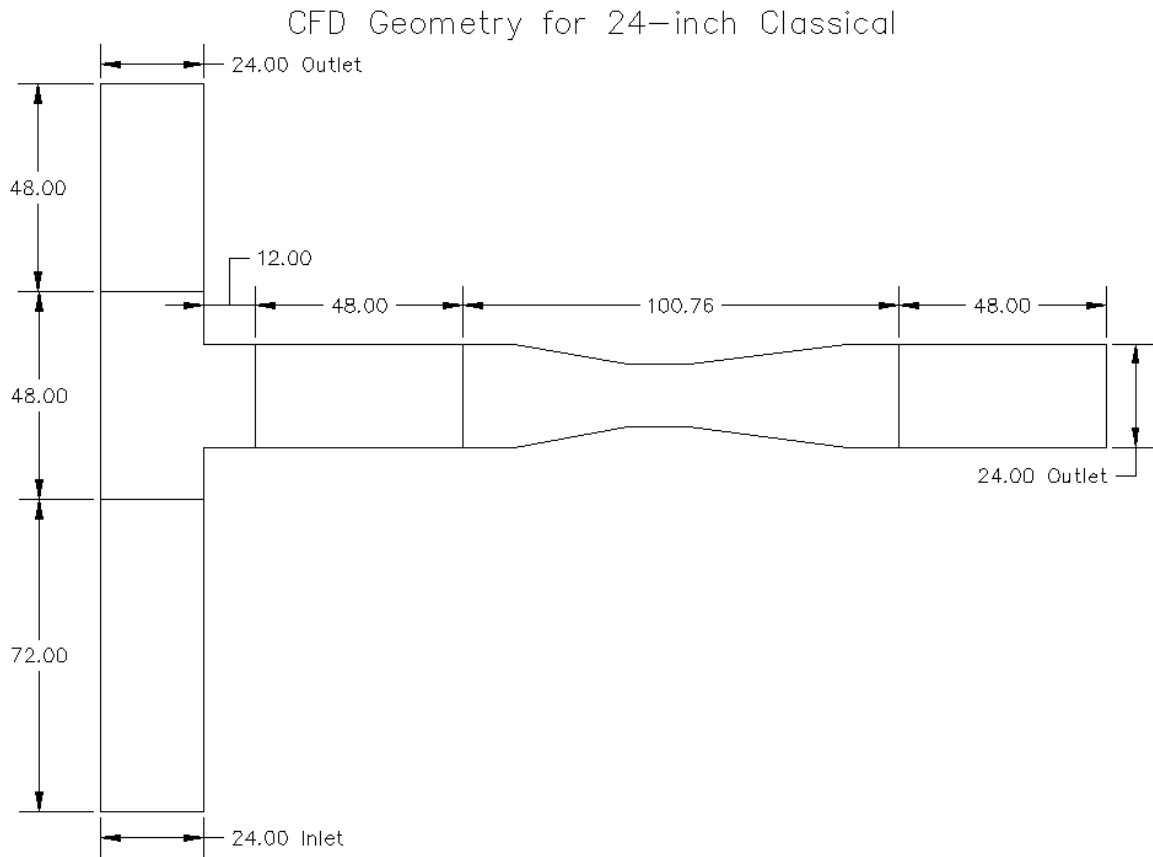


Figure 10. Lengths and diameters used for the 24-in. 0.6 beta Classical installation in CFD. All values are in inches.

For the 6-in. classical Venturi at 5D the CFD geometry used was the same as that of Figure 9, except that the 23.33 inches of the UVT is replaced with 22.37 inches of a classical Venturi. The geometry for the 6-in. UVT at 5D downstream of a sharp tee is the same as in Figure 9, except the tee corner was made sharp. For the 24-in. 0.7 beta geometry only the Venturi length in Figure 10 needs to be changed from 100.76 in. to 87.57 in.

Contour Plots

For each plot, the y-axis is the ratio of flow (Q) entering the branch of the tee to the total flow entering the tee (a.k.a. flow split). On the x-axis is the Reynolds number at the inlet of the Venturi. The black dots on the plots represent modeled points. By knowing the flow split and Reynolds number at the inlet of the Venturi, a ratio by which to adjust, the discharge coefficient (C_d) can be found. For some Venturi installations, the 20% flow split model results modeled as a negative differential pressure and therefore a C_d could not be calculated as an imaginary number would result. Because of this some contour plots only go from 0.4 to 1.0 on the y-axis.

The contour plots were automated by adding to the Python code discussed in Appendix C. The code obtains the plotting information from the database using the pandas dataframe, which provides the points to interpolate between. The Python packages SciPy, Matplotlib (Hunter 2007), and NumPy are used in the code to create the contour plots. Using the NumPy package, arrays of data from the dataframe are created for Reynolds number, flow split, and $C_d/C_{d_straight}$. The minimum and maximum of the Reynolds number and flow split data are then used to define a mesh grid of the data using NumPy. Using the arrays and grid developed up to this point in the code, interpolated values of $C_d/C_{d_straight}$ are calculated, using the cubic interpolation method, and stored in a variable using the SciPy griddata function. With the Matplotlib contour function and the XY-grid and interpolated values, the contour plots are created. Additional code then adds a color bar, the model results as points, and other plot formatting for effective

presentation. By using the data in the dataframe for a particular installation the contour plot covers the full modeled range of flow splits and Reynolds numbers.

CHAPTER IV

RESULTS AND DISCUSSION

6-in. Physical Laboratory Data and CFD Modeling Results

The first validation of the CFD modeling results using physical data focused on the straight-line Venturi installation for the 6-in. UVT. For Tap Set 1 (refer to Chapter III for discussion of which tap set is which) the lab calibration averaged discharge coefficient, C_d , was 0.9817. For Tap Set 2, the averaged C_d was 0.9794. The CFD averaged C_d was 1.6% and 1.4% lower for Tap Set 1 and 2 at 0.9657 and 0.966, respectively. A plot comparing the physical and CFD data for the straight-line calibration is shown in Figure 11.

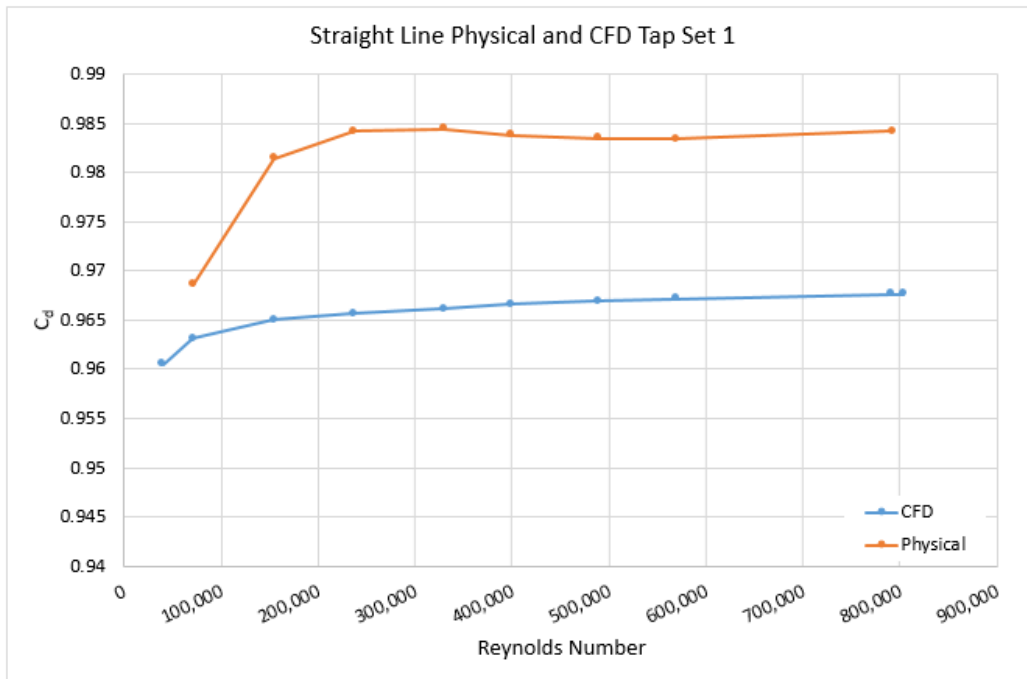


Figure 11. Plot of discharge coefficient, C_d , versus Reynolds number for the physical laboratory data and CFD straight-line UVT installation. Tap Set 1 is typical of Tap Set 2, 3, and 4 for the straight-line UVT installation.

Comparison between observations and CFD model results for the 0D and 5D installations was done by graphing percent deviation from the straight-line C_d versus the Reynolds number entering the UVT (Figure 12). The percent deviation was calculated using interpolation to get a straight-line C_d at the same Reynolds number as the 0D or 5D installation.

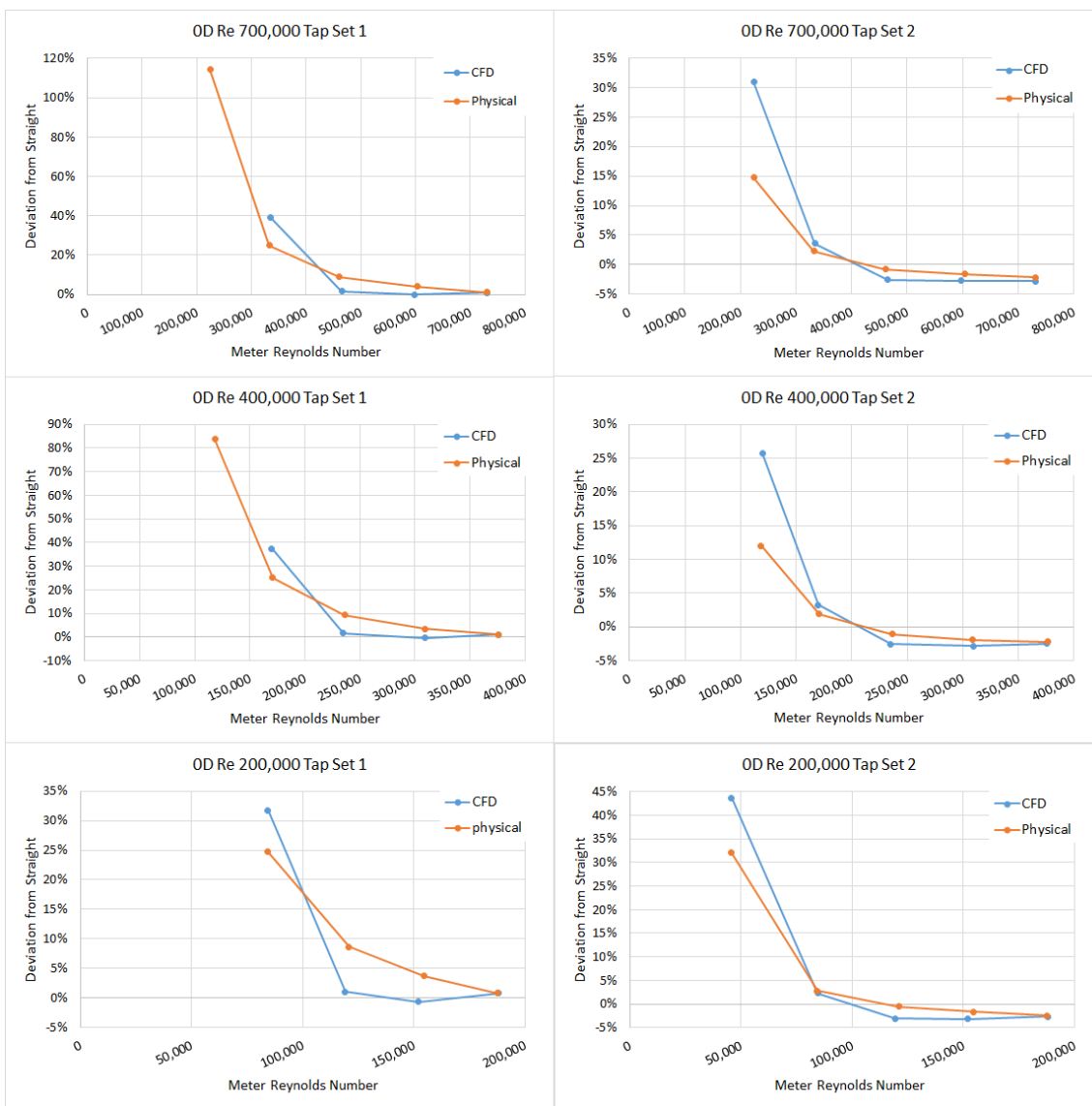


Figure 12. Percent deviation from straight versus Reynolds number entering the UVT for the 0D installation at the three Reynolds numbers entering the tee tested in the UWRL.

CFD model results follow the same general trend as the physical data. The 60%, 80%, and 100% flow splits result in the smallest deviation for both tap sets. By the 40% and 20% flow splits for Tap Set 1, the percent deviation is more extreme. The 20% flow split CFD data point was not included in Figure 12 graphs for Tap Set 1 due to negative pressure differentials, which places a negative under the square root in Equation 4 and makes it impossible to calculate a real value for C_d . The percent deviation for Tap Set 2 is not nearly as extreme as Tap Set 1 at 40% and 20% flow splits.

It is difficult to determine from Figure 12 if the relationship is dependent on the Reynolds number or the percentage of flow split. To better see this relationship, plots combining the three plots for Tap Set 1 and the three plots for Tap Set 2 and changing the x-axis to flow split (or Reynolds number ratio of flow entering the UVT to the flow entering the tee) were made (Figure 13 and Figure 14). Figure 13 shows the physical data fall on top of each other for the three different Reynolds numbers entering the tee, except the 20% split which is not shown on the plot due to being higher than 40% deviation. The CFD model results also plot nearly on top of each other. The data for Tap Set 2 likewise plot nearly on top of each other except for the 20% data (Figure 14). This would suggest that the data is more dependent on the Reynolds number ratio rather than the specific Reynolds number for the ranges evaluated.

The OD installation was the most difficult for the CFD physics models used in STAR-CCM+, refer to Chapter III for a full list of the physics models used, to model, especially for Tap Set 1. The physics models (Figure 13 and Figure 14) do model the deviation from straight extremely well, being nearly 0.5% or less than the physical

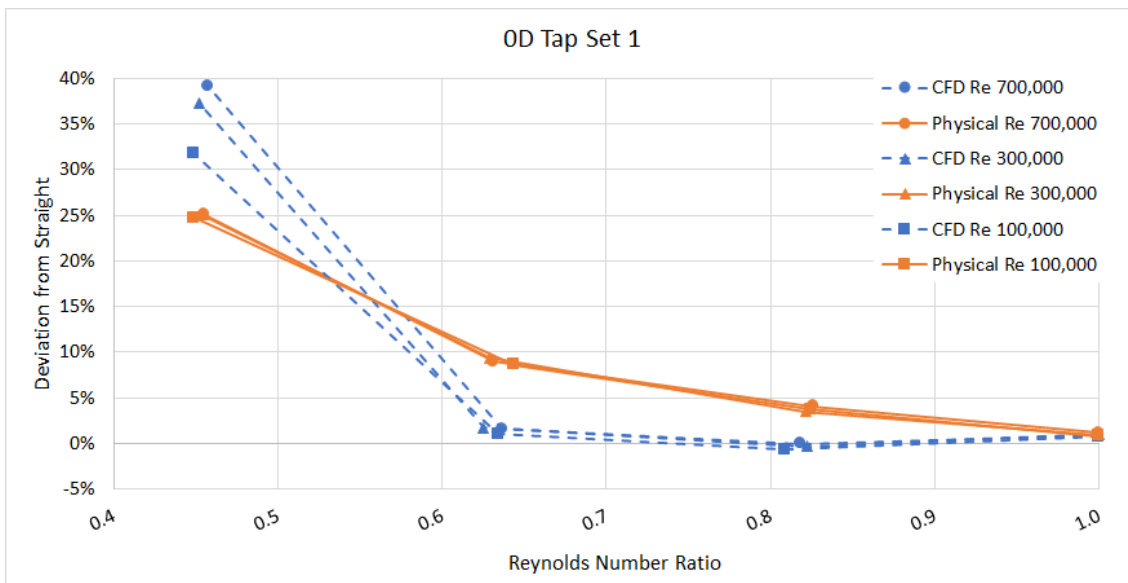


Figure 13. Tap Set 1 all three main Reynolds numbers tested/modeled plotted together as percent deviation versus Reynolds number ratio, with the exception of the 0.2 Reynolds number ratio data due to higher deviations from straight than 40%.

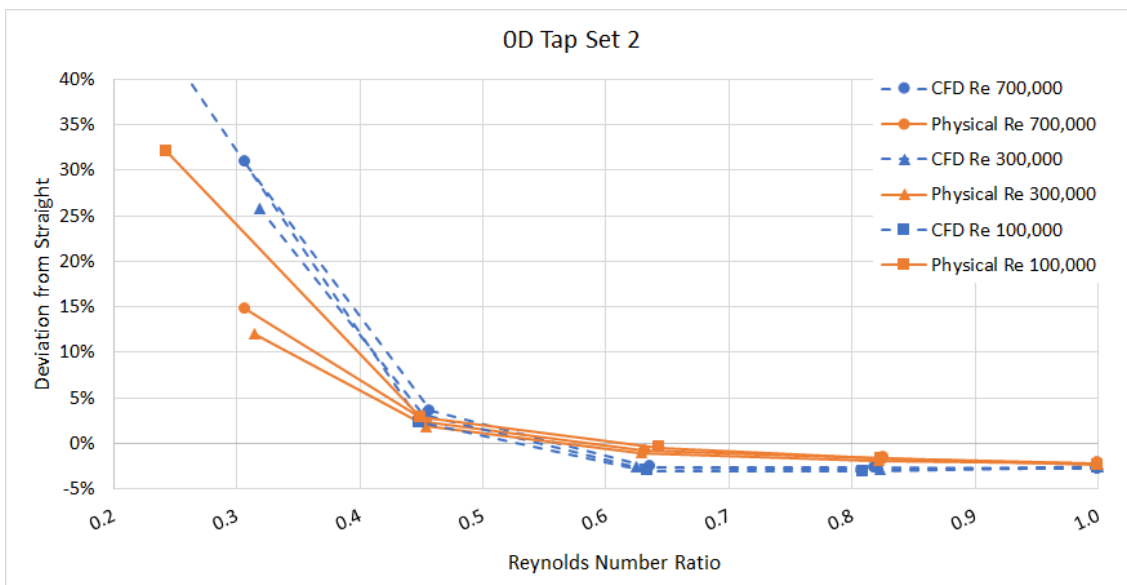


Figure 14. Tap Set 2 all three main Reynolds numbers tested/modeled plotted together as percent deviation versus Reynolds number ratio, with the exception of one CFD 0.2 Reynolds number ratio data point which had a deviation from straight higher than 40%.

model, at 100% of the flow entering the UVT on the branch. Tap Set 1 quickly diverges and is nearly 5% lower than the physical laboratory data by the 80% flow split the CFD and nearly 10% lower than the physical by 60% of the flow entering the UVT. At 40% and 20% of flow entering the UVT, CFD results did not accurately capture the 0D installation at Tap Set 1.

Tap Set 2, on the other hand, is more accurately captured in the CFD results with a greater amount of consistency and accuracy than Tap Set 1. Again, at the 100% flow split the difference between CFD model results and physical laboratory data deviation from straight is small, within 0.5%. At 80%, the difference is closer to 1 or 2% lower than physical laboratory data, at 60% of flow the difference is 2 or 3%, and at 40% of flow, the difference is back to 1 or 1.5%. At the 20% flow split the difference from straight, while not nearly as extreme as for Tap Set 1, is high and not well predicted by the physics models used. Two screenshots of the velocity vectors for the 6-in. UVT 0D installation at 82% and 45% of flow entering the UVT helps to visualize why the physics models struggle to accurately model Tap Set 1 well (Figure 15).

The physics models do model the 0D installation well at Tap Set 2 for flow splits 40% and above. It would be recommended that a Venturi not be placed at 0D, but if it must then the differential pressure should be read from Tap Set 2 because there is not an eddy near or over the upstream tap making it difficult to get a good pressure reading. It is acknowledged that the physical laboratory data at the 0D installation for Tap Set 1 did not read a negative pressure like the CFD simulation at the low flow split. However, the

percent deviation was extreme at the low flow splits for the physical laboratory data (Figure 12).

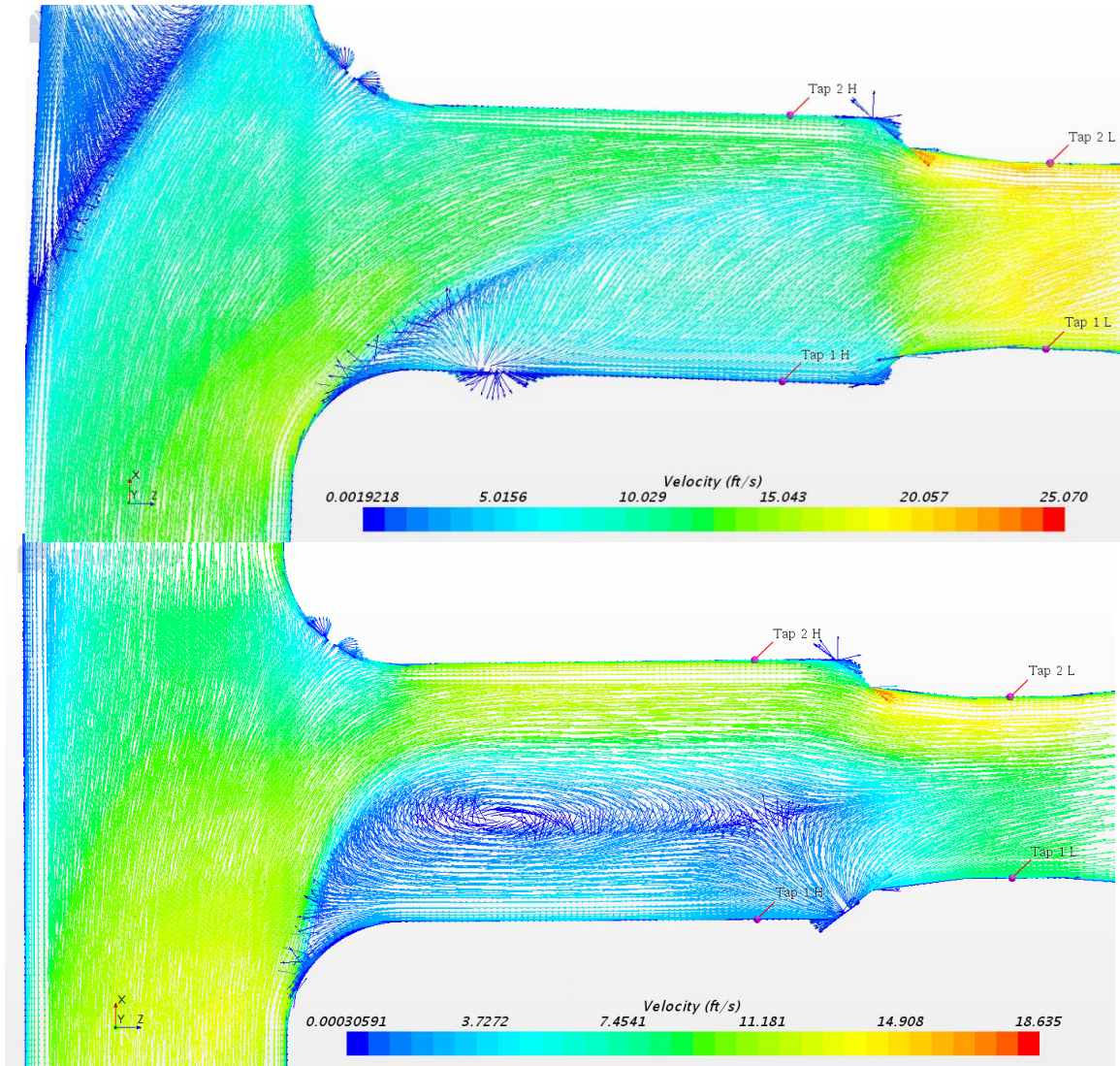


Figure 15. Screenshots of the velocity vector scene for the 82% and 45% flow splits entering the UVT. On top is the 82% split screenshot and on the bottom is the 45% split screenshot. In both screenshots, flow is coming from the bottom moving to the top and right.

In Figure A1, a contour plot for Tap Set 2 shows that the straight-line, or calibrated, discharge coefficient can be adjusted by a multiplying factor to improve the accuracy of the flow measurement. Figure A2 removes the 20% flow split data to better contour the 40% to 100% flow split range. Figure A3 shows the contour plot of the physical data for Tap Set 2. Figure A4 shows the same physical data contour plot as Figure A3 without the 20% flow split data to improve the usability of the physical data contour plot. It is important to note that the CFD contour plots are of the ratio of CFD model results C_d to CFD model results $C_{d_straight}$. Likewise, the physical laboratory data contour plots are of the ratio of physical laboratory data C_d to physical laboratory data $C_{d_straight}$. Knowing this the similarity between Figure A2 and Figure A4 speaks to the ability of CFD to model Tap Set 2 in the 0D above 40% flow split installation.

Though Tap Set 1 is not the recommended tap set, Figure A5, Figure A6, and Figure A7 show CFD and physical laboratory data contour plots for Tap Set 1. These plots should be used with the understanding that the lower the flow split, the larger the percent difference between the CFD and physical laboratory data. Also, contour plots for Tap Sets 3 and 4 are given in Figure A8 and Figure A9. However, without physical laboratory data to compare to for Tap Sets 3 and 4 (which were not present on the physical meter tested), it is difficult to say how large or small the difference between the CFD and physical percent difference from straight would be.

Looking at the same aspects of the 6-in UVT 5D installation, the individual deviation from straight versus the UVT Reynolds number plots (Figure 16) is a bit misleading. At first glance, the CFD model results appear not to capture the deviation

from straight well but looking closer at the y-axis reveals how much smaller the range is compared to the 0D installation.

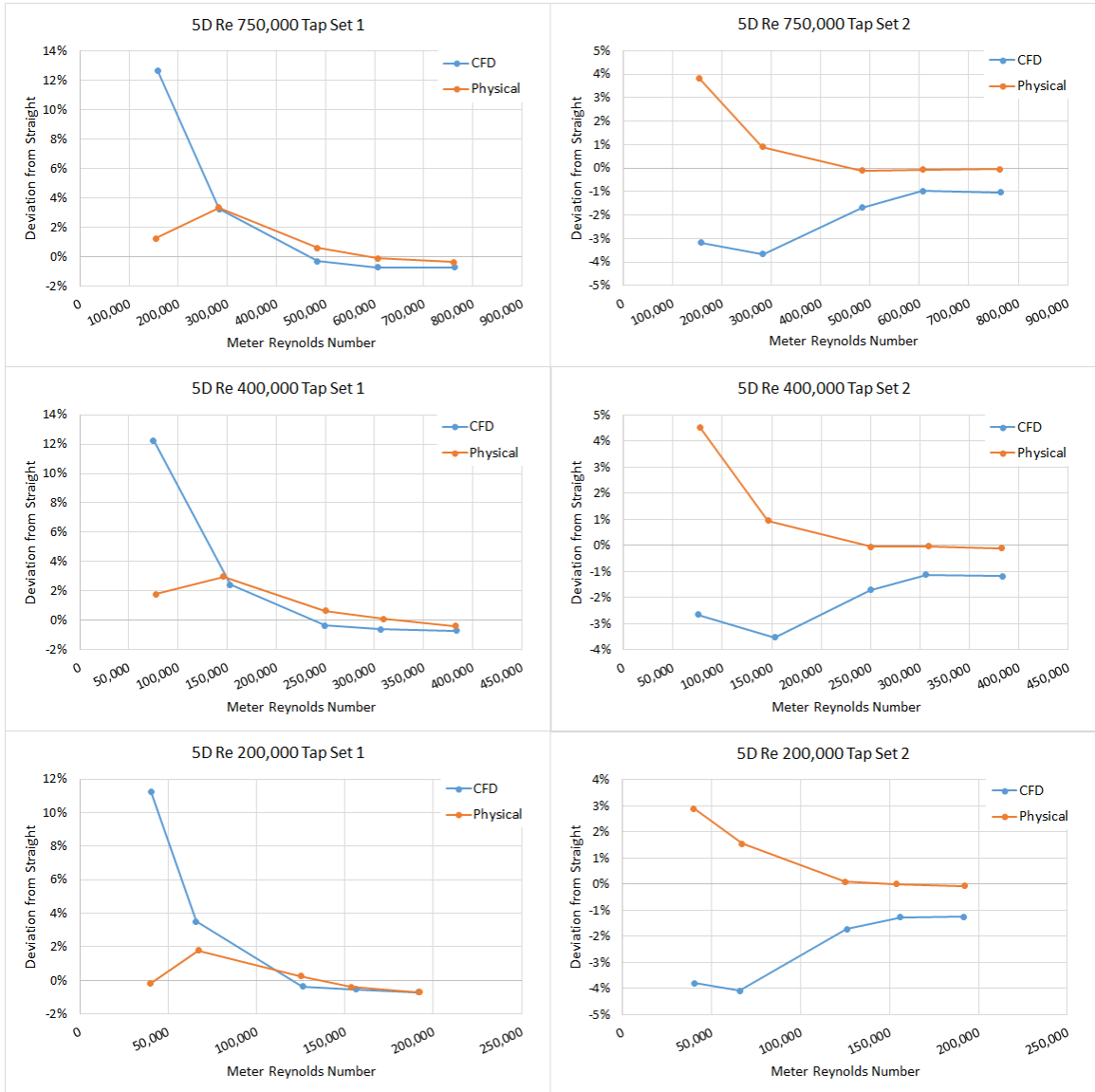


Figure 16. Percent deviation from straight versus Reynolds number entering the UVT for the 5D installation at the three Reynolds numbers entering the tee tested in the UWRL.

Like Figure 13 and Figure 14 for the 0D installation, Figure 17 and Figure 18 plot the data on one graph using the same y-axis limits as Figure 13 and Figure

14. Figure 17 and Figure 18 help show how closely the CFD model results do represent the physical laboratory data. However, the CFD physics models still struggled to model the 0.2 Reynolds number ratio, a.k.a. the 20% flow split, at 5D very well.

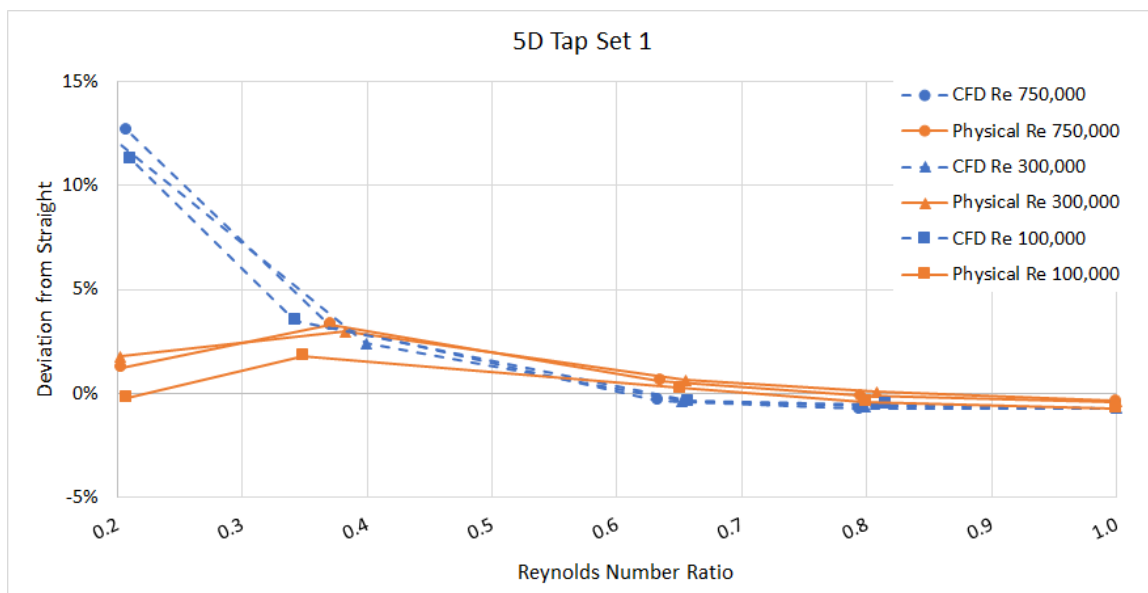


Figure 17. Tap Set 1 all three main Reynolds numbers tested/modeled plotted together as percent deviation versus Reynolds number ratio.

The CFD physics models do model the 5D installation well at both tap sets for flow splits 60% and above. Tap Set 1 is modeled well to the 40% flow split but Tap Set 2 breaks with the trend and goes down instead of up. To understand if this was due to the meter geometry or tee corner, two additional 6-in installations were modeled. One installation was the UVT at 5D with a sharp cornered tee and the other installation was a 6-in. classical Venturi at 5D with a round-cornered tee. The model results for these two installations are presented and discussed after the 0.7 beta ratio 24-in. classical Venturi model results.

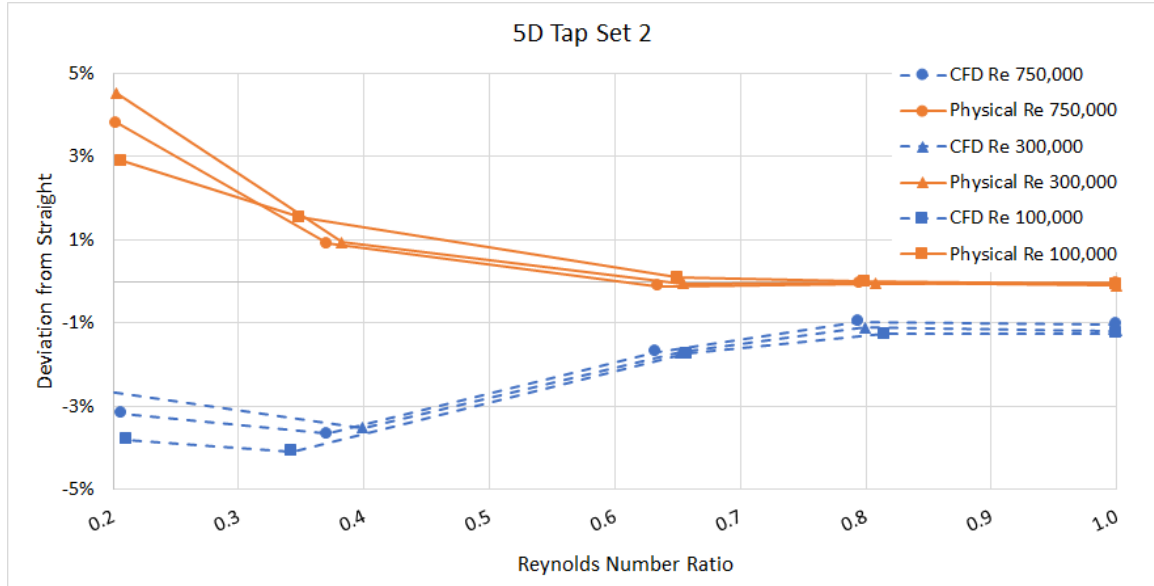


Figure 18. Tap Set 2 all three main Reynolds numbers tested/modeled plotted together as percent deviation versus Reynolds number ratio.

If the 6-in UVT is placed at 5D downstream on the branch of a tee junction, the recommended tap set to use in order to read differential pressure would be Tap Set 1. The contour plot for Tap Set 1 at 5D (Figure A10) can be used to determine the ratio to adjust the calibrated discharge coefficient to improve flow measurement. Figure A11 shows the contour plot of the physical data for Tap Set 1 at 5D.

Figure A12 and Figure A13 show the contour plots for the CFD and physical data of Tap Set 2. Contour plots for Tap Sets 3 and 4 are given in Figure A14 and Figure A15. Again, without physical data to compare to for Tap Set 3 and 4 it is difficult to say how large or small the difference between the CFD model results and physical laboratory data percent difference from straight would be. However, at the 5D installation, it is assumed that the relationship will be similar to that of Tap Sets 1 and 2 and would likely be the average of the two tap sets.

24-in. 0.6 Beta Ratio CFD Model Results

The 6-in. UVT CFD model results both verified the CFD physics models as viable in modeling the Venturi placed downstream of a tee, while also identifying weaknesses of the chosen physics models. For example, the difficulty modeling flow splits 20% or less and the difficulty modeling the 0D installation. Recognizing these limitations, it was decided to not run the grid converged 24-in classical 0.6 beta ratio simulations at a 0D installation, but rather a 2D, 5D, and 10D installations. The 20% split for each installation and flow rate entering the tee was still modeled, but it is stressed that if the information is to be used for low flow splits, it should be done with the understanding of its limitations and uncertainty.

Figure 19 shows the CFD calibration curve for Tap Sets 1-4, which Tap Sets are defined in Figure 4, of a 24-in. classical Venturi with a 0.6 beta ratio. These plots show the straight-line data are acceptable to be used to calculate the percent deviation from straight for the 2D, 5D, and 10D installations. The straight-line data is acceptable based on the work of Sharp et al. (2018) where a classical Venturi was laboratory calibrated and used to validate CFD results.

Figure 20, Figure 21, and Figure 22 show all of the 25 data points for the 24-in 0.6 beta ratio Classical Venturi plotted together for each tap set. For the 2D installation (Figure 20) the four tap sets show nearly identical behavior. As the flow split entering the inlet of the classical Venturi decreases the deviation from straight increases. The trend is similar to that shown in the 6-in 0D installation for the UVT physical data points, but to a lower percent deviation as would be expected as the installation is 2D further away for

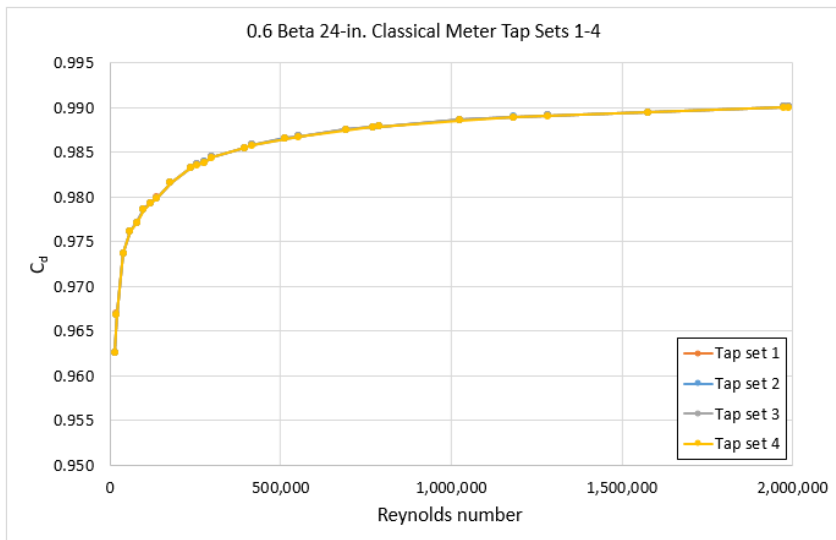


Figure 19. CFD calibrated discharge coefficient curves in a straight-line installation for the 0.6 beta 24-in. classical Venturi.

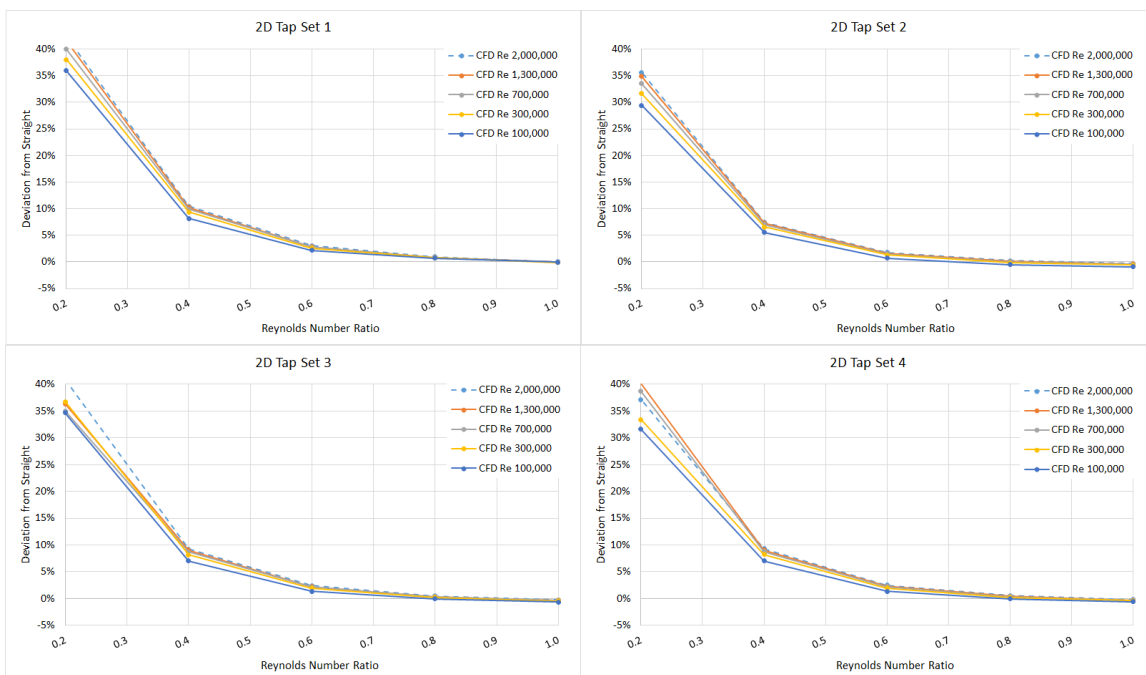


Figure 20. All five CFD modeled main Reynolds numbers for Tap Sets 1-4 of the 0.6 beta 24-in Classical Venturi in the 2D installation plotted together as percent deviation versus Reynolds number ratio. Note that the y-axis is between -5% and 40%.

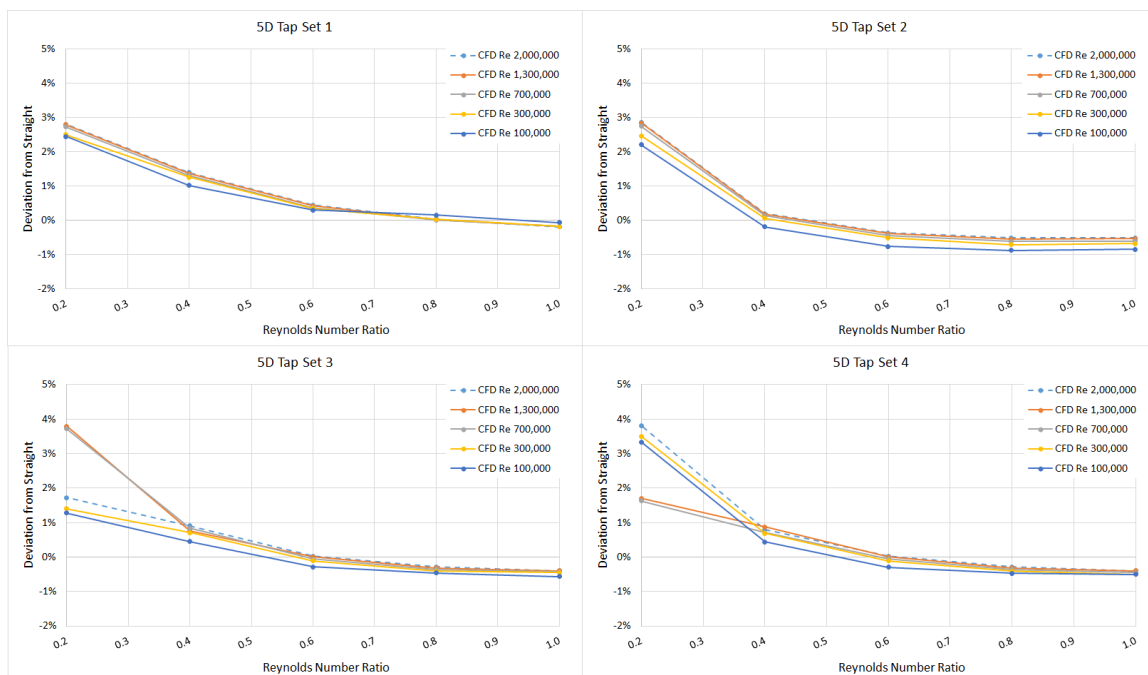


Figure 21. All five CFD modeled main Reynolds numbers for Tap Sets 1-4 of the 0.6 beta 24-in Classical Venturi in the 5D installation plotted together as percent deviation versus Reynolds number ratio. Note that the y-axis is between -2% and 5%.

the tee junction. The trend for the 24-in 0.6 beta 5D installation (Figure 21), is nearly identical to that of the 6-in 5D physical data with a very small percent deviation from straight 60% and above and under 5% deviation from straight below 60% flow split. By 10D (Figure 22), deviation from straight is nearly zero, which is consistent with the ASME standard 10 diameters for “zero additional uncertainty” for a 0.6 beta classical Venturi in the most difficult situation (ASME 2008b).

Contour plots to help adjust the discharge coefficient for the 0.6 beta 24-in. classical Venturi are also found in appendix A. Plots for Tap Sets 1-4 of the 2D installation correspond to Figure A16-Figure A19, for Tap Sets 1-4 of the 5D installation Figure A20-Figure A23, and for Tap Sets 1-4 of the 10D installation Figure A24-Figure

A27. These plots, like those created for the 6-in UVT, are used by finding the corresponding Reynolds number entering the Venturi and flow split to find an interpolated ratio of $C_d/C_{d_straight}$ by which to adjust the discharge coefficient to improve the flow measurement calculation. It should be noted that the 24-in. simulations used a sharp-edged tee, not the round-edged tee used for the 6-in. simulations.

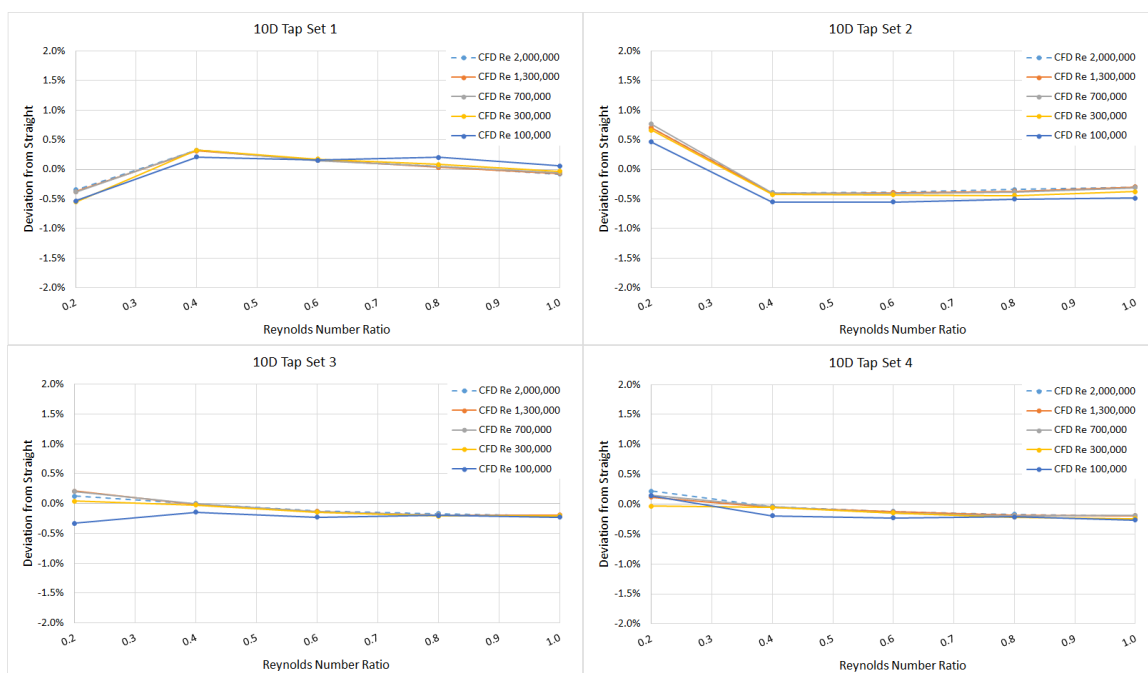


Figure 22. All five CFD modeled main Reynolds numbers for Tap Sets 1-4 of the 0.6 beta 24-in Classical Venturi in the 10D installation plotted together as percent deviation versus Reynolds number ratio. Note the y-axis is between -2% and 2%.

24-in. 0.7 Beta Ratio CFD Model Results

The straight-line discharge coefficient versus Reynolds number curves for the 0.7 beta 24-in. classical Venturi looked like those in Figure 19 for the 0.6 beta 24-in. classical Venturi, but are shifted up by about 0.002. The larger beta size resulted in the simulations having larger deviations from straight-line CFD model results sooner than with the 0.6

beta model results of the same 24-in. classical Venturi. Figure 23 shows how difficult the CFD simulation for OD is at that larger beta ratio and classical Venturi geometry than the 0.7 beta ratio 6-in. UVT. Comparing the 0.6 beta (Figure 20-Figure 22) to the 0.7 beta (Figure 24-Figure 26) deviation from straight versus Reynolds number ratio plots, the 0.7 beta deviates exponentially more. Therefore, if a classical Venturi is to be used in the installation described, a smaller beta ratio classical Venturi produced more stable discharge coefficients.

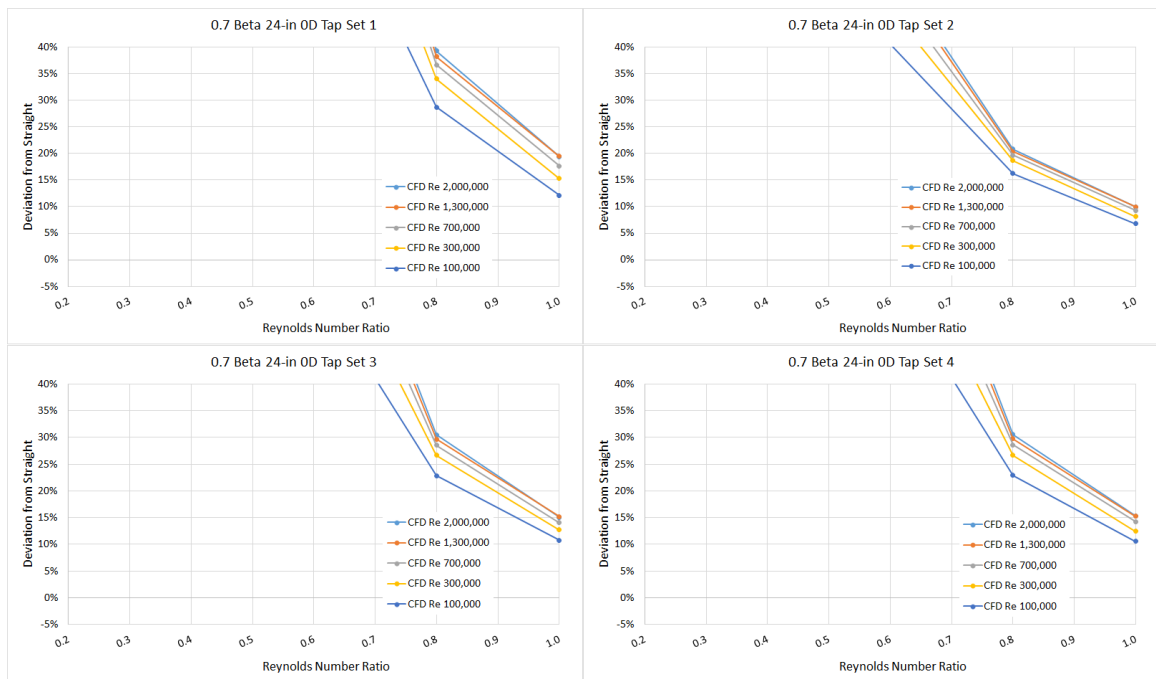


Figure 23. All five CFD modeled main Reynolds numbers for Tap Sets 1-4 of the 0.7 beta 24-in Classical Venturi in the OD installation plotted together as percent deviation versus Reynolds number ratio. Note that the y-axis is between -5% and 40%.

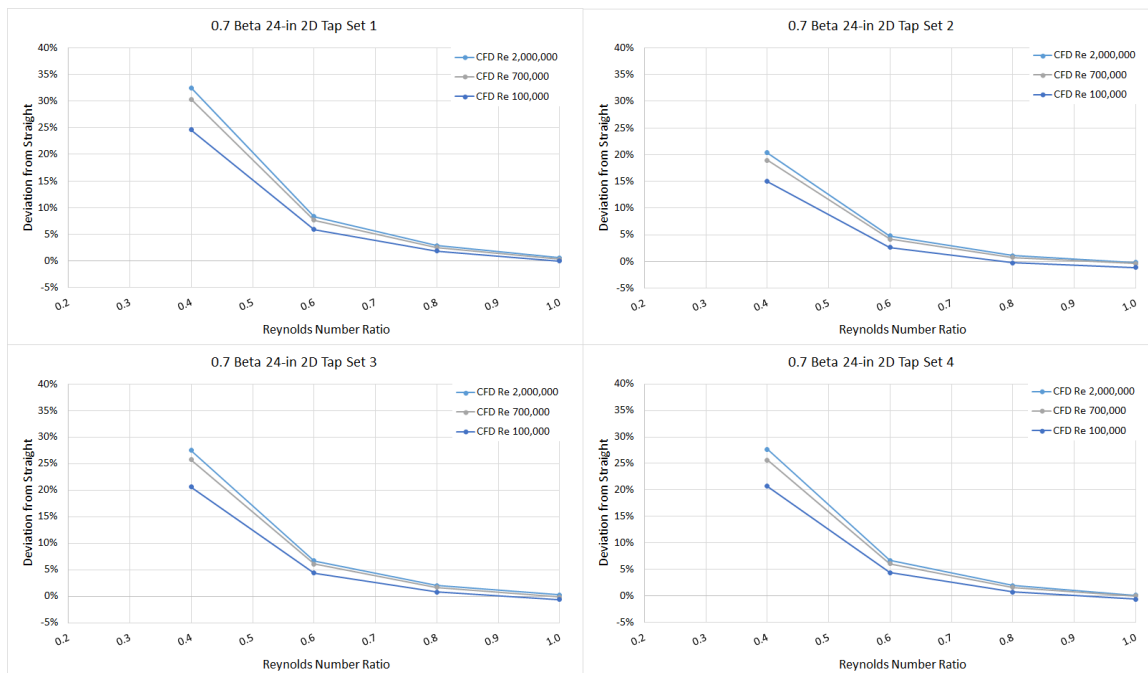


Figure 24. All three CFD modeled main Reynolds numbers for Tap Sets 1-4 of the 0.7 beta 24-in Classical Venturi in the 2D installation plotted together as percent deviation versus Reynolds number ratio. Note that the y-axis is between -5% and 40%.

If a 0.7 beta classical Venturi is used, then, like the other two Venturi meters discussed, contour plots are provided in Appendix A for 0D (Figure A28-Figure A31), 2D (Figure A32-Figure A35), 5D (Figure A36-Figure A39), and 10D (Figure A40-Figure A43).

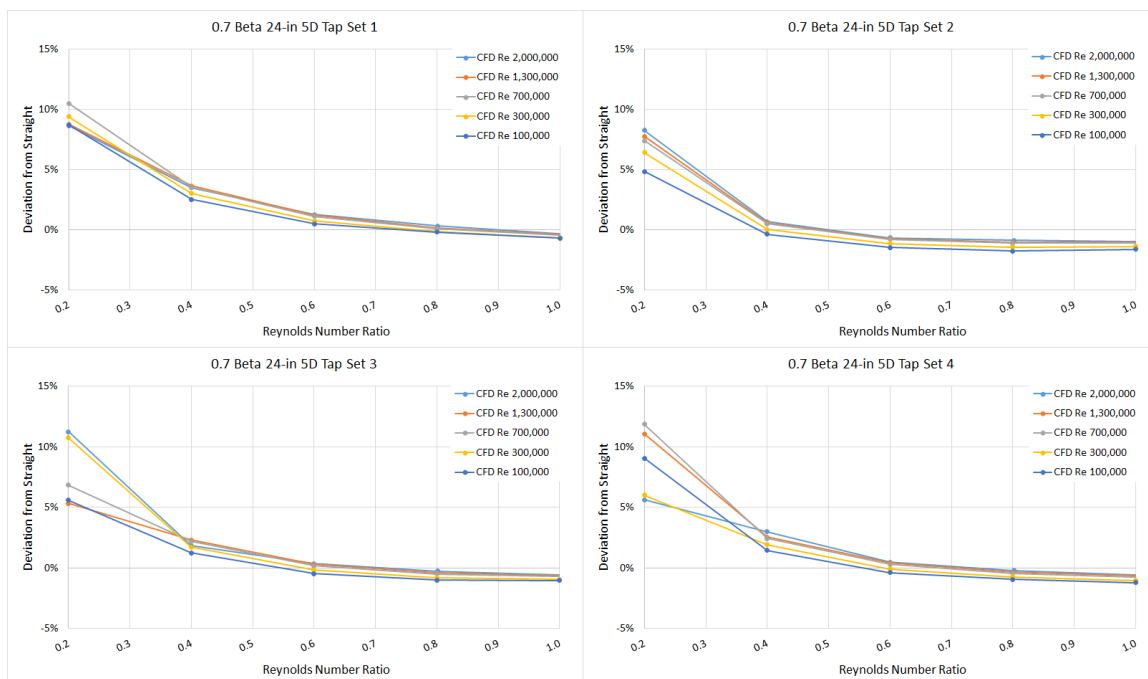


Figure 25. All five CFD modeled main Reynolds numbers for Tap Sets 1-4 of the 0.7 beta 24-in Classical Venturi in the 5D installation plotted together as percent deviation versus Reynolds number ratio. Note that the y-axis is between -5% and 15%.

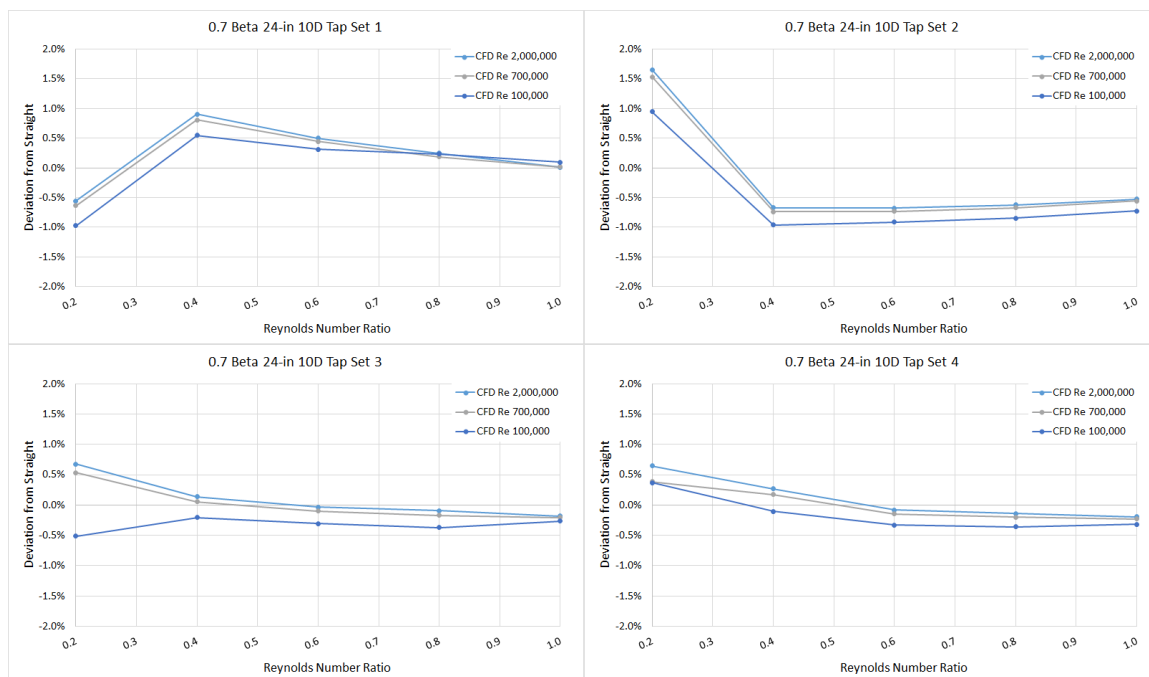


Figure 26. All three CFD modeled main Reynolds numbers for Tap Sets 1-4 of the 0.7 beta 24-in Classical Venturi in the 10D installation plotted together as percent deviation versus Reynolds number ratio. Note that the y-axis is between -2% and 2%.

Additional 6-in. 0.7 Beta Ratio CFD Model Results

When Tap Set 2 of the 6-in. UVT in the 5D installation (Figure 18) was discussed previously, it was noted that it was uncertain whether the break-in trend below the 60% flow split was due to Venturi geometry, pipe size, or tee corner. To determine which of these variables is likely causing the CFD model results of Figure 18 the 6-in. UVT was modeled in the 5D installation downstream of a sharp cornered tee (Figure 27 and Figure 28) and a classical Venturi geometry was modeled in the 5D installation downstream of the round-cornered tee (Figure 29 and Figure 30). As the results for physical laboratory data and CFD model results have all shown to not be Reynolds number dependent but rather Reynolds number ratio, or flow split, dependent these additional installations were

only run at one Reynolds number entering the tee and five flow splits. While Tap Set 2 was the focus of this additional modeling (Figure 28 and Figure 30), Tap Set 1 model results are also presented to show the effect of these variables on the model results at Tap Set 1 (Figure 27 and Figure 29).

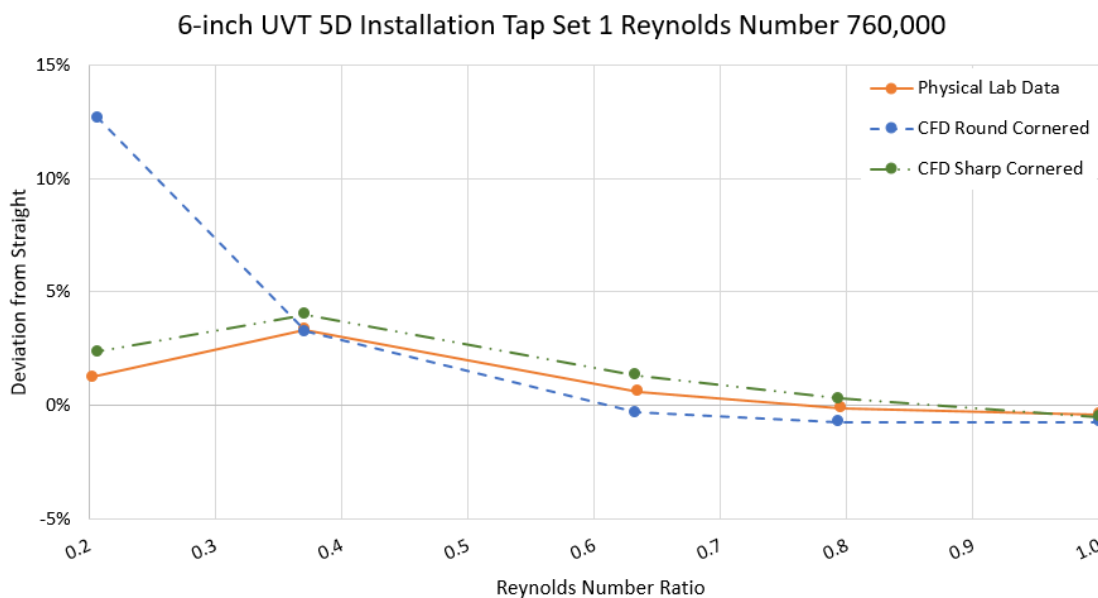


Figure 27. CFD model results for Tap Set 1 of a 6-in. UVT in the 5D installation downstream of a sharp cornered tee at a Reynolds number of 760,000 entering the tee.

The additional CFD modeling indicates the downward trend of Tap Set 2 at 5D is due to the Venturi geometry rather than pipe size or tee corner. Figure 28 the UVT is modeled downstream of a tee with a sharp corner and the downward trend is still evident. Figure 30 shows that a 6-in. classical Venturi did not exhibit the downward trend of the 6-in. UVT. Therefore, Venturi geometry was identified as the variable affecting the CFD model results at 5D Tap Set 2.

The CFD model results were also affected, by varying amounts, by pipe size and

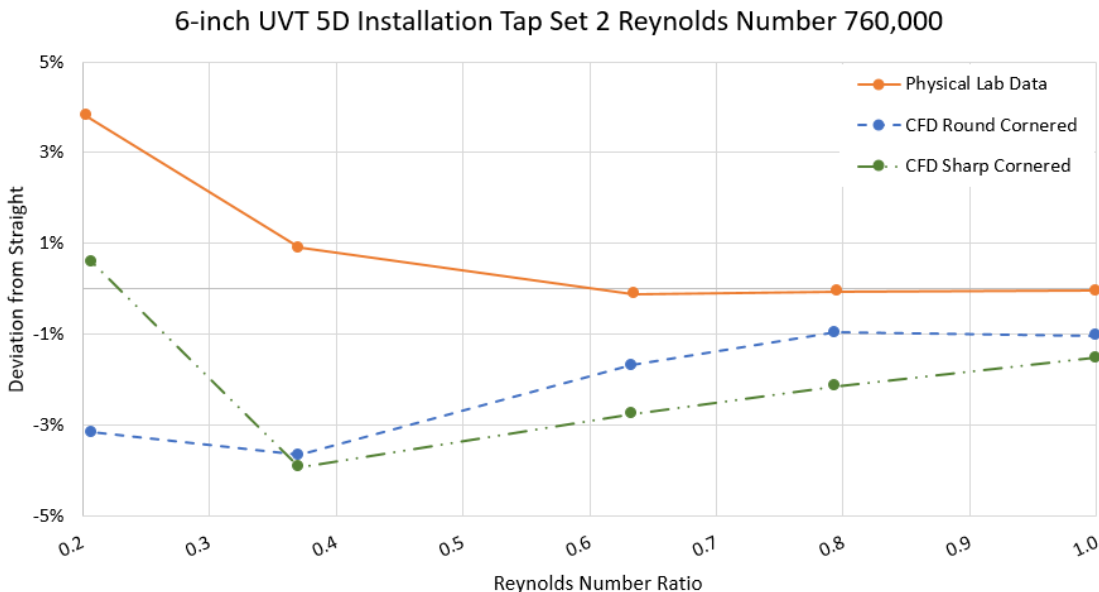


Figure 28. CFD model results for Tap Set 2 of a 6-in. UVT in the 5D installation downstream of a sharp cornered tee at a Reynolds number of 760,000 entering the tee.

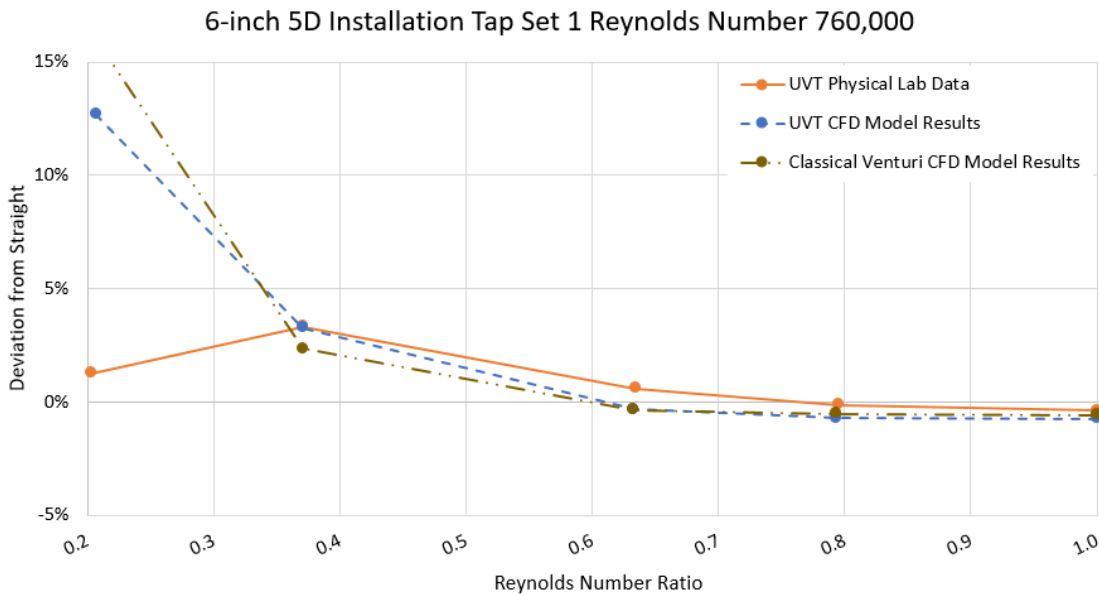


Figure 29. CFD model results for Tap Set 1 of a 6-in. classical Venturi in the 5D installation downstream of a round-cornered tee at a Reynolds number of 760,000 entering the tee.

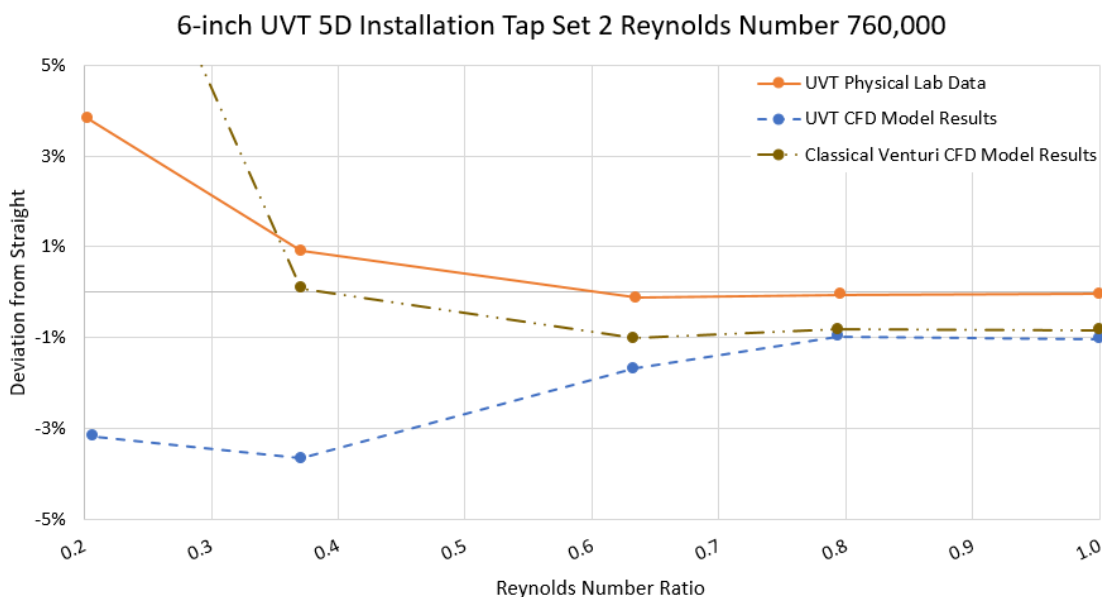


Figure 30. CFD model results for Tap Set 2 of a 6-in. classical Venturi in the 5D installation downstream of a round-cornered tee at a Reynolds number of 760,000 entering the tee.

tee corner. Figure 29 and Figure 30 suggest that the pipe size has little influence on the CFD model results as the 6-in. 0.7 beta classical Venturi plots a similar trend to that of the 24-in. 0.7 beta classical Venturi (Figure 25). The presence of the sharp tee corner seems to shift the trend up or down depending on the Tap Set. In Figure 27, the UVT trend line was shifted up for Tap Set 1 using the sharp-cornered tee, while in Figure 28, the trend line for the UVT was shifted down by using the sharp-cornered tee.

Using the Results

The following example problem demonstrates how to use the contour plots, found in the Appendix, in order to adjust the discharge coefficient.

A 24-in. classical Venturi, with a 0.6 beta ratio, was installed 48 inches downstream on the branch of a tee junction. The Venturi came with a straight-line

calibrated discharge coefficient of 0.985. The tap set used to read differential pressure is the tap set in the plane on the inside curve of the tee, herein referred to as Tap Set 1. It is known that the flow entering the tee junction has a Reynolds number of 1.5×10^6 and it is desired to have 45% of the flow entering the branch while the remaining 55% continues through the run of the tee junction. The objective is to find a multiplier for the calibrated discharge coefficient so flow rate can be more accurately calculated. $\rho_f = 62.42 \text{ lb/ft}^3$ and $\Delta P = 1.356 \text{ psi}$.

First, the target Venturi Reynolds number needs to be calculated.

$$Re_{meter} = Re_{total} * 45\% = 1.5 * 10^6 * 0.45 = 0.675 * 10^6$$

Knowing the flow split and Reynolds number entering the Venturi allows for the use of Figure A16 to find the $C_d/C_{d_stright}$ ratio to correct the given C_d . Figure 31 shows the use of Figure A16. A rough interpolation between 1.06 and 1.08 gives the $C_d/C_{d_stright} = 1.072$.

The adjusted discharge coefficient is:

$$C_d = 0.985 * 1.072 = 1.0559$$

Calculate the throat area.

$$A_t = \frac{\pi}{4} * \left(\frac{24 * 0.6}{12} \right)^2 = 1.13097 \text{ ft}^2$$

Convert the differential pressure from psi to psf.

$$\Delta P = 1.356 * 144 = 195.264 \frac{\text{lb}}{\text{ft}^2}$$

Lastly, use Equation 4 to calculate the flow rate, Q .

$$Q = 1.0559 * 1.13097 * \sqrt{\frac{2 * 32.17405 * 195.264}{(1 - 0.6^4) * 62.42}} = 18.16 \text{ cfs}$$

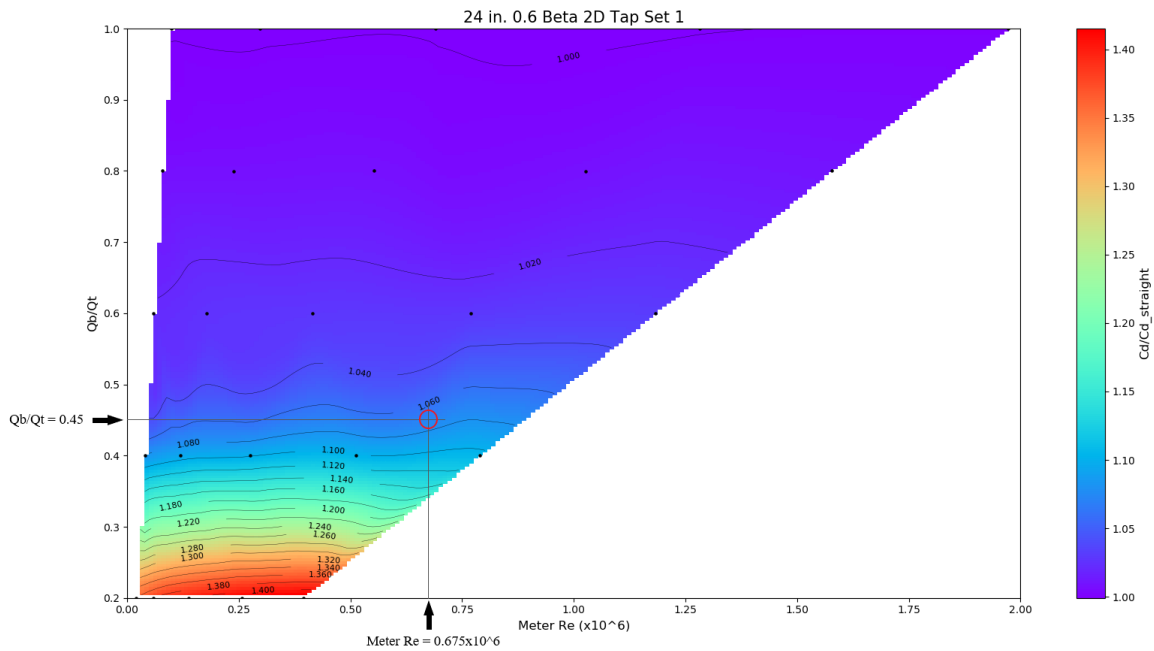


Figure 31. Contour plot for Tap Set 1 of the 24-in. 0.6 beta ratio Classical Venturi. The plot has lines and arrows identifying the Venturi Reynolds number and flow split for the example problem. The red circle identifies where the lines cross and the $C_d/C_{d_straight}$ ratio is read.

If the calibrated discharge coefficient is not adjusted and used as the given 0.985 then the calculated flow rate will be:

$$Q = 0.985 * 1.13097 * \sqrt{\frac{2 * 32.17405 * 195.264}{(1 - 0.6^4) * 62.42}} = 16.94 \text{ cfs}$$

This is a percent difference of:

$$\text{percent difference} = \frac{16.94 - 18.16}{18.16} * 100\% = -6.72\%$$

The percent difference between the flow rate calculated with the adjusted discharge coefficient and the non-adjusted coefficient in this example provides insight into the error in using the straight-line discharge coefficient to calculate the flow rate in installations not suitable for straight-line flow conditions. As the percentage of flow entering the Venturi increases the expected percent difference in flow rate would be expected to decrease. While the percentage of flow entering the Venturi decreases, the expected percent difference in flow rate would be expected to increase. Installation location would also be expected to influence the percent difference in flow rate. The closer the Venturi is located to the tee, the higher the percent difference.

CHAPTER V

CONCLUSIONS

Venturi flowmeters are robust and can function in many different and difficult situations. One such situation is downstream of a tee junction. To get the most accurate reading of flow from the Venturi, it is necessary to calibrate the Venturi in a laboratory setting with the same installation. However, calibration may not be feasible and there may be times when the Venturi has already been installed. In cases like these, CFD models can help individuals understand how the Venturi may be performing. They may then produce discharge coefficient ratios to correct the manufacturer given discharge coefficients or straight line calibrated discharge coefficients to more accurately determine the flow rate.

In this thesis, the CFD physics models were verified as an effective tool for modeling a Venturi located a short distance downstream of a tee junction while also identifying areas the physics models fall short. Some of the notable shortcomings are an inability to correctly model installations at flow splits 20% or less and difficulty simulating the OD installation, especially for the 24-in. 0.7 beta classical Venturi.

Considerable effort was made to ensure the simulation results for the 6-in and 24-in Venturi were mesh (or grid) independent. Plots of physical laboratory data and CFD model results show that the percent deviation from straight is related to the Reynolds number ratio, also known as flow split, of flow entering the Venturi to flow entering the tee and not the particular Reynolds number entering at the inlet of the Venturi.

From the physical laboratory data and CFD model results of the Venturi in a straight-line, or unobstructed, installation and in different locations downstream of a tee, ratios of tee installation discharge coefficient to straight-line discharge coefficient at the same Reynolds number were calculated. The discharge coefficient ratios were plotted in contour plots for the different tee installations. The example presented in Chapter IV illustrates how to use the contour plots to adjust the straight-line, or manufacturer provided, discharge coefficient and calculate the flow rate. The example also provides insight into the percent difference in the calculated flow rate if the discharge coefficient is not adjusted.

At 100% of flow entering the Venturi on the branch of the tee, the percent difference from the straight-line discharge coefficient is nearly negligible for some installations. As the flow split entering the Venturi decreases, the difference in percent difference from straight for physical laboratory data and CFD model results increases and is dependent on the Venturi installation. For the 0D installation, the contour plots have the least uncertainty for the 80-100% flow splits entering the Venturi. The 0D installation should be avoided due to the severely distorted velocity profile of approach, but if use is required, a laboratory calibration is suggested before using the methods described in this research. The 2D installation was represented better by the CFD model above a 40% flow split entering the Venturi, with difficulty at the lower flow splits. Using 5D and 10D installations, the CFD modeling results in lower deviations from the straight-line discharge coefficient.

Overall, the research helps introduce the idea of calibrating a Venturi downstream of a tee junction over a range of flow splits and Reynolds numbers to create a contour plot of discharge coefficient ratios which can be referenced and used to adjust a straight-line discharge coefficient and improve flow measurement accuracy. The contour plots and other results from this research should not be considered a standard.

There are possibilities for future research that are beyond the scope of this thesis and should be considered. One possibility is using multiple taps around the Venturi to average the discharge coefficient as is suggested in Stauffer's (2019) thesis. Another possibility would be taking the contour plots generated as part of this thesis and testing the uncertainty of them with physical laboratory data, particularly the 24-in Classical Venturi, which was not physically tested as part of this thesis. Further research can also build on this thesis for installations not tested, particularly a 1D, 3D, 4D, or 6-9D installation. It could be an interesting study to reproduce the results of this research with a flow conditioner, for example, a plate with multiple orifice openings, placed on the tee junction branch to see if $C_d/C_{d_{straight}}$ could be reduced to a range the CFD physics models could reproduce in a 0D installation. One could also look at other Venturi designs and tee configurations.

This research is significant in presenting an idea for improving flow measurement accuracy when a Venturi is placed downstream of a tee branch and laboratory calibration is not feasible. By improving flow measurement accuracy, overcharges for water delivered, which can result in costly legal battles, challenging system operations, or undercharging for water delivered resulting in lost revenue all due to an incorrect

measurement of flow can be avoided. By reducing the error in flow measurement both the water provider and water user economically benefit.

A summary of key findings is as follows:

1. CFD is a powerful tool that can be used to predict characteristic trends of discharge coefficients of Venturi meters installed downstream of the branch on tee junctions.
2. The discharge coefficient deviations from the straight-line discharge coefficient were a function of the ratio of Reynolds number exiting the tee branch to the Reynolds number entering the tee (or flow split) and not the absolute Reynolds number.
3. The larger deviations from straight for all distances from the tee occur at the low flow splits. The largest deviations overall occur at the OD installation.
4. The 0.7 beta ratio was found to deviate from straight more than the 0.6 beta ratio.
5. The Classical Venturi geometry modeled a more predictable deviation from straight trend than did the UVT between the different installations. Other Venturi geometries would be expected to influence the deviation from straight trends.
6. Tee geometry (sharp versus round cornered) had an effect on model results by shifting the trend lines up or down depending on tap set location.
7. 24-in. and 6-in. model results for the Classical Venturi indicate size has little effect on the deviation from straight trend.

8. Using either physical laboratory data or CFD results correction factors for the given straight-line discharge coefficient can be calculated. Plotting the correction factors as a contour plot allows for a correction factor to be found for an operational range of Reynolds numbers and flow splits.

REFERENCES

- Abdulwahhab, M., Injeti, N. K., and Dakhil, S. F. (2013). “Numerical prediction of pressure loss of fluid in a T-junction.” *International journal of energy and environment*, 4(2), 253–264.
- ASME. (2006). *Test uncertainty: An American national standard*. ASME PTC 19.1-2005, New York.
- ASME. (2008a). “Procedure for estimation and reporting of uncertainty due to discretization in CFD applications.” *Journal of Fluids Engineering*, 130(7), 4.
- ASME. (2008b). *Addenda to ASME MFC-3M-2004: measurement of fluid flow in pipes using orifice, nozzle, and venturi*. ASME MFC-3M-2004, New York.
- Cascetta, F. (1995). “Short history of the flowmetering.” *ISA Transactions*, 34(3), 229–243.
- Costa, N. P., Maia, R., Proença, M. F., and Pinho, F. T. (2006). “Edge Effects on the Flow Characteristics in a 90deg Tee Junction.” *Journal of Fluids Engineering*, 128(6), 1204–1217.
- Finnemore, E. J., and Franzini, J. B. (2002). “Venturi meter.” *Fluid mechanics with engineering applications*, McGraw-Hill, USA, 515–518.
- Hunter, J. D. (2007). “Matplotlib: A 2D Graphics Environment.” *Computing in Science & Engineering*, 9(3), 90–95.
- McKinney, W. (2010). “Data Structures for Statistical Computing in Python.” *The 9th Python in Science Conference*, 51–56.

- Miller, R. W. (1996a). "Chapter 10: Differential producers: Design information." *Flow Measurement Engineering Handbook*, McGraw-Hill, USA, 55–65.
- Miller, R. W. (1996b). "Chapter 9: Engineering Equations." *Flow Measurement Engineering Handbook*, McGraw-Hill, USA, 5–10.
- Sharp, Z. B., Johnson, M. C., and Barfuss, S. L. (2018). "Optimizing the ASME Venturi Recovery Cone Angle to Minimize Head Loss." *Journal of Hydraulic Engineering*, 144(1), 04017057.
- Siemens. (2020). "Reynolds-Averaged Navier-Stokes (RANS) Turbulence Models." <https://documentation.thesteveportal.plm.automation.siemens.com/starccmplus_1atest_en/index.html#page/STARCCMP%2FGUID-7237C585-2707-4FCC-BB3F-E2376C68B114.html> (Feb. 28, 2020).
- Stauffer, T. (2019). "Hydraulic average of multiple tap sets to improve performance of venturi flowmeters with upstream disturbance." Master's, Utah State University, Logan, Ut.
- Stoker, D. M., Barfuss, S. L., and Johnson, M. C. (2012). "Ultrasonic flow measurement for pipe installations with nonideal conditions." *Journal of Irrigation and Drainage Engineering*, 138(11), 993–998.
- UWRL. (2019). "Flowmeter, Pipe, Pump, & Valve Testing." *Utah State University Utah Water Research Laboratory*, <<https://uwrl.usu.edu/hydraulics/hydraulic-testing>> (Oct. 29, 2019).

APPENDICES

APPENDIX A

SIMULATION TABLE AND CONTOUR PLOTS

Table A1. Parameters used for the CFD 6-in. and 24-in. 0.6 beta ratio GCI simulations.

Pipe Size (in)	Installation	Unit Weight (pcf)	Dynamic Viscosity (Pa-s)	Number of Prism Layers	Prism Layer Stretching	Interface Mass Flow Rate (lb/s)	Flow Split Entering the Venturi
6	straight	62.40915	0.0013072	11	1.45	14	1
6	straight	62.40915	0.0013072	12	1.45	24.89	1
6	straight	62.40915	0.0013072	13	1.45	54.22	1
6	straight	62.40915	0.0013072	14	1.45	83.22	1
6	straight	62.40915	0.0013072	16	1.45	115.52	1
6	straight	62.40915	0.0013072	17	1.45	140.02	1
6	straight	62.40915	0.0013072	17	1.45	171.7	1
6	straight	62.40915	0.0013072	17	1.45	199.57	1
6	straight	62.40915	0.0013072	18	1.45	277.6	1
6	straight	62.40915	0.0013072	18	1.45	281.8	1
6	0D	62.41868	0.0013883	18	1.45	272	1
6	0D	62.41868	0.0013883	18	1.45	272	0.8185
6	0D	62.41868	0.0013883	18	1.45	272	0.6367
6	0D	62.41868	0.0013883	18	1.45	272	0.4573
6	0D	62.41868	0.0013883	18	1.45	272	0.3068
6	0D	62.41868	0.0013883	16	1.45	140	1
6	0D	62.41868	0.0013883	16	1.45	140	0.8226
6	0D	62.41868	0.0013883	16	1.45	140	0.6251
6	0D	62.41868	0.0013883	16	1.45	140	0.4517
6	0D	62.41868	0.0013883	16	1.45	140	0.3187
6	0D	62.41868	0.0013883	15	1.45	70	1
6	0D	62.41868	0.0013883	15	1.45	70	0.809
6	0D	62.41868	0.0013883	15	1.45	70	0.634
6	0D	62.41868	0.0013883	15	1.45	70	0.449
6	0D	62.41868	0.0013883	15	1.45	70	0.243
6	5D	62.41603	0.0013615	19	1.45	279	1
6	5D	62.41603	0.0013615	19	1.45	279	0.794
6	5D	62.41603	0.0013615	19	1.45	279	0.633
6	5D	62.41603	0.0013615	19	1.45	279	0.371
6	5D	62.41603	0.0013615	19	1.45	279	0.207

6	5D	62.41603	0.0013615	17	1.45	140	1
6	5D	62.41603	0.0013615	17	1.45	140	0.799
6	5D	62.41603	0.0013615	17	1.45	140	0.652
6	5D	62.41603	0.0013615	17	1.45	140	0.399
6	5D	62.41603	0.0013615	17	1.45	140	0.196
6	5D	62.41603	0.0013615	15	1.45	70	1
6	5D	62.41603	0.0013615	15	1.45	70	0.8149
6	5D	62.41603	0.0013615	15	1.45	70	0.6575
6	5D	62.41603	0.0013615	15	1.45	70	0.3426
6	5D	62.41603	0.0013615	15	1.45	70	0.2107
24	straight	62.41603	0.0013615	10	1.45	21.438	1
24	straight	62.41603	0.0013615	10	1.45	28.58347	1
24	straight	62.41603	0.0013615	12	1.45	57.16694	1
24	straight	62.41603	0.0013615	13	1.45	85.42348	1
24	straight	62.41603	0.0013615	13	1.45	113.898	1
24	straight	62.41603	0.0013615	14	1.45	142.373	1
24	straight	62.41603	0.0013615	14	1.45	170.847	1
24	straight	62.41603	0.0013615	14	1.45	199.322	1
24	straight	62.41603	0.0013615	15	1.45	256.271	1
24	straight	62.41603	0.0013615	16	1.45	341.695	1
24	straight	62.41603	0.0013615	16	1.45	370.169	1
24	straight	62.41603	0.0013615	16	1.45	398.644	1
24	straight	62.41603	0.0013615	17	1.45	427.118	1
24	straight	62.41603	0.0013615	17	1.45	569.491	1
24	straight	62.41603	0.0013615	18	1.45	597.966	1
24	straight	62.41603	0.0013615	18	1.45	740.338	1
24	straight	62.41603	0.0013615	18	1.45	797.287	1
24	straight	62.41603	0.0013615	19	1.45	996.609	1
24	straight	62.41603	0.0013615	19	1.45	1110.507	1
24	straight	62.41603	0.0013615	19	1.45	1138.982	1
24	straight	62.41603	0.0013615	20	1.45	1480.677	1
24	straight	62.41603	0.0013615	20	1.45	1708.473	1
24	straight	62.41603	0.0013615	21	1.45	1850.846	1
24	straight	62.41603	0.0013615	21	1.45	2277.964	1
24	straight	62.41603	0.0013615	22	1.45	2847.455	1
24	straight	62.41603	0.0013615	22	1.45	2870	1
24	2D	62.41603	0.0013615	21	1.45	2847.455	1
24	2D	62.41603	0.0013615	21	1.45	2847.455	0.8
24	2D	62.41603	0.0013615	21	1.45	2847.455	0.6

24	2D	62.41603	0.0013615	21	1.45	2847.455	0.4
24	2D	62.41603	0.0013615	21	1.45	2847.455	0.2
24	2D	62.41603	0.0013615	20	1.45	1850.846	1
24	2D	62.41603	0.0013615	20	1.45	1850.846	0.8
24	2D	62.41603	0.0013615	20	1.45	1850.846	0.6
24	2D	62.41603	0.0013615	20	1.45	1850.846	0.4
24	2D	62.41603	0.0013615	20	1.45	1850.846	0.2
24	2D	62.41603	0.0013615	19	1.45	996.609	1
24	2D	62.41603	0.0013615	19	1.45	996.609	0.8
24	2D	62.41603	0.0013615	19	1.45	996.609	0.6
24	2D	62.41603	0.0013615	19	1.45	996.609	0.4
24	2D	62.41603	0.0013615	19	1.45	996.609	0.2
24	2D	62.41603	0.0013615	17	1.45	427.118	1
24	2D	62.41603	0.0013615	17	1.45	427.118	0.8
24	2D	62.41603	0.0013615	17	1.45	427.118	0.6
24	2D	62.41603	0.0013615	17	1.45	427.118	0.4
24	2D	62.41603	0.0013615	17	1.45	427.118	0.2
24	2D	62.41603	0.0013615	14	1.45	142.373	1
24	2D	62.41603	0.0013615	14	1.45	142.373	0.8
24	2D	62.41603	0.0013615	14	1.45	142.373	0.6
24	2D	62.41603	0.0013615	14	1.45	142.373	0.4
24	2D	62.41603	0.0013615	14	1.45	142.373	0.2
24	5D	62.41603	0.0013615	21	1.45	2847.455	1
24	5D	62.41603	0.0013615	21	1.45	2847.455	0.8
24	5D	62.41603	0.0013615	21	1.45	2847.455	0.6
24	5D	62.41603	0.0013615	21	1.45	2847.455	0.4
24	5D	62.41603	0.0013615	21	1.45	2847.455	0.2
24	5D	62.41603	0.0013615	20	1.45	1850.846	1
24	5D	62.41603	0.0013615	20	1.45	1850.846	0.8
24	5D	62.41603	0.0013615	20	1.45	1850.846	0.6
24	5D	62.41603	0.0013615	20	1.45	1850.846	0.4
24	5D	62.41603	0.0013615	20	1.45	1850.846	0.2
24	5D	62.41603	0.0013615	18	1.45	996.609	1
24	5D	62.41603	0.0013615	18	1.45	996.609	0.8
24	5D	62.41603	0.0013615	18	1.45	996.609	0.6
24	5D	62.41603	0.0013615	18	1.45	996.609	0.4
24	5D	62.41603	0.0013615	18	1.45	996.609	0.2
24	5D	62.41603	0.0013615	16	1.45	427.118	1
24	5D	62.41603	0.0013615	16	1.45	427.118	0.8

24	5D	62.41603	0.0013615	16	1.45	427.118	0.6
24	5D	62.41603	0.0013615	16	1.45	427.118	0.4
24	5D	62.41603	0.0013615	16	1.45	427.118	0.2
24	5D	62.41603	0.0013615	14	1.45	142.373	1
24	5D	62.41603	0.0013615	14	1.45	142.373	0.8
24	5D	62.41603	0.0013615	14	1.45	142.373	0.6
24	5D	62.41603	0.0013615	14	1.45	142.373	0.4
24	5D	62.41603	0.0013615	14	1.45	142.373	0.2
24	10D	62.41603	0.0013615	22	1.45	2847.455	1
24	10D	62.41603	0.0013615	22	1.45	2847.455	0.8
24	10D	62.41603	0.0013615	22	1.45	2847.455	0.6
24	10D	62.41603	0.0013615	22	1.45	2847.455	0.4
24	10D	62.41603	0.0013615	22	1.45	2847.455	0.2
24	10D	62.41603	0.0013615	21	1.45	1850.846	1
24	10D	62.41603	0.0013615	21	1.45	1850.846	0.8
24	10D	62.41603	0.0013615	21	1.45	1850.846	0.6
24	10D	62.41603	0.0013615	21	1.45	1850.846	0.4
24	10D	62.41603	0.0013615	21	1.45	1850.846	0.2
24	10D	62.41603	0.0013615	19	1.45	996.609	1
24	10D	62.41603	0.0013615	19	1.45	996.609	0.8
24	10D	62.41603	0.0013615	19	1.45	996.609	0.6
24	10D	62.41603	0.0013615	19	1.45	996.609	0.4
24	10D	62.41603	0.0013615	19	1.45	996.609	0.2
24	10D	62.41603	0.0013615	17	1.45	427.118	1
24	10D	62.41603	0.0013615	17	1.45	427.118	0.8
24	10D	62.41603	0.0013615	17	1.45	427.118	0.6
24	10D	62.41603	0.0013615	17	1.45	427.118	0.4
24	10D	62.41603	0.0013615	17	1.45	427.118	0.2
24	10D	62.41603	0.0013615	14	1.45	142.373	1
24	10D	62.41603	0.0013615	14	1.45	142.373	0.8
24	10D	62.41603	0.0013615	14	1.45	142.373	0.6
24	10D	62.41603	0.0013615	14	1.45	142.373	0.4
24	10D	62.41603	0.0013615	14	1.45	142.373	0.2

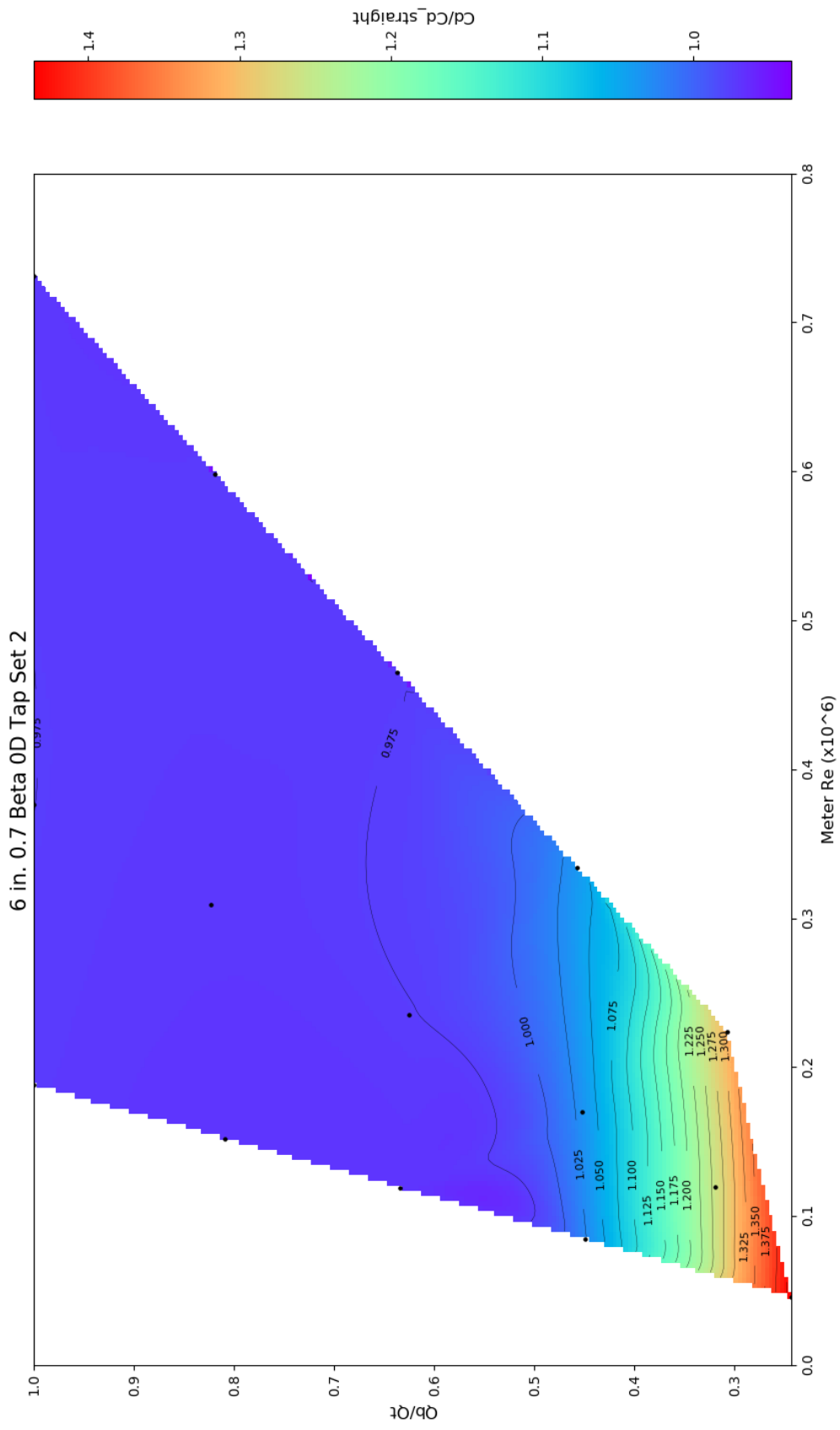


Figure A1. Contour plot for Tap Set 2 of the CFD 6-in. 0.7 beta ratio OD installation.

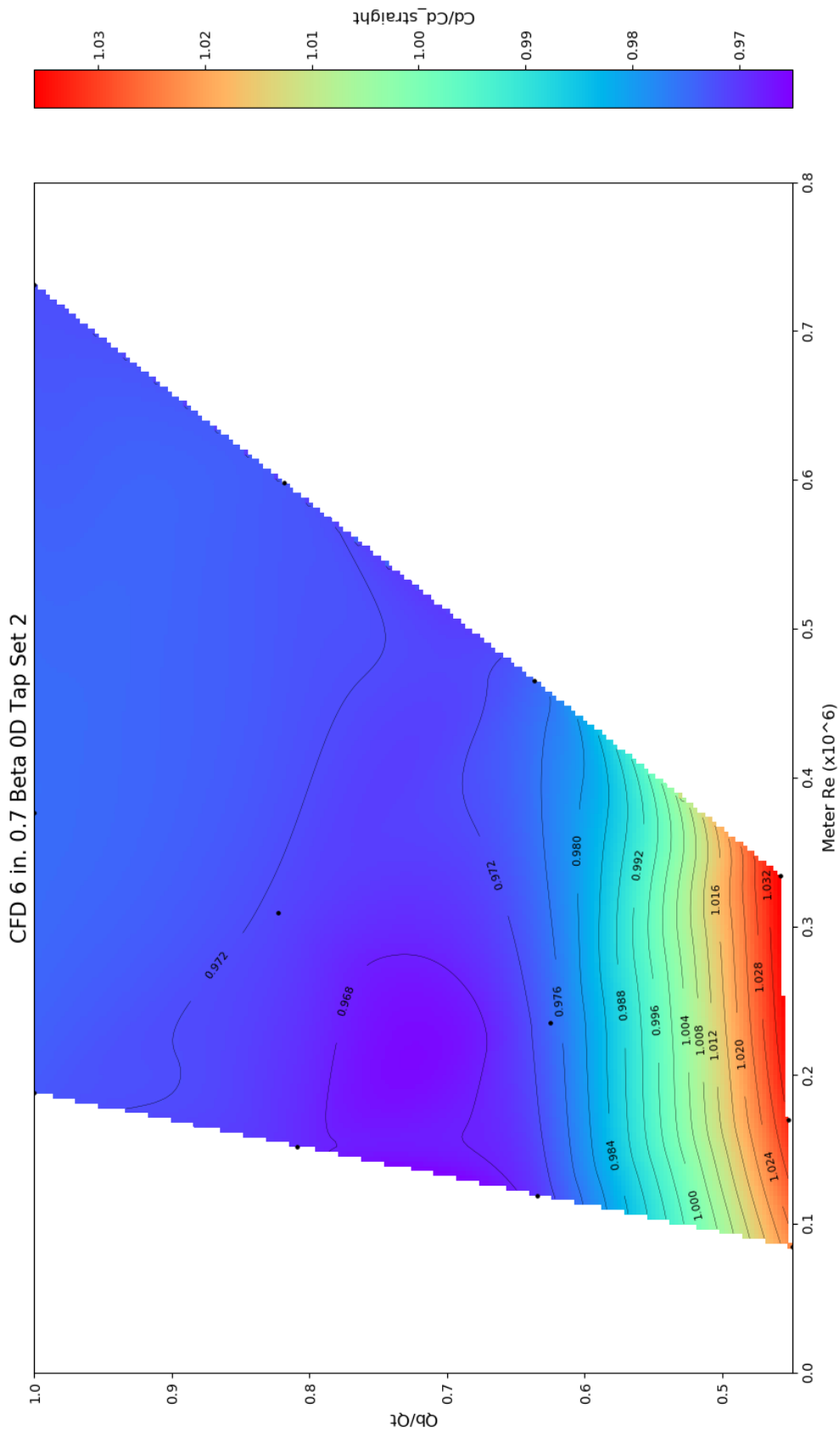


Figure A2. Contour plot for Tap Set 2 of the CFD 6-in. 0.7 beta ratio OD installation without 20% flow split data.

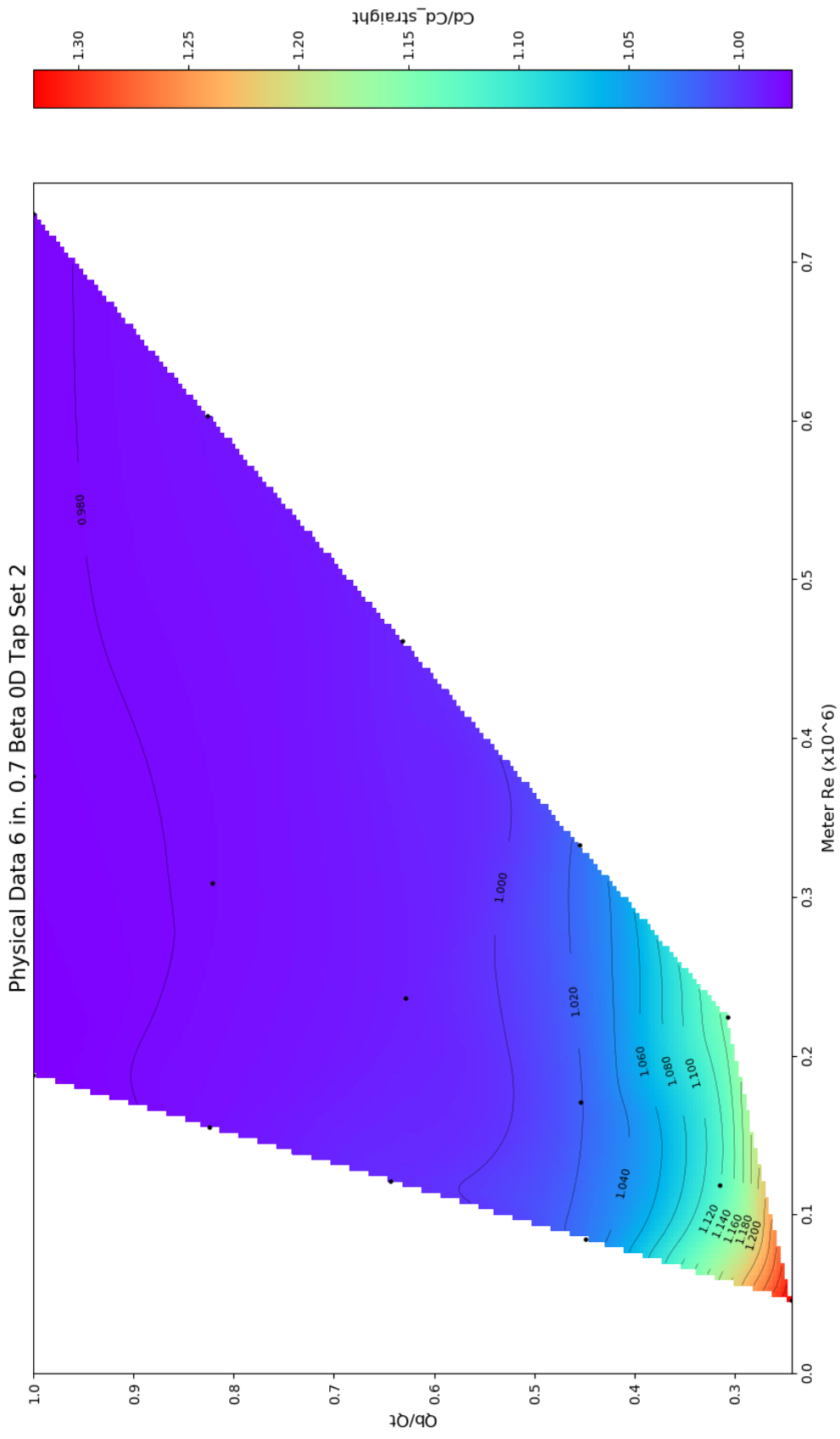


Figure A3. Contour plot for Tap Set 2 of the physical 6-in. 0.7 beta ratio OD installation.

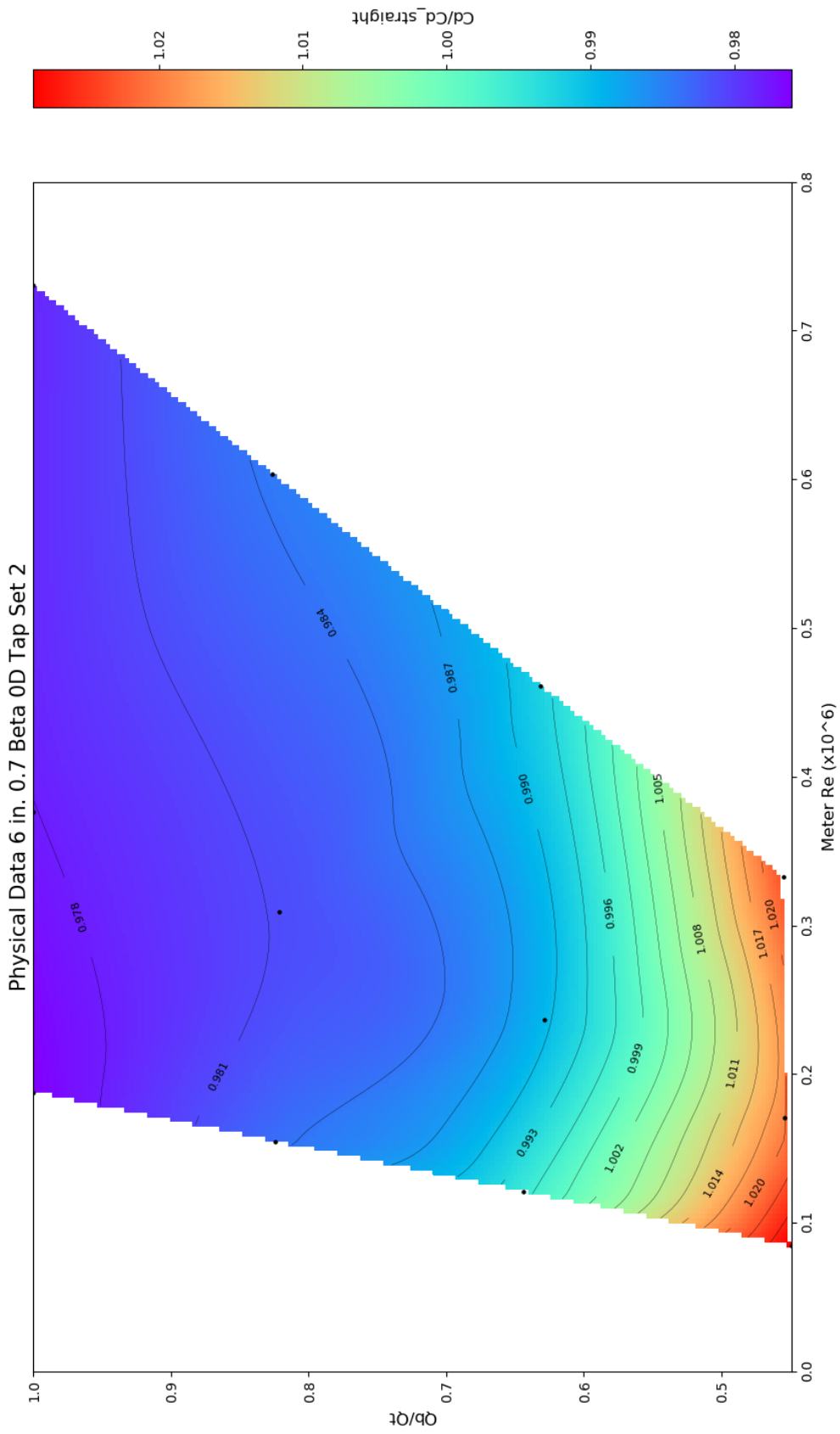


Figure A4. Contour plot for Tap Set 2 of the physical 6-in. 0.7 beta ratio 0D installation without 20% flow split data.

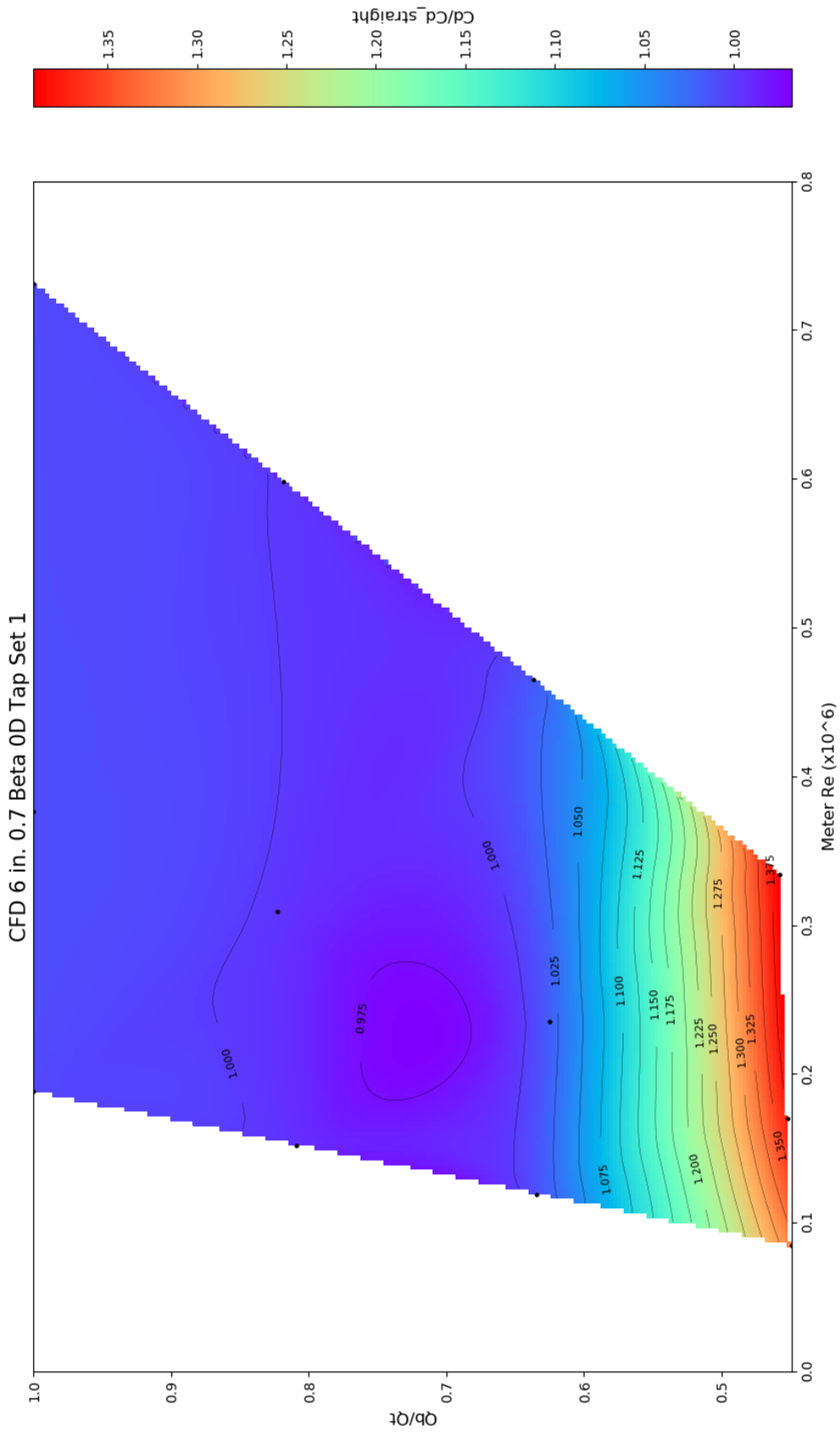


Figure A5. Contour plot for Tap Set 1 of the CFD 6-in. 0.7 beta ratio OD installation without 20% flow split data.

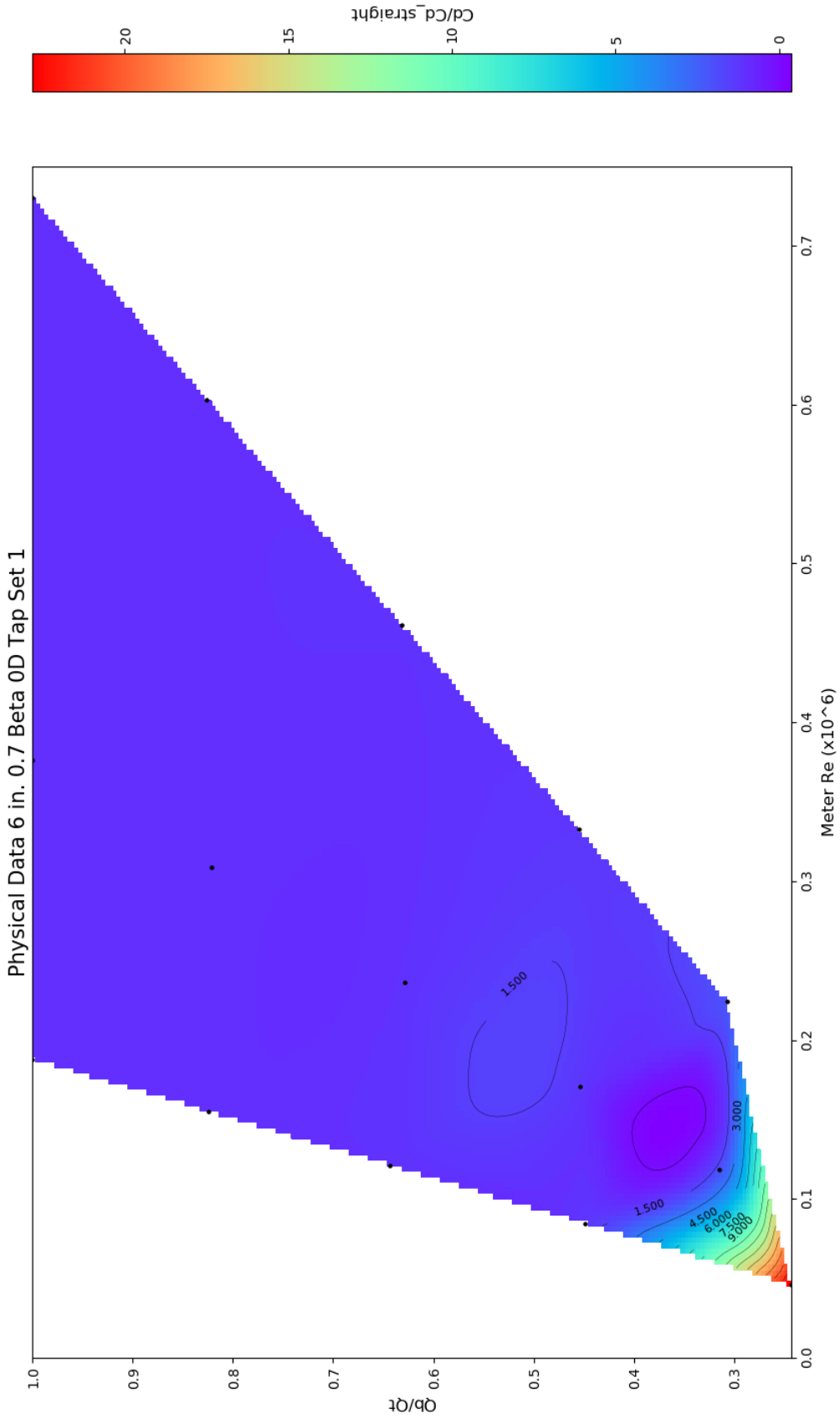


Figure A6. Contour plot for Tap Set 1 of the physical 6-in. 0.7 beta ratio OD installation.

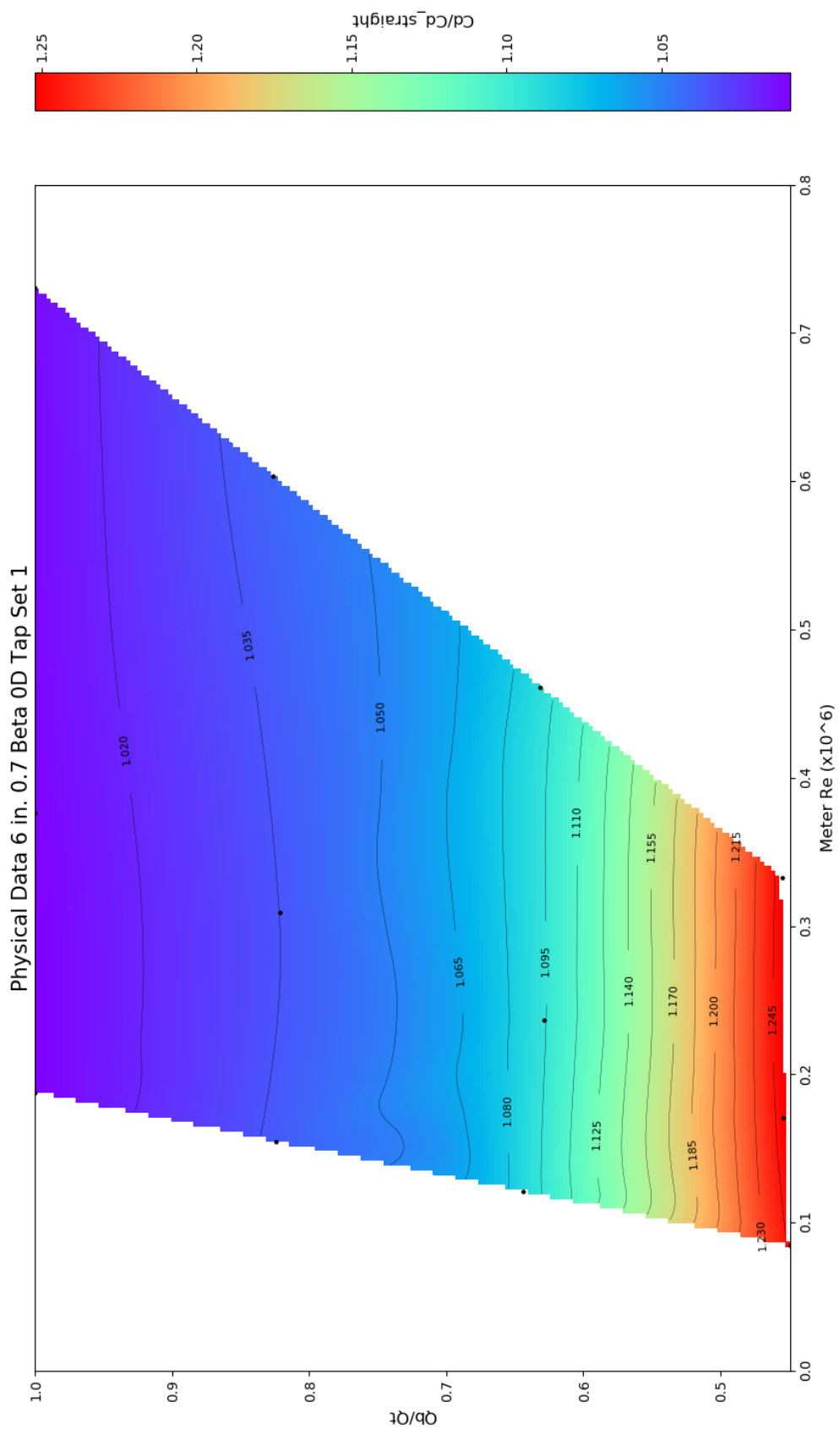


Figure A7. Contour plot for Tap Set 1 of the physical 6-in. 0.7 beta ratio OD installation without 20% flow split data.

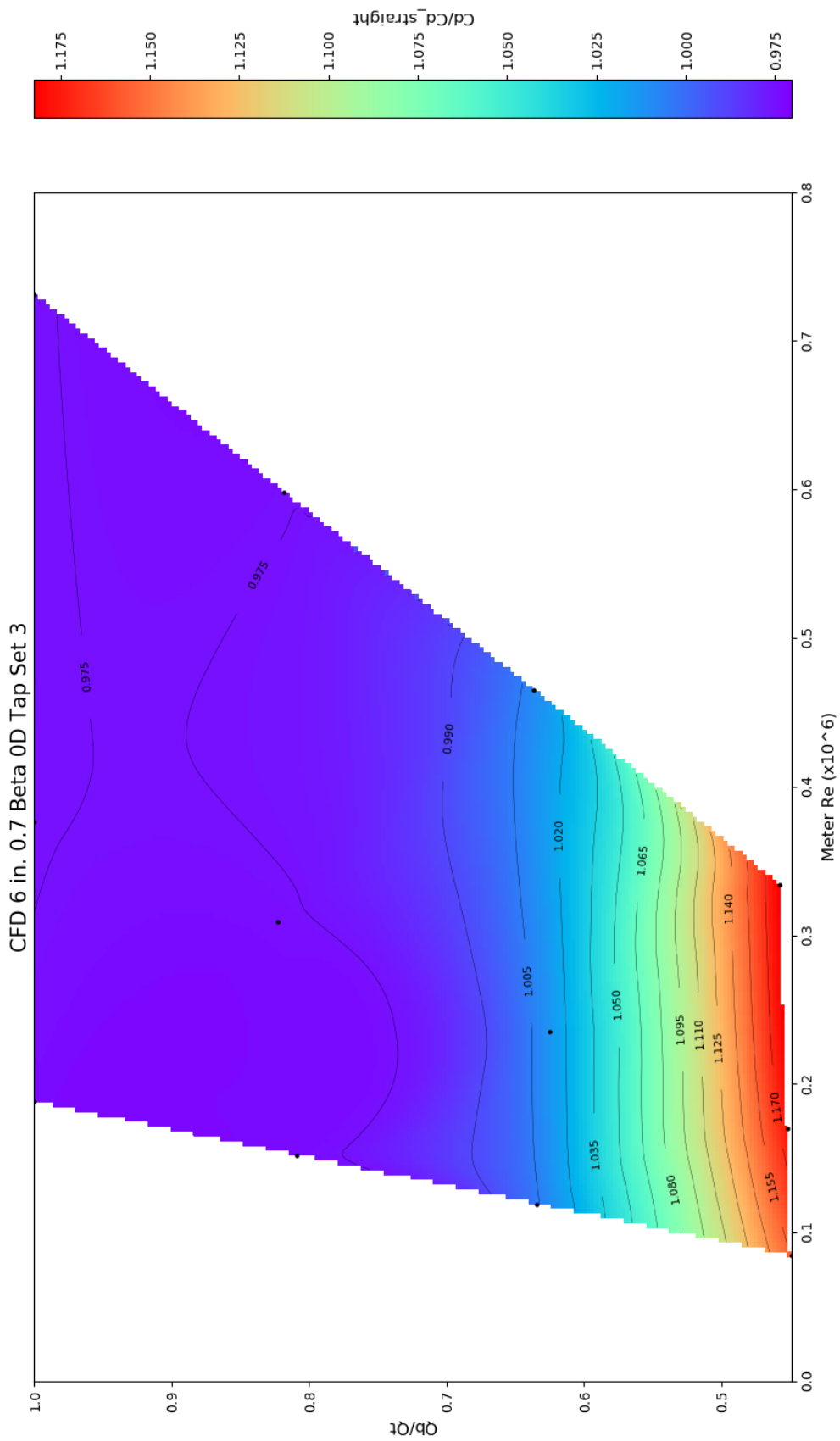


Figure A8. Contour plot for Tap Set 3 of the CFD 6-in. 0.7 beta ratio OD installation without 20% flow split data.

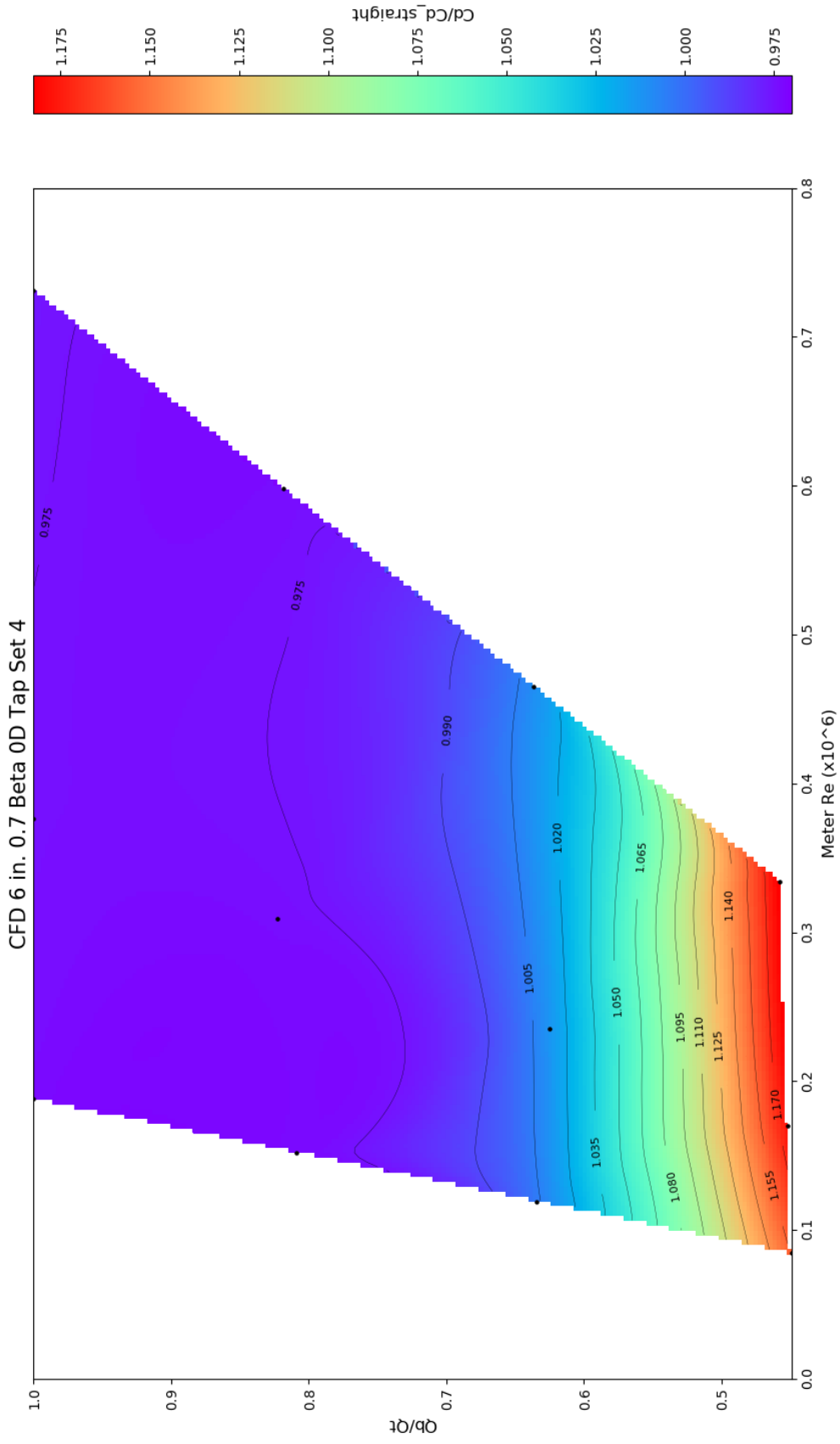


Figure A9. Contour plot for Tap Set 4 of the CFD 6-in. 0.7 beta ratio OD installation without 20% flow split data.

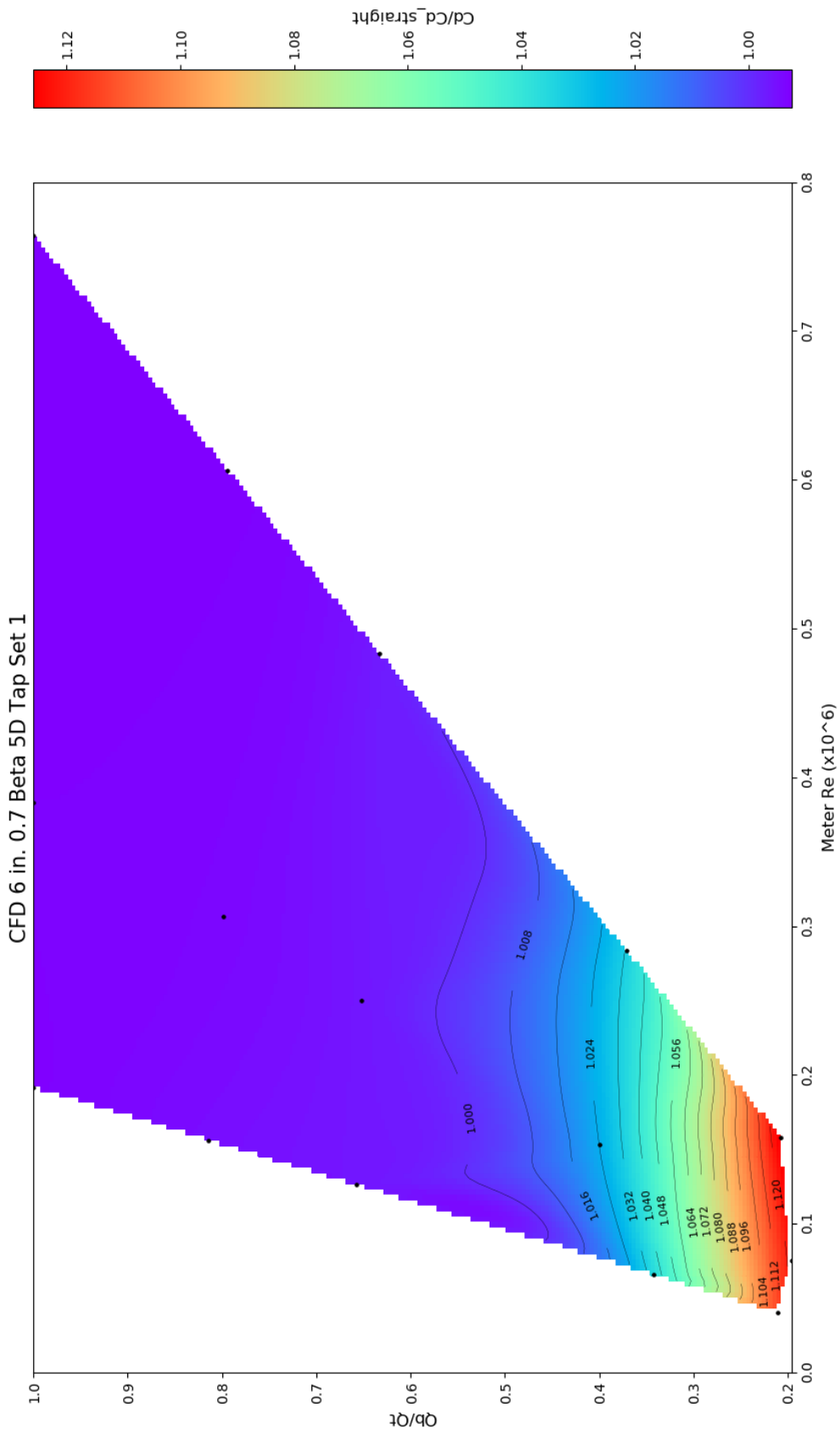


Figure A10. Contour plot for Tap Set 1 of the CFD 6-in. 0.7 beta ratio 5D installation.

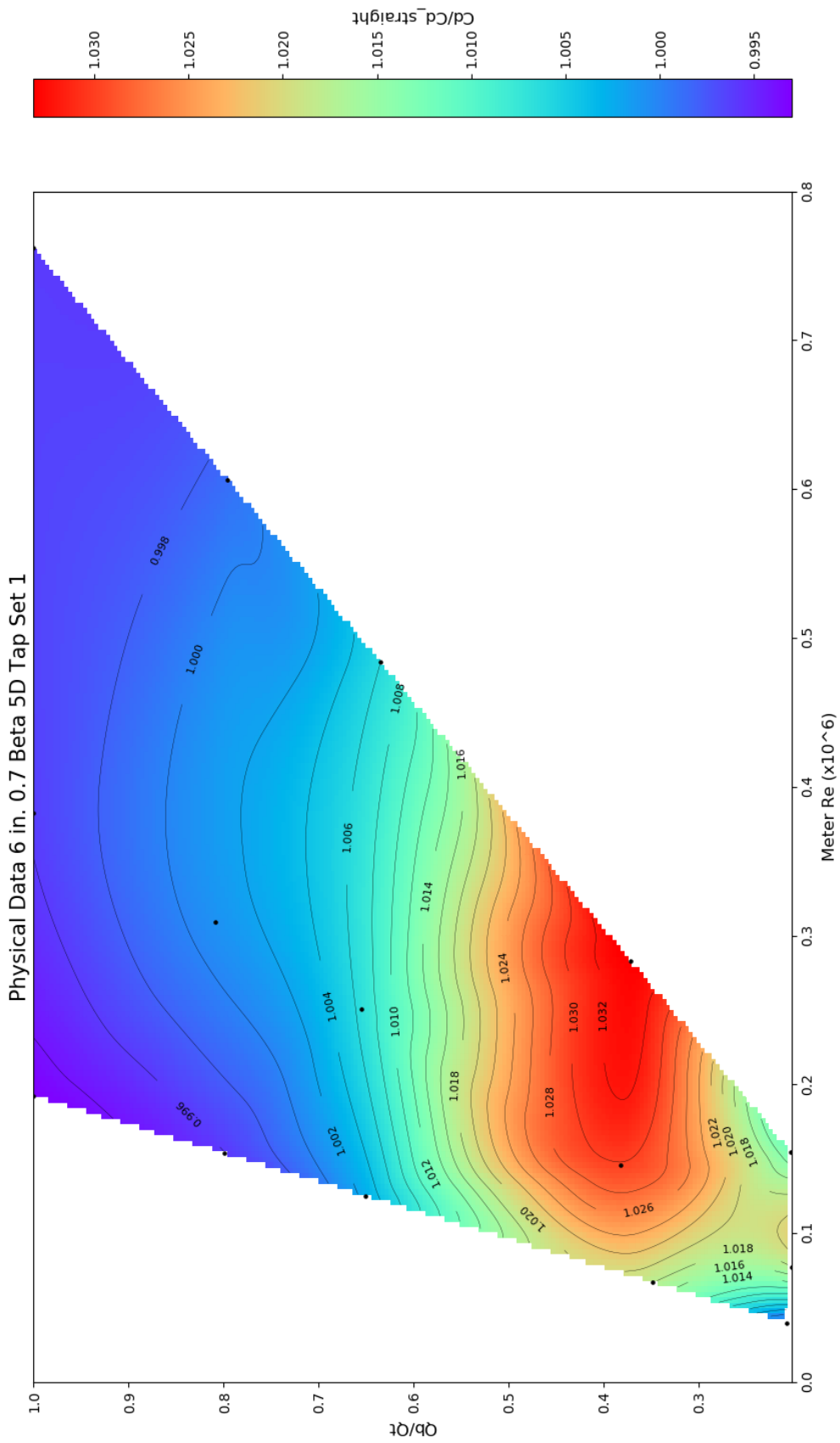


Figure A11. Contour plot for Tap Set 1 of the Physical 6-in. 0.7 beta ratio 5D installation.

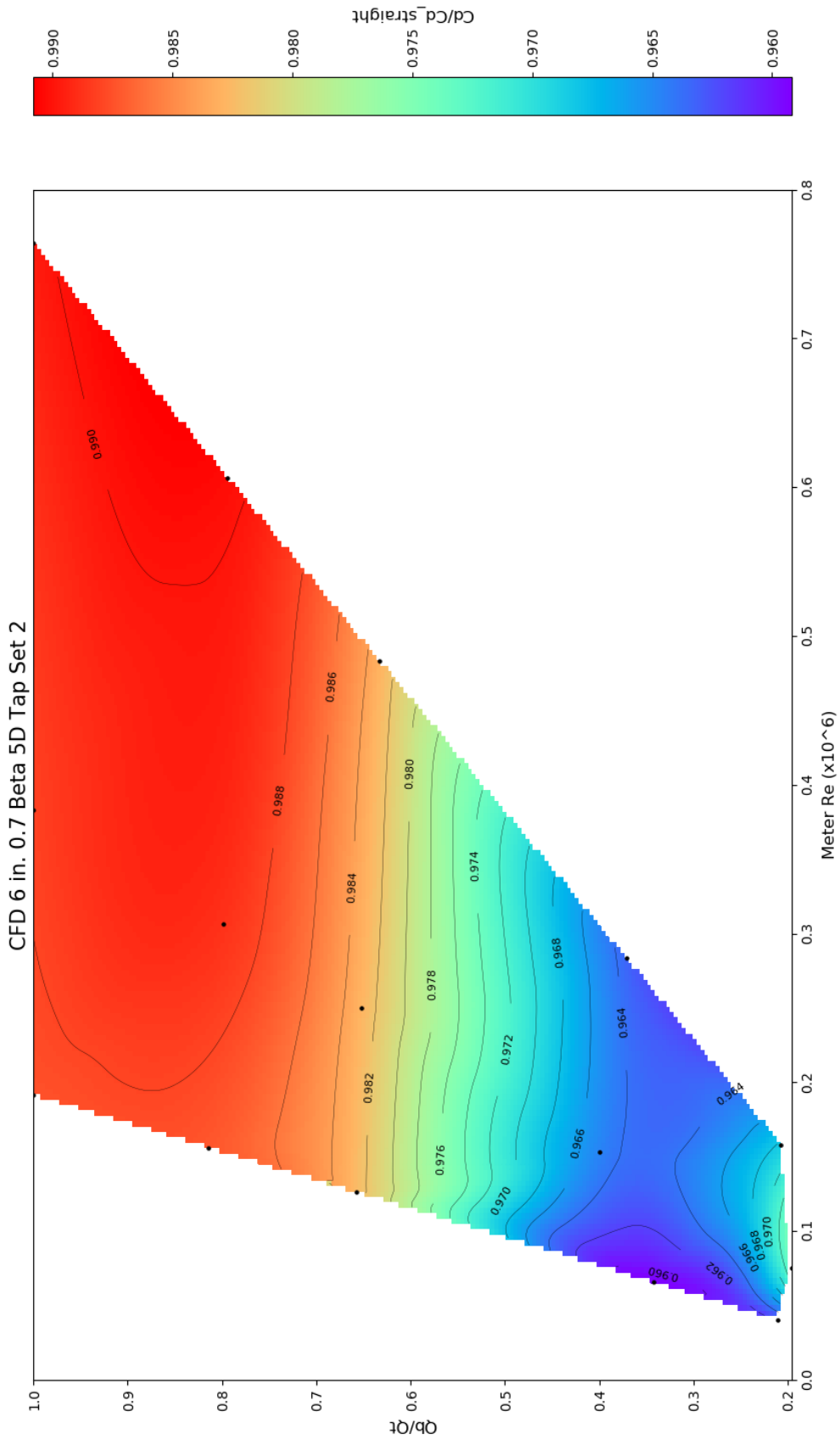


Figure A12. Contour plot for Tap Set 2 of the CFD 6-in. 0.7 beta ratio 5D installation.

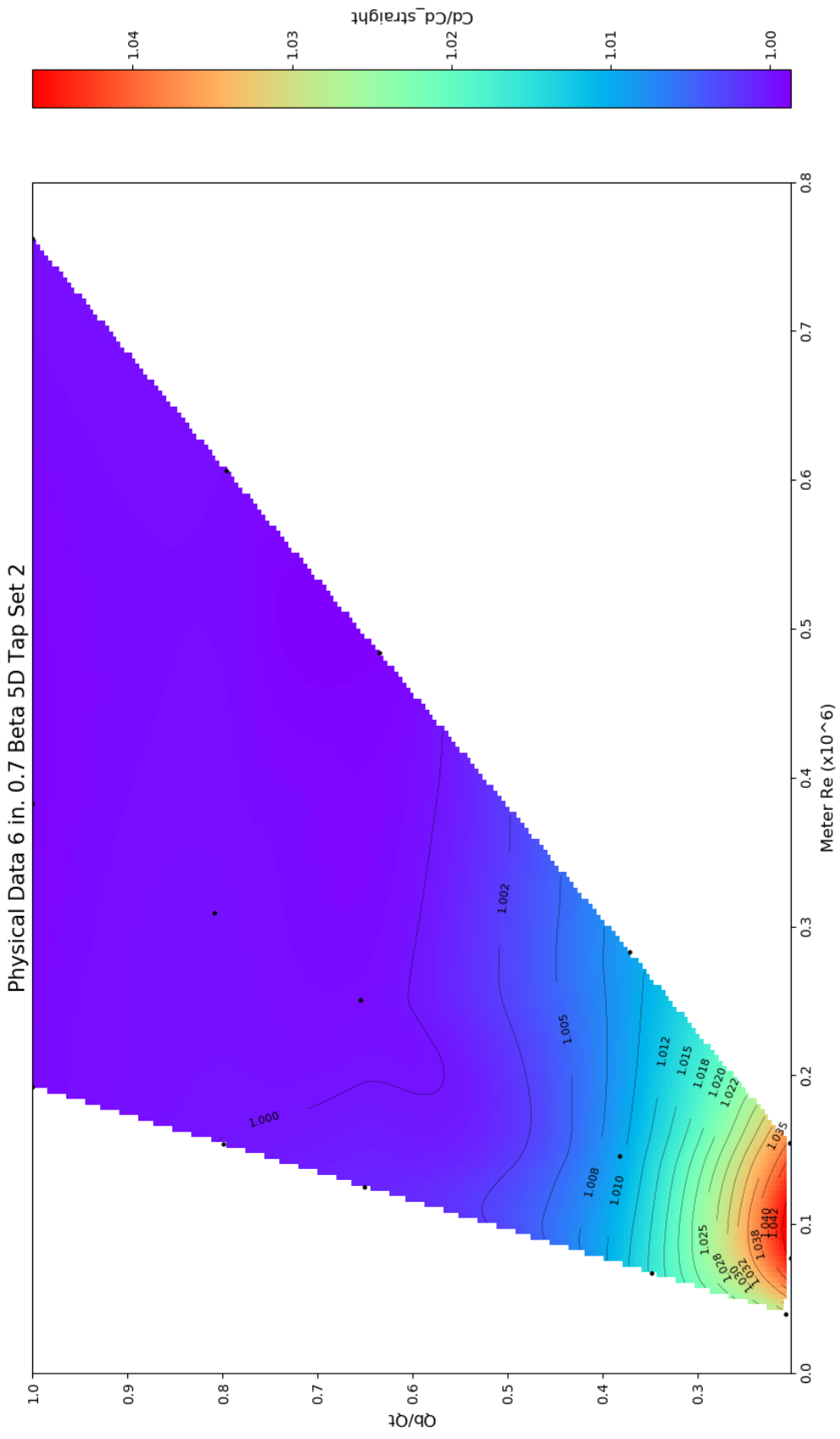


Figure A13. Contour plot for Tap Set 2 of the Physical 6-in. 0.7 beta ratio 5D installation.

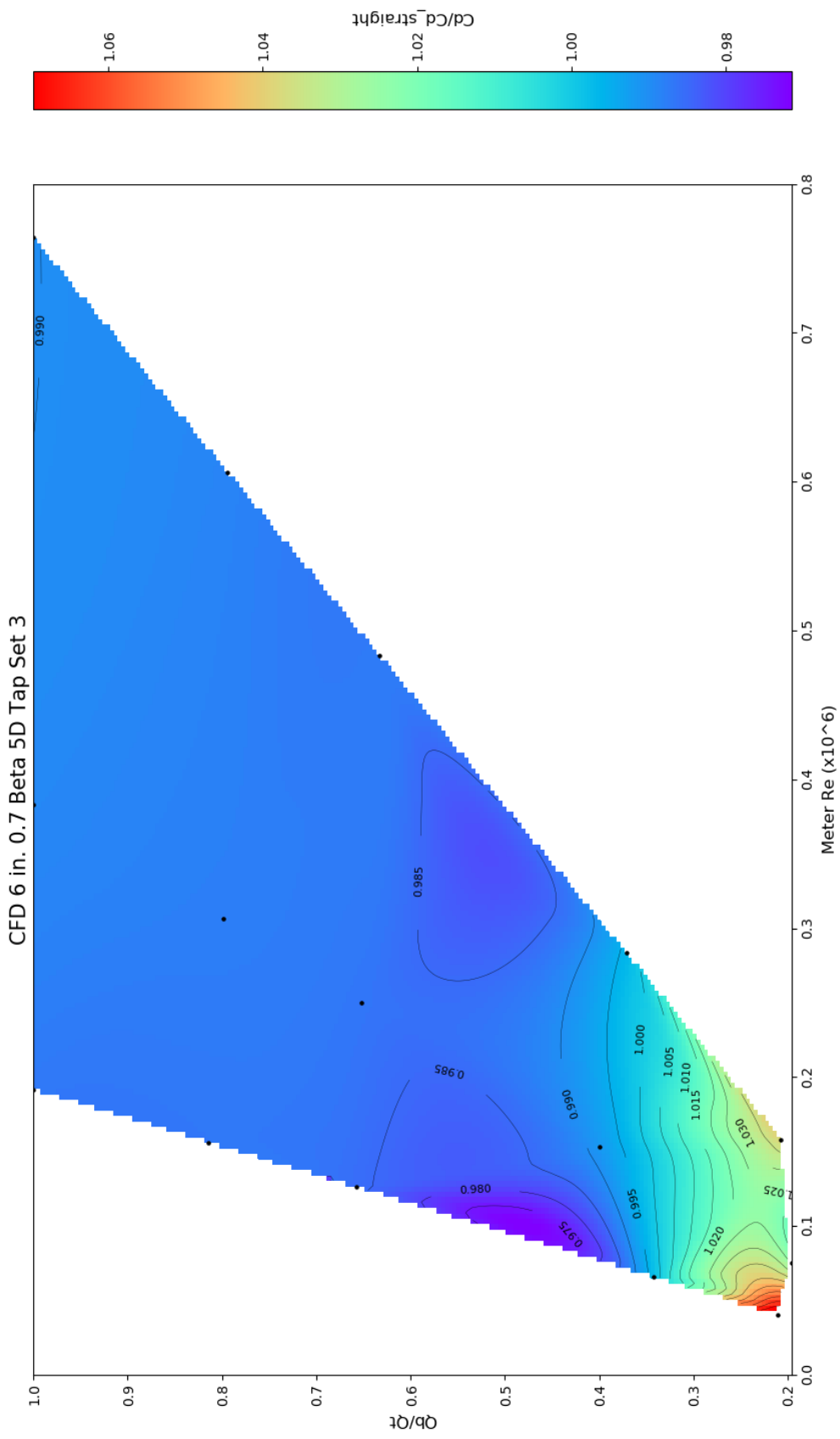


Figure A14. Contour plot for Tap Set 3 of the CFD 6-in. 0.7 beta ratio 5D installation.

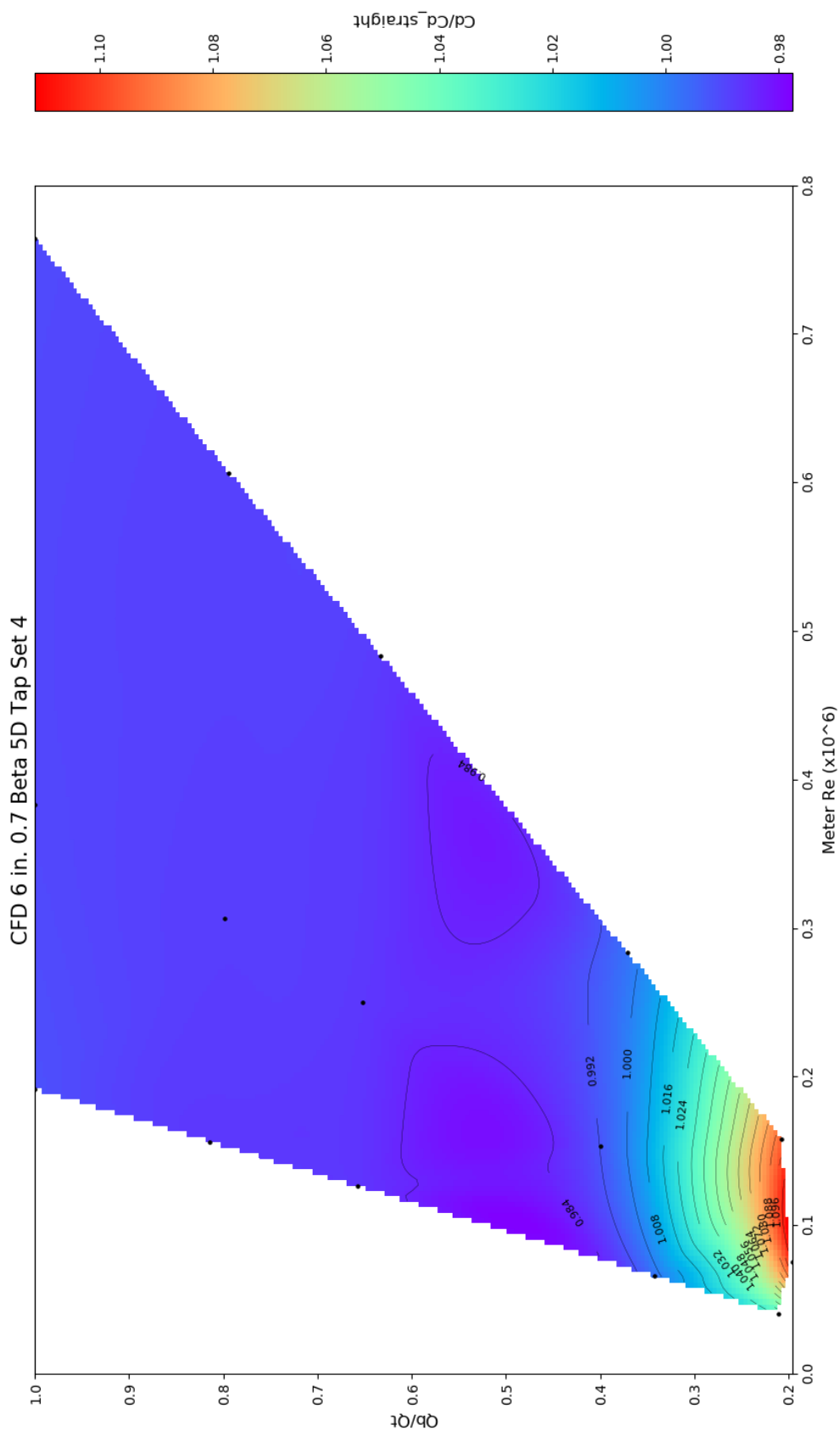


Figure A15. Contour plot for Tap Set 4 of the CFD 6-in. 0.7 beta ratio 5D installation.

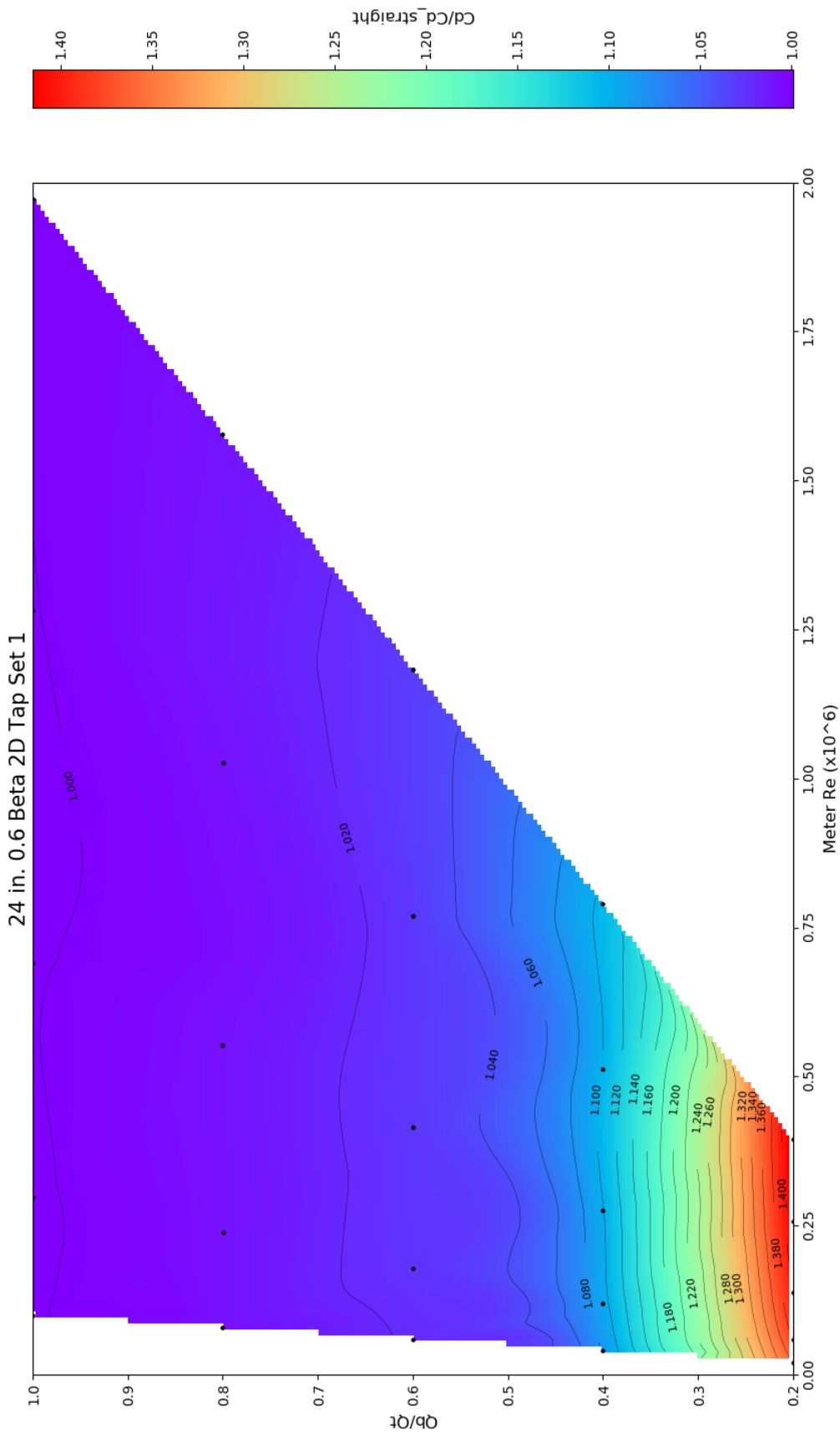


Figure A16. Contour plot for Tap Set 1 of the CFD 24-in. 0.6 beta ratio 2D installation.

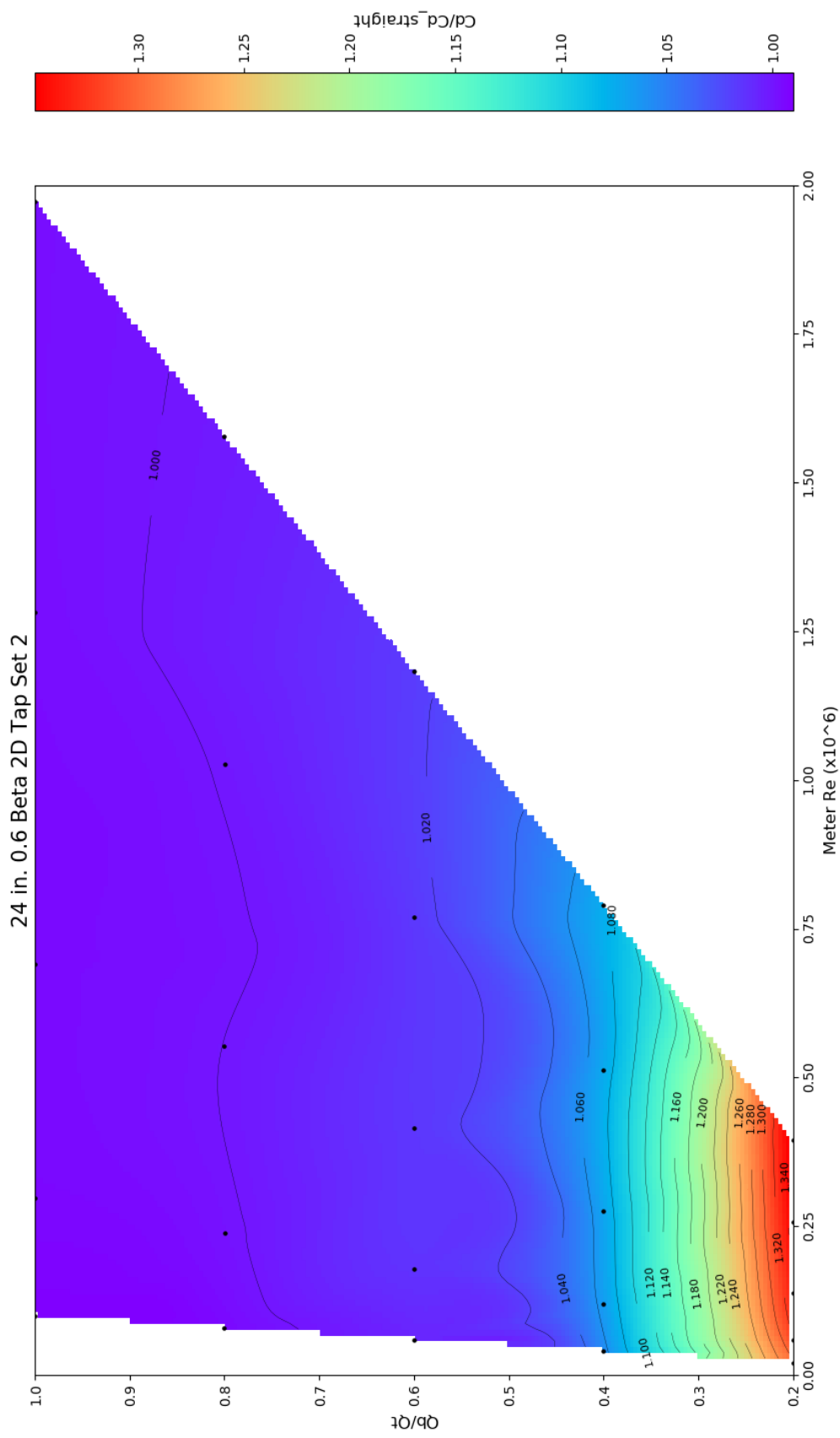


Figure A17. Contour plot for Tap Set 2 of the CFD 24-in. 0.6 beta ratio 2D installation.

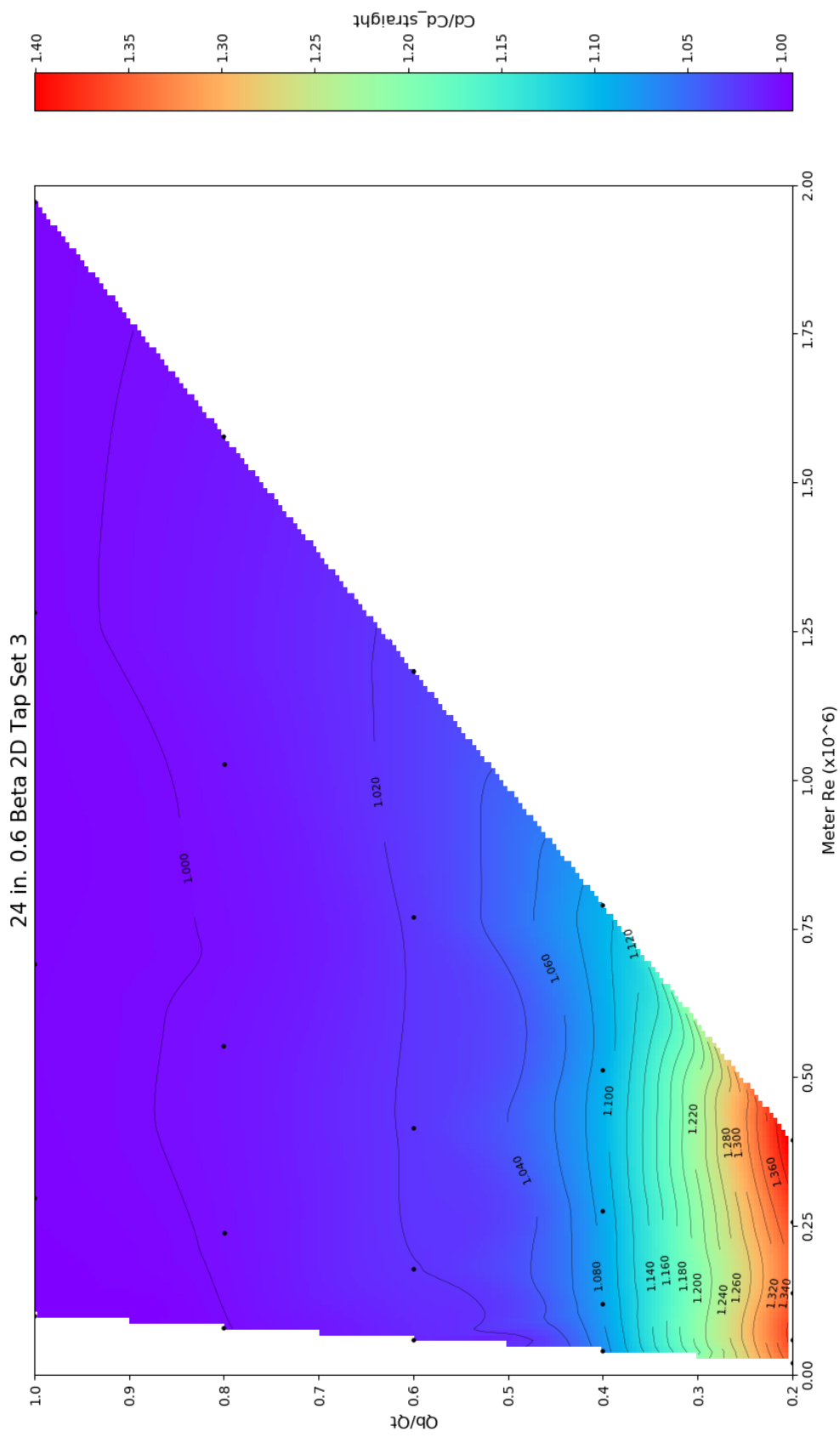


Figure A18. Contour plot for Tap Set 3 of the CFD 24-in. 0.6 beta ratio 2D installation.

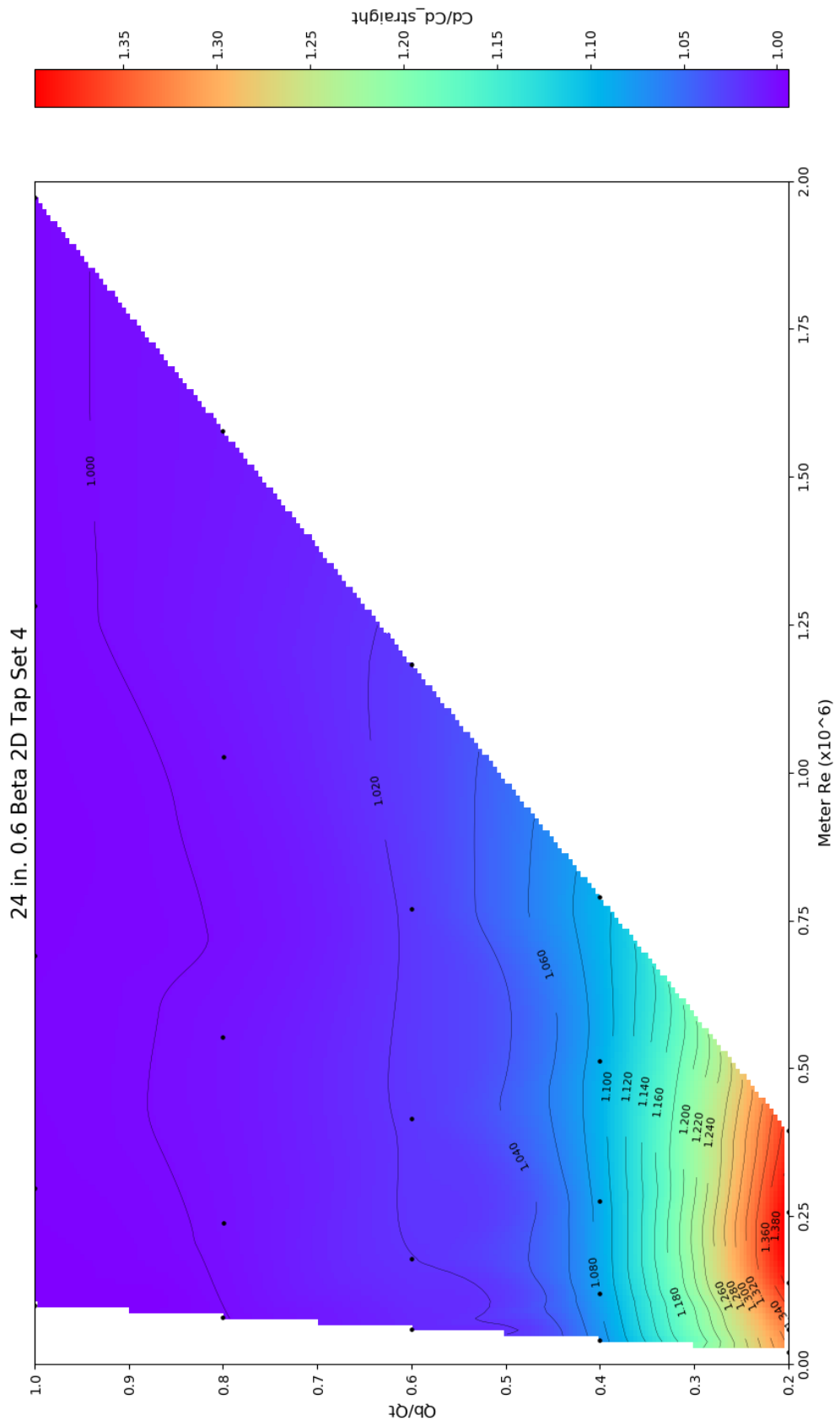


Figure A19. Contour plot for Tap Set 4 of the CFD 24-in. 0.6 beta ratio 2D installation.

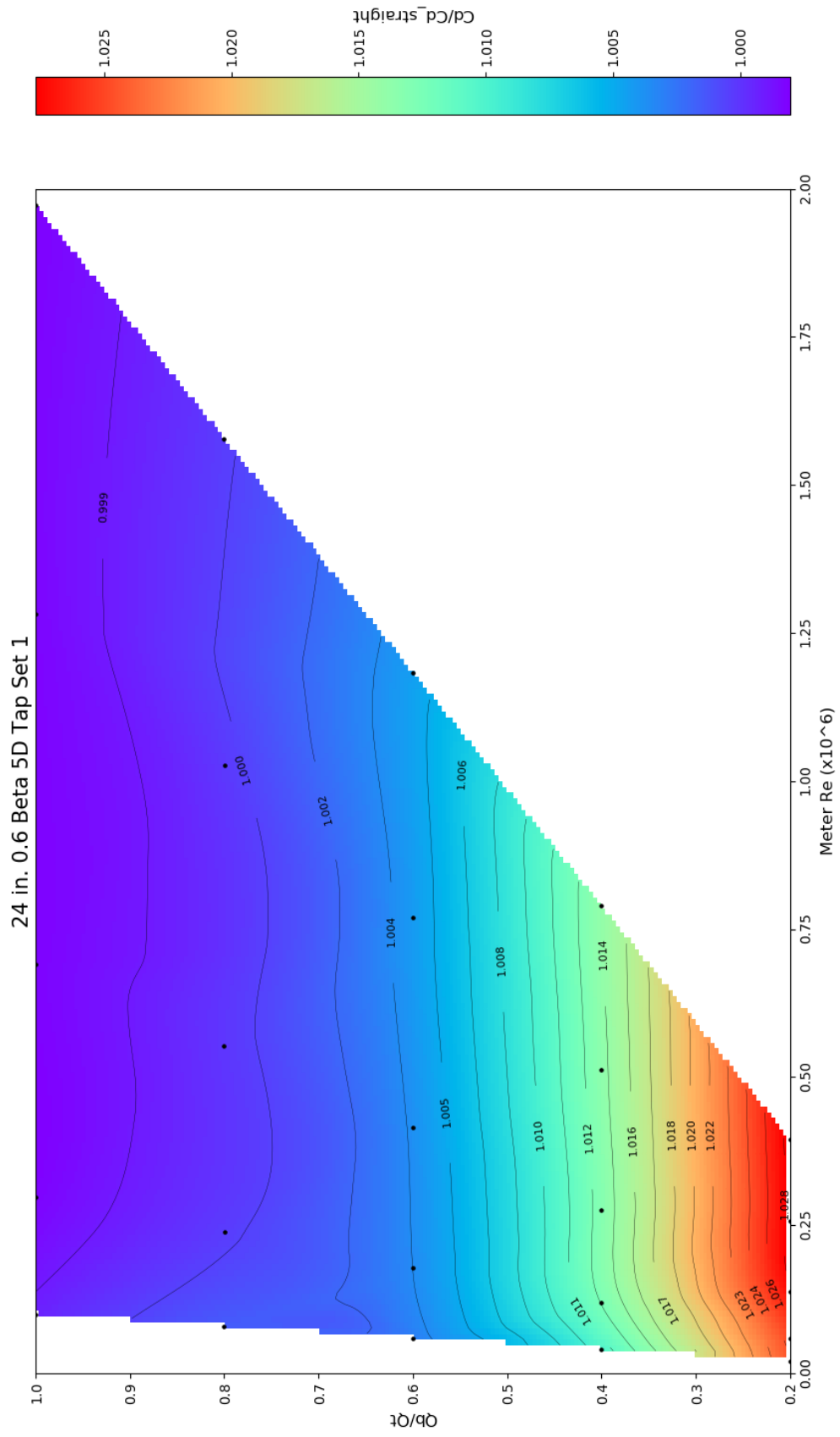


Figure A20. Contour plot for Tap Set 1 of the CFD 24-in. 0.6 beta ratio 5D installation.

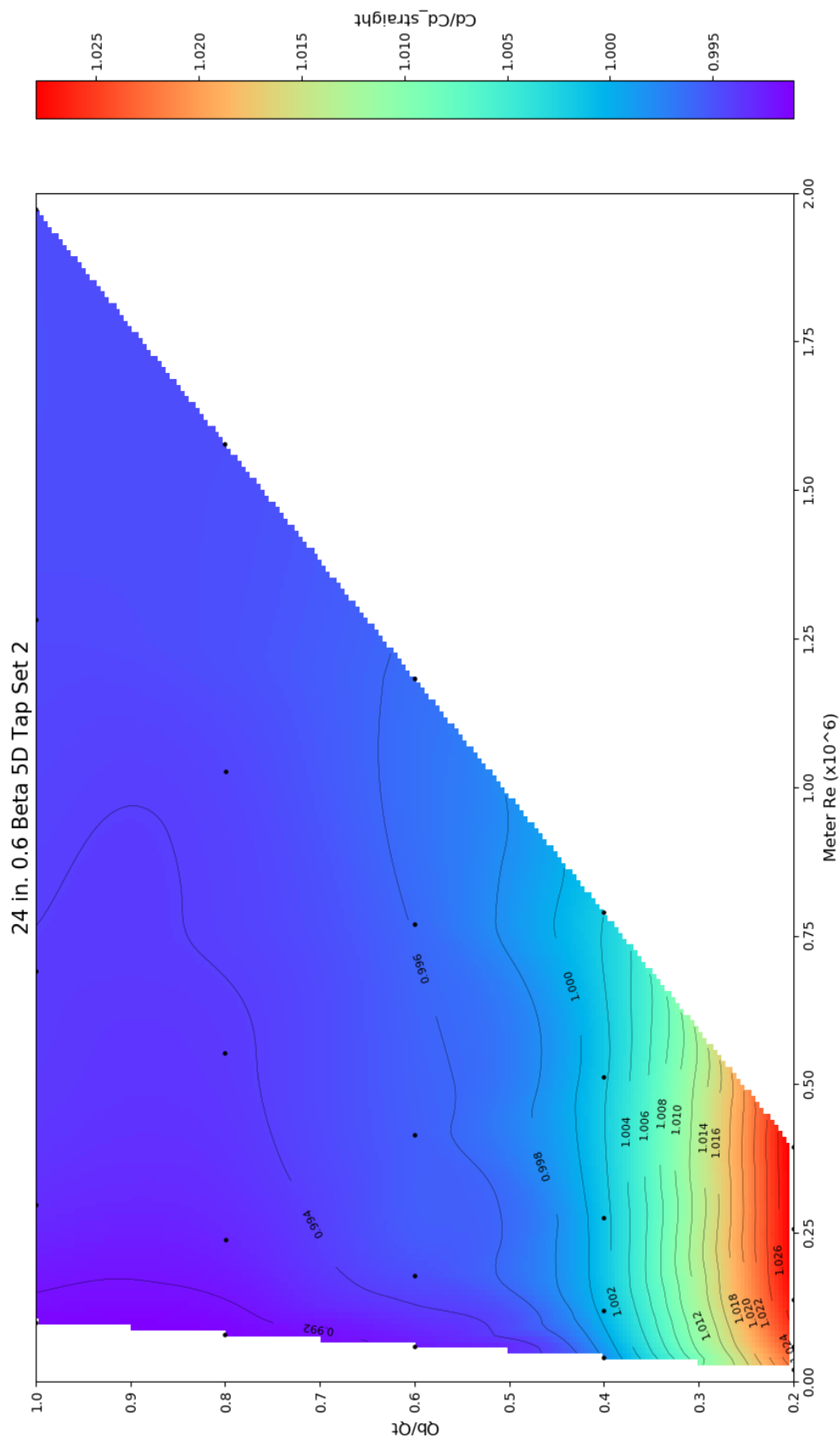


Figure A21. Contour plot for Tap Set 2 of the CFD 24-in. 0.6 beta ratio 5D installation.

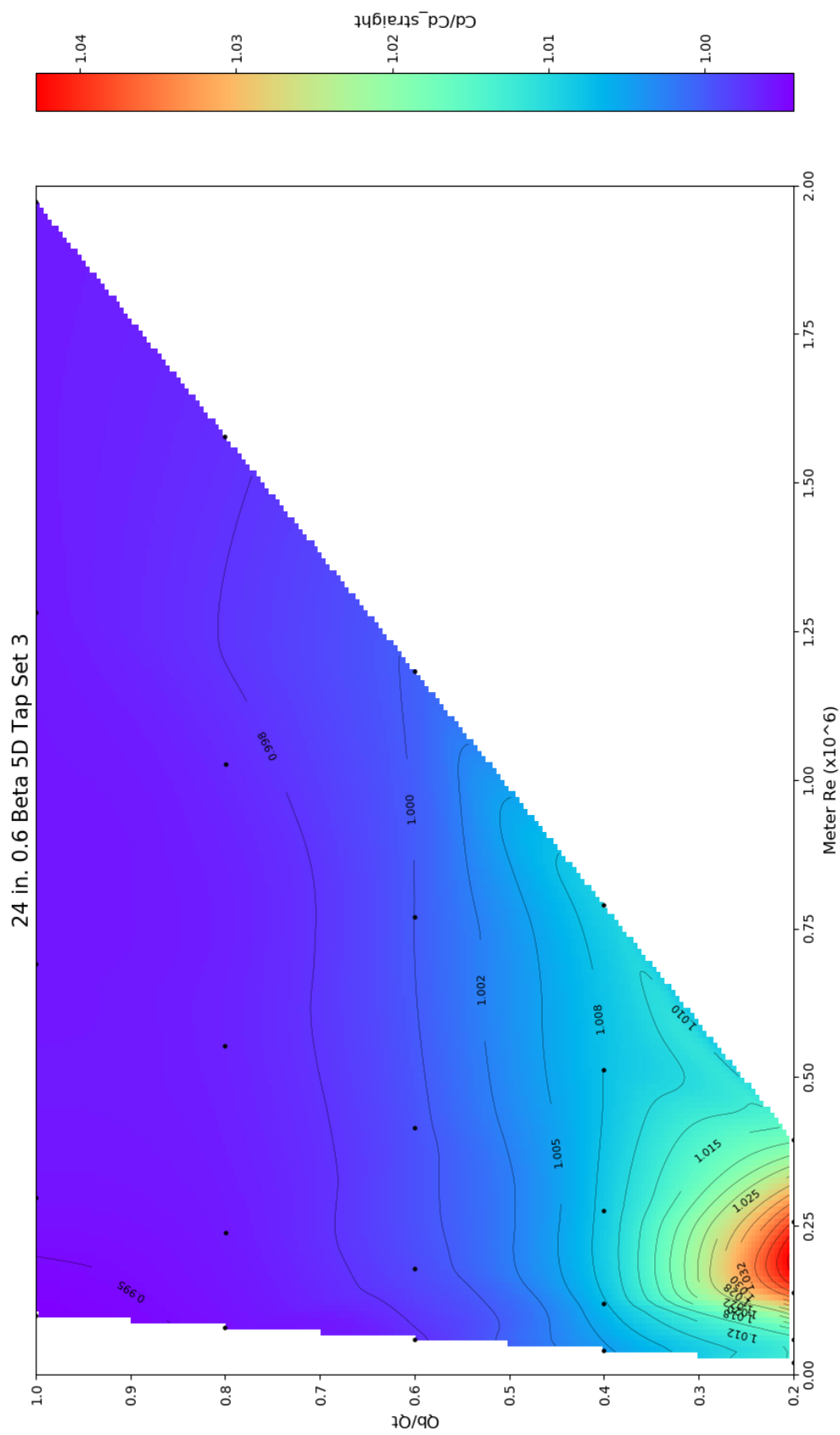


Figure A22. Contour plot for Tap Set 3 of the CFD 24-in. 0.6 beta ratio 5D installation.

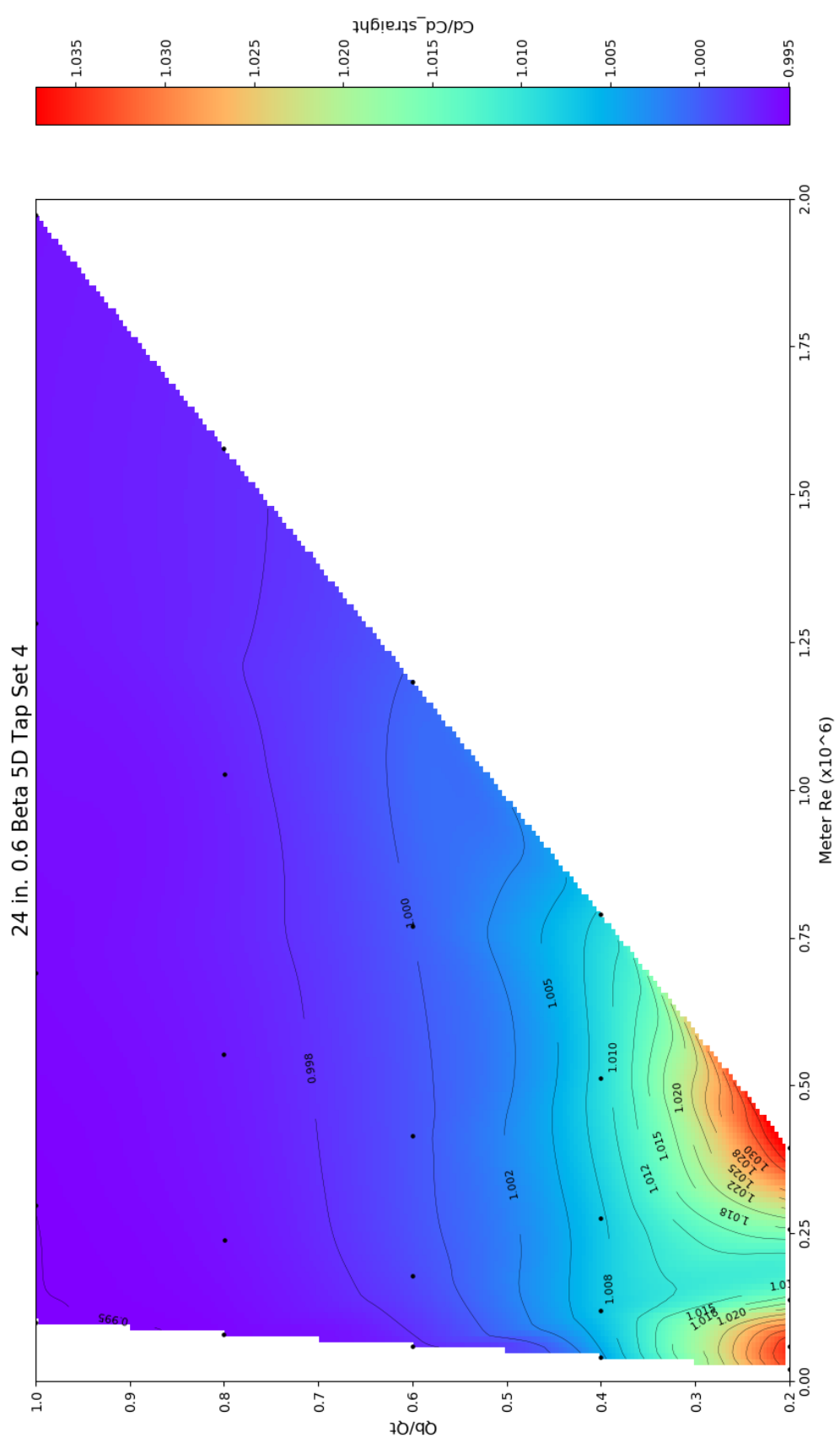


Figure A23. Contour plot for Tap Set 4 of the CFD 24-in. 0.6 beta ratio 5D installation.

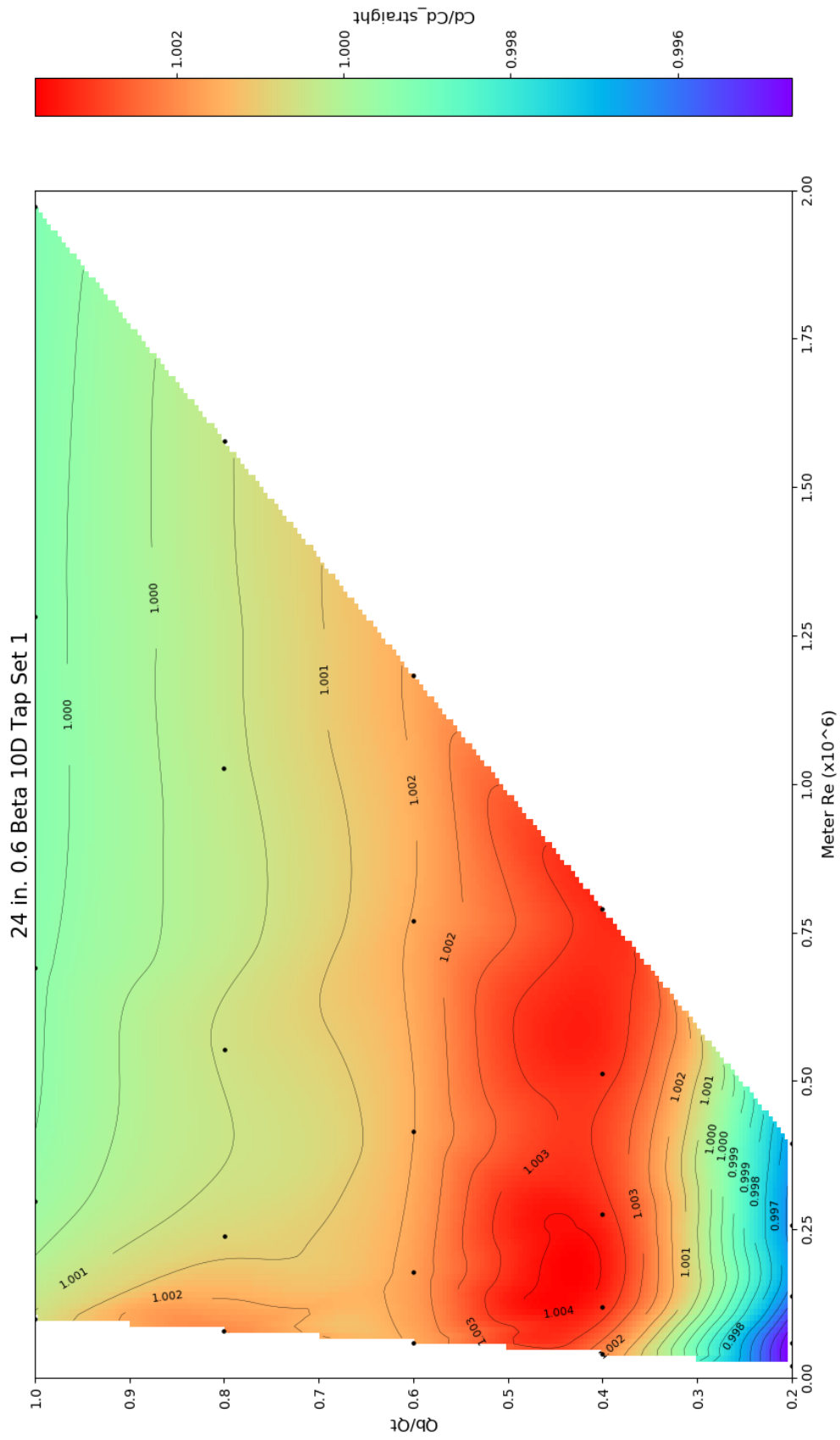


Figure A24. Contour plot for Tap Set 1 of the CFD 24-in. 0.6 beta ratio 10D installation.

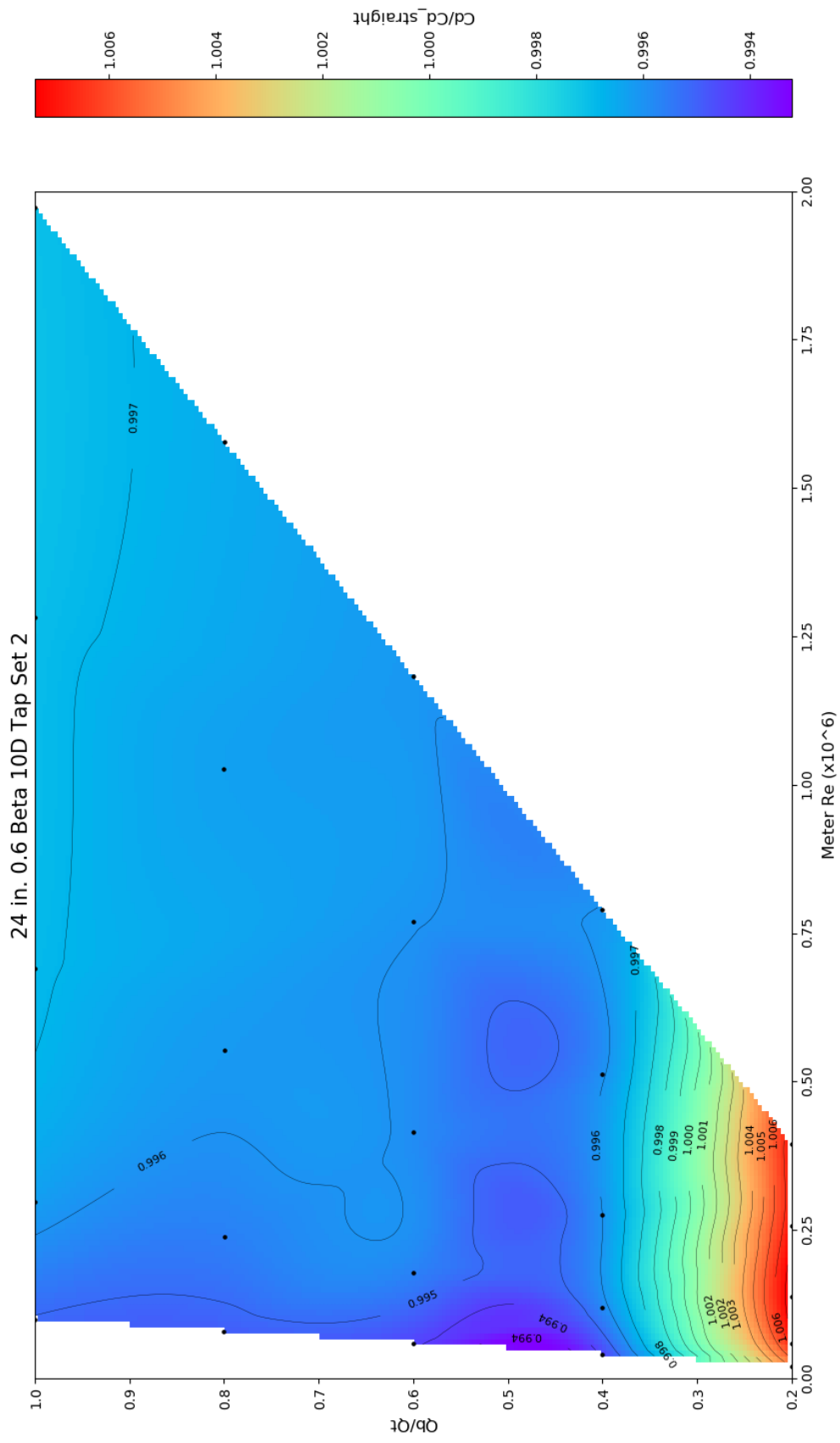


Figure A25. Contour plot for Tap Set 2 of the CFD 24-in. 0.6 beta ratio 10D installation.

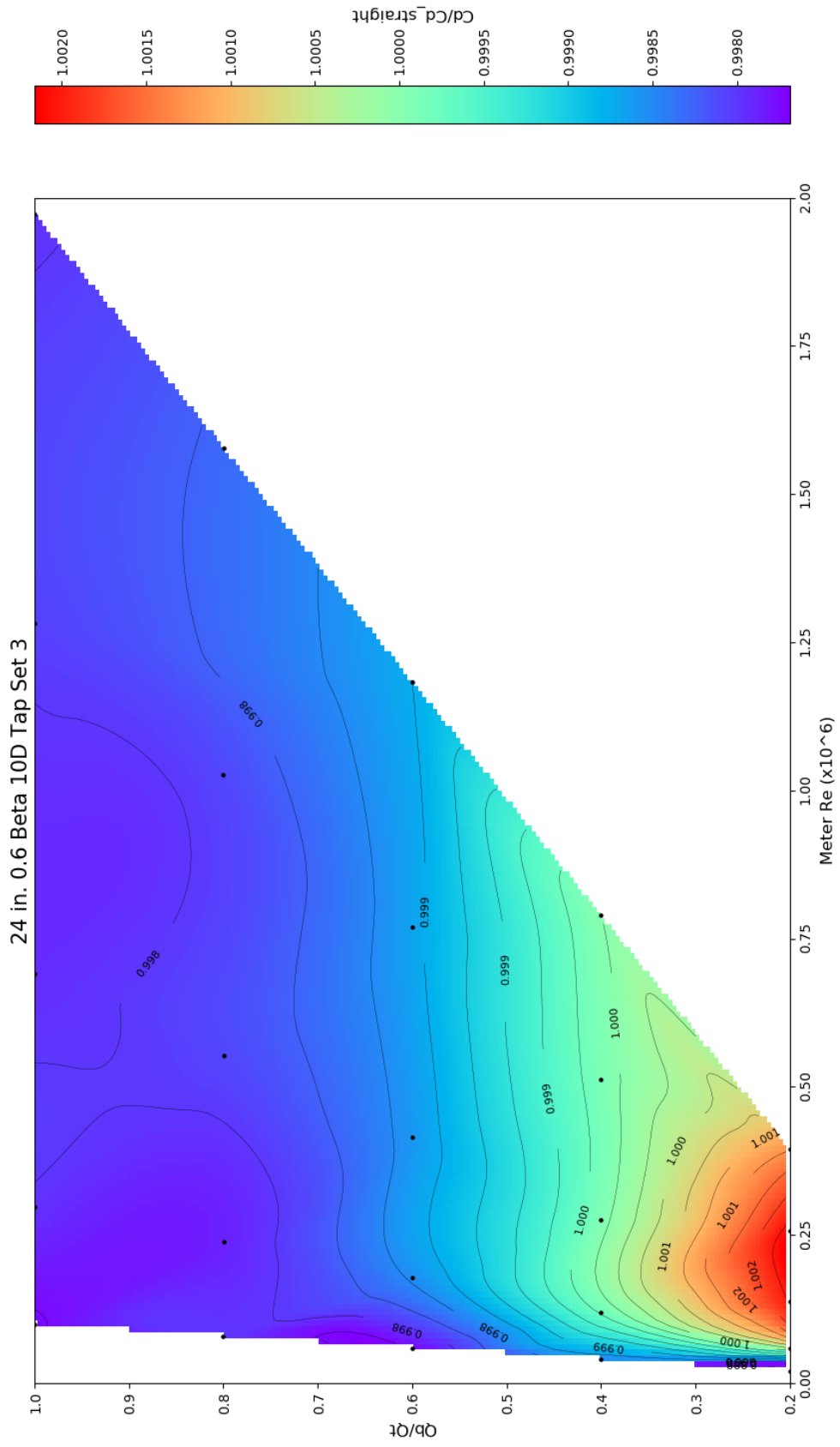


Figure A26. Contour plot for Tap Set 3 of the CFD 24-in. 0.6 beta ratio 10D installation.

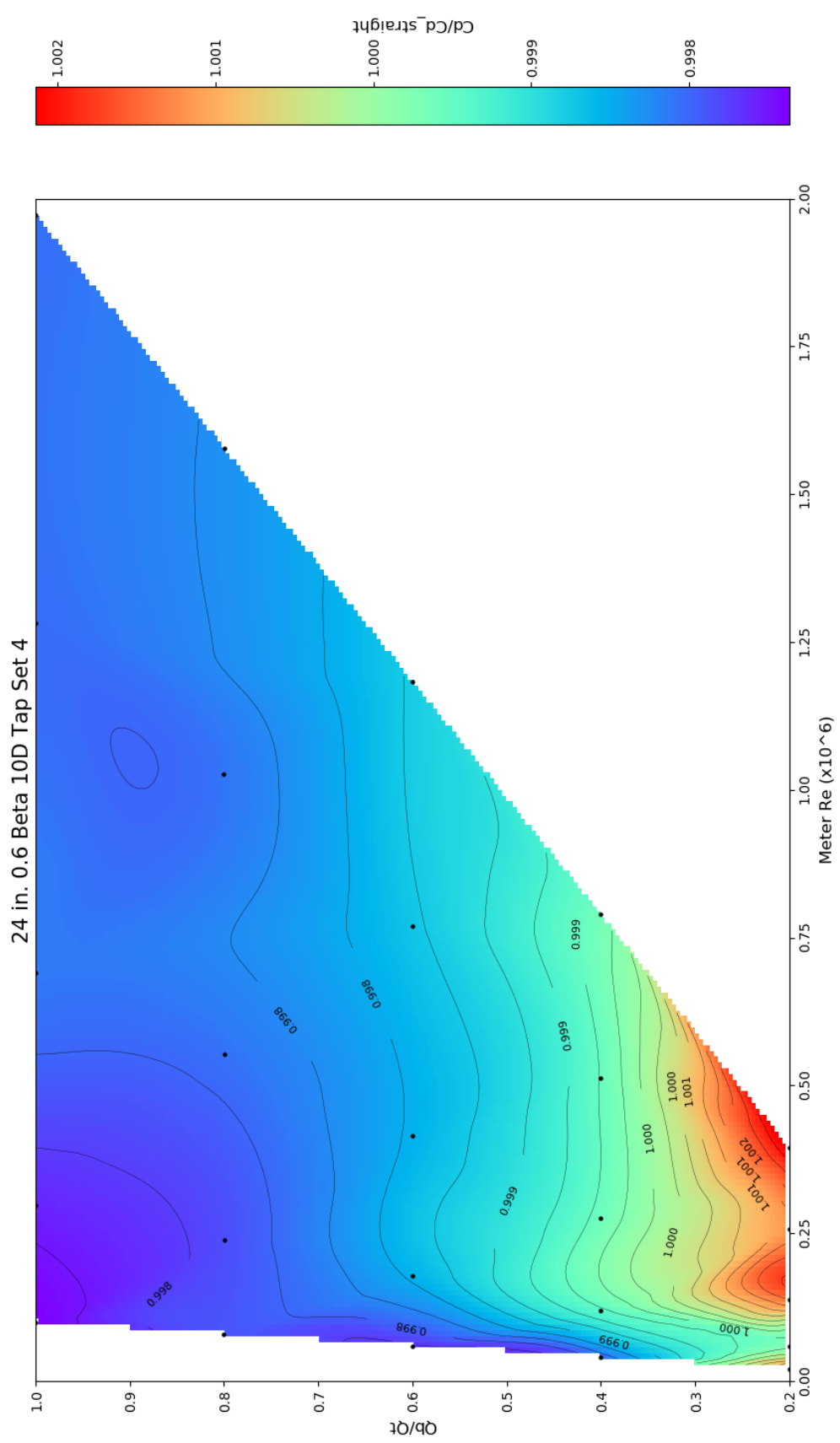


Figure A27. Contour plot for Tap Set 4 of the CFD 24-in. 0.6 beta ratio 10D installation.

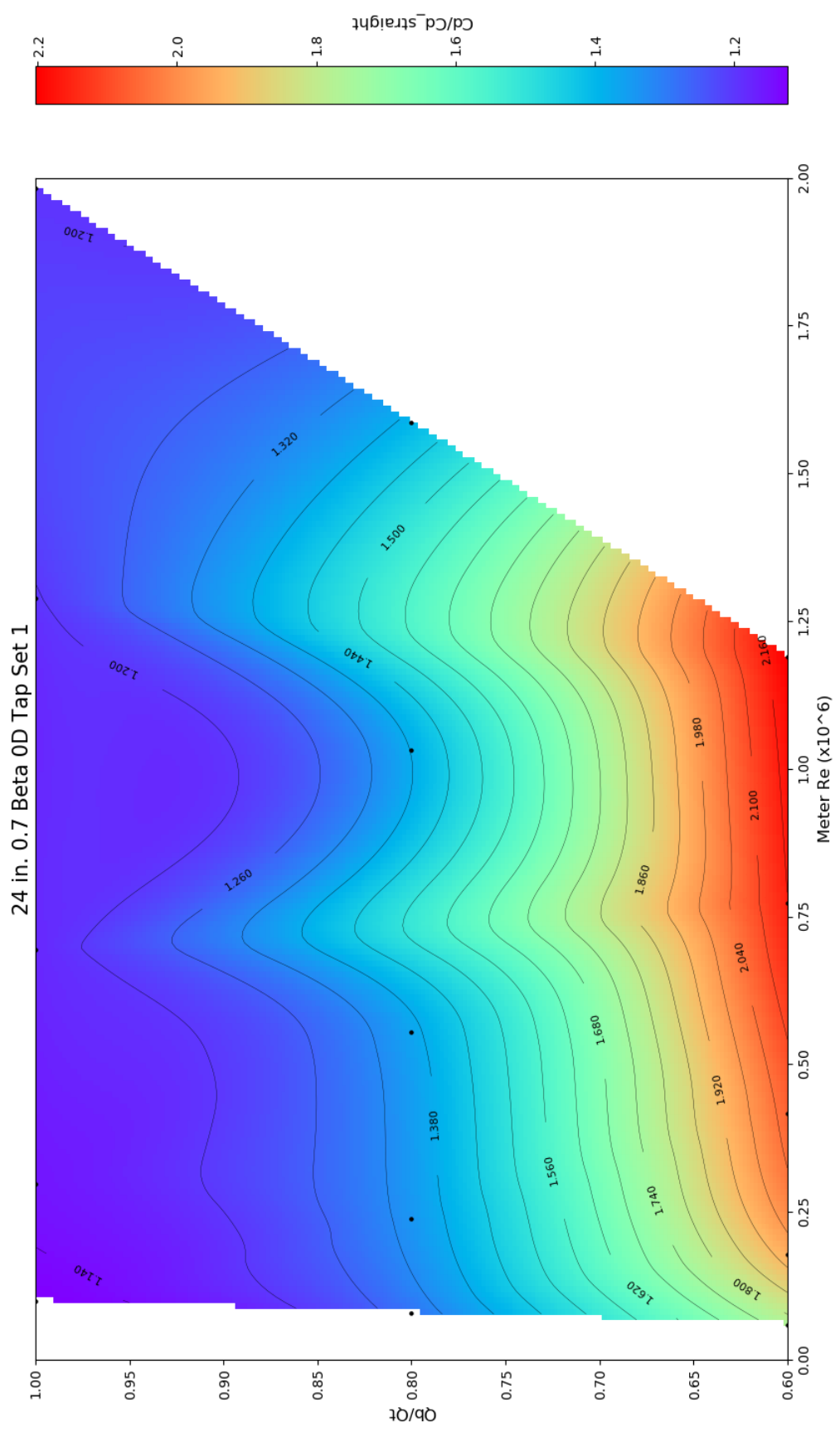


Figure A28. Contour plot for Tap Set 1 of the CFD 24-in. 0.7 beta ratio OD installation without 40% or 20% flow split data.

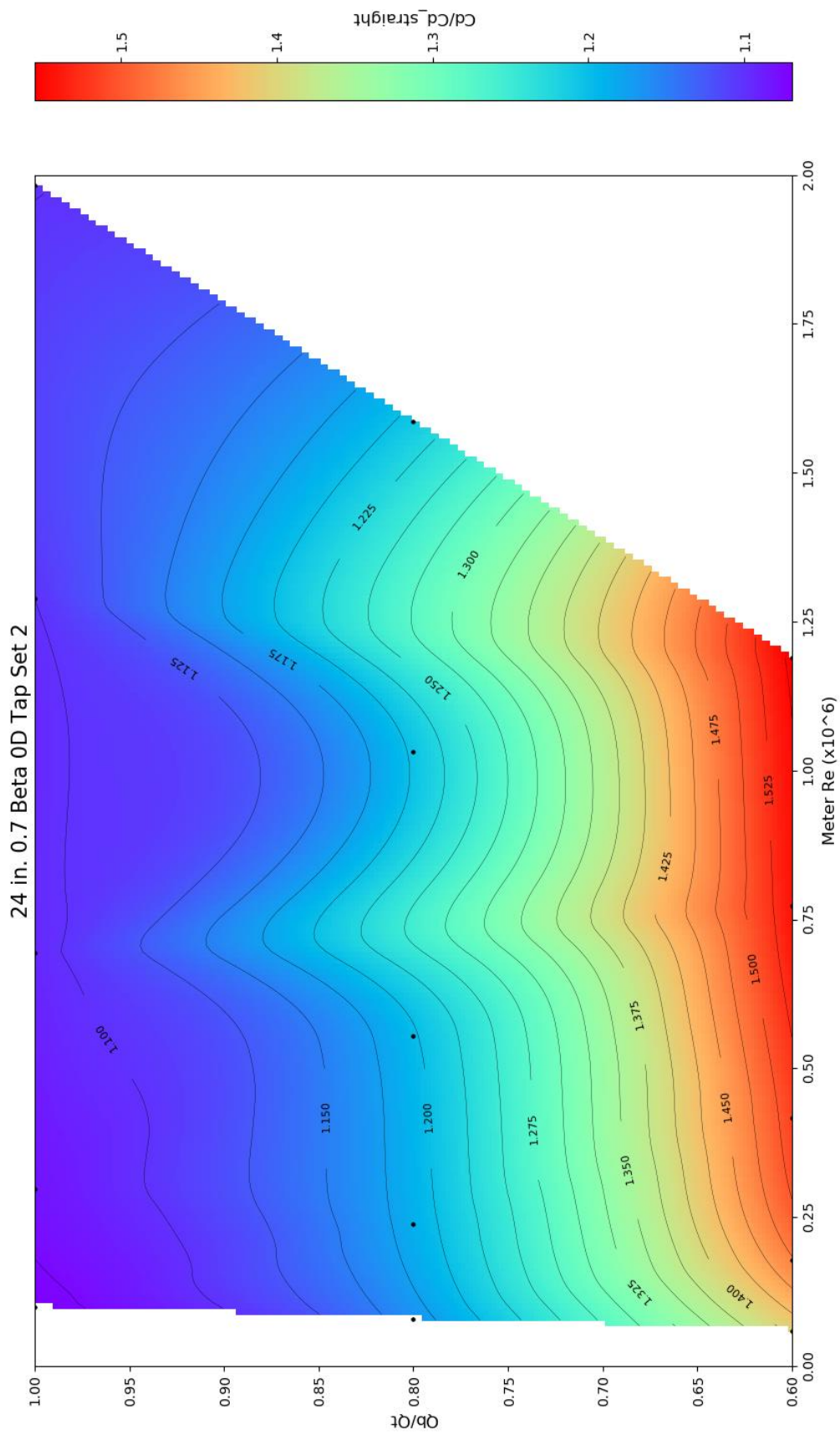


Figure A29. Contour plot for Tap Set 2 of the CFD 24-in. 0.7 beta ratio OD installation without 40% or 20% flow split data.

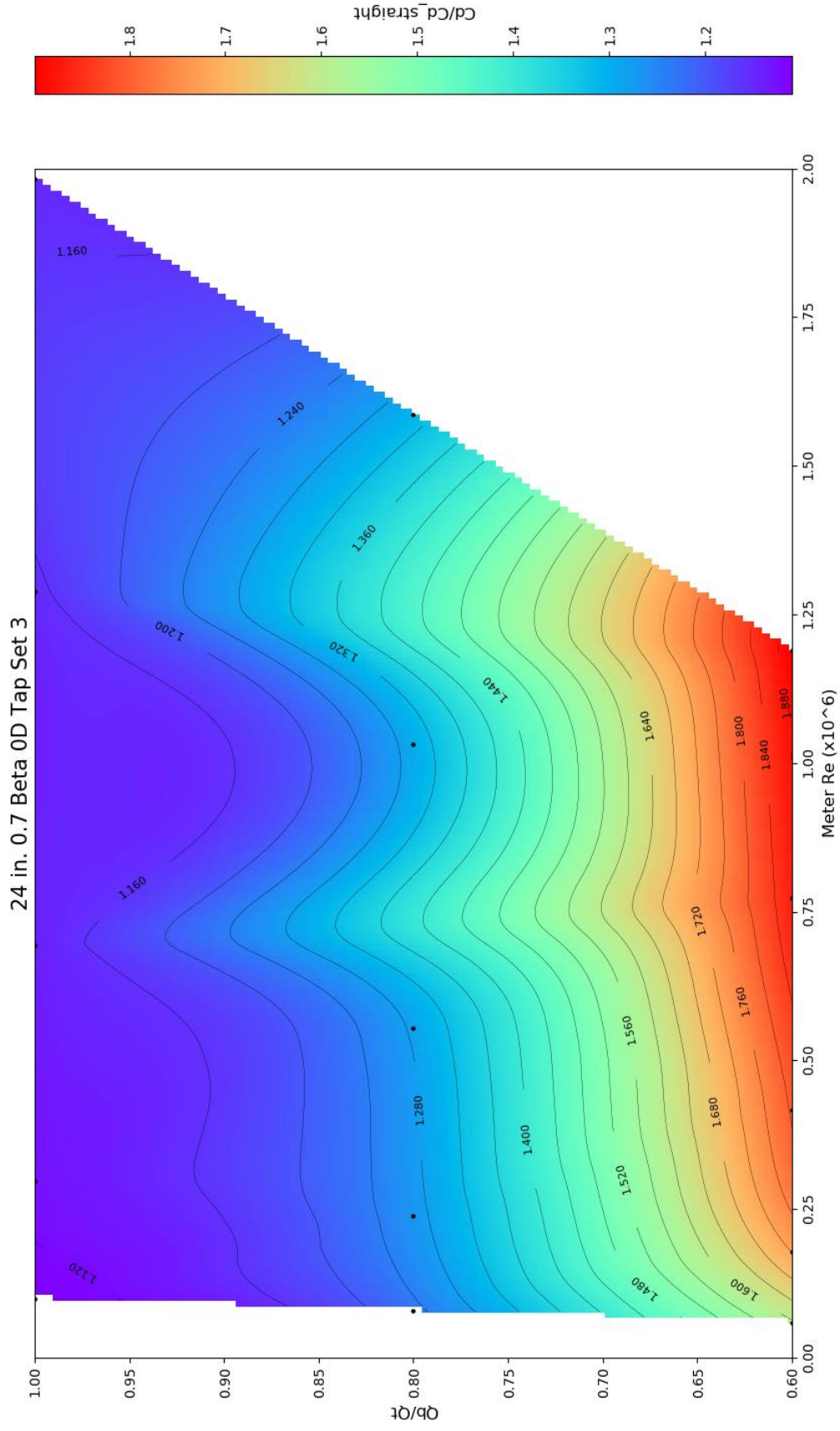


Figure A30. Contour plot for Tap Set 3 of the CFD 24-in. 0.7 beta ratio OD installation without 40% or 20% flow split data.

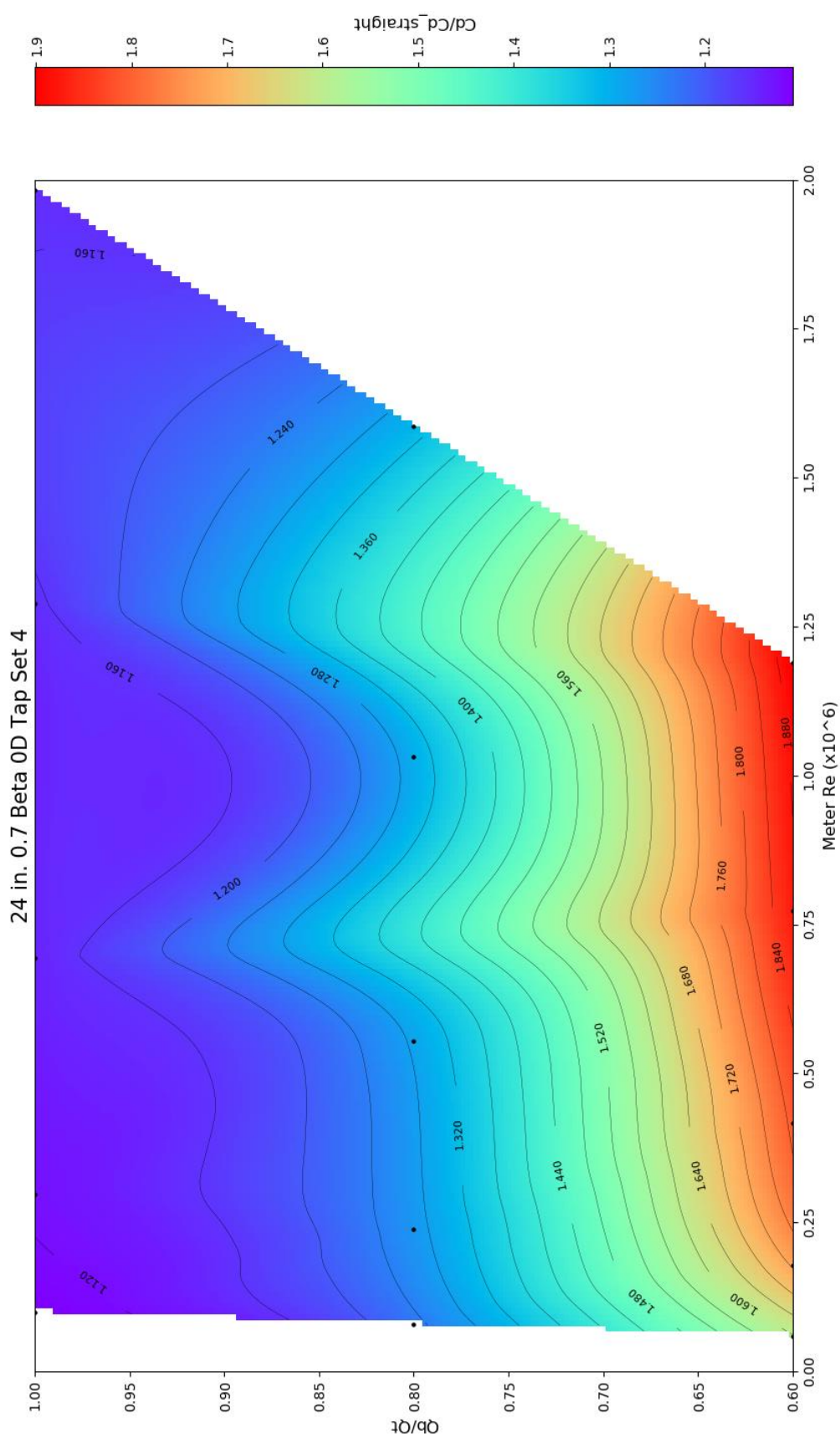


Figure A31. Contour plot for Tap Set 4 of the CFD 24-in. 0.7 beta ratio OD installation without 40% or 20% flow split data.

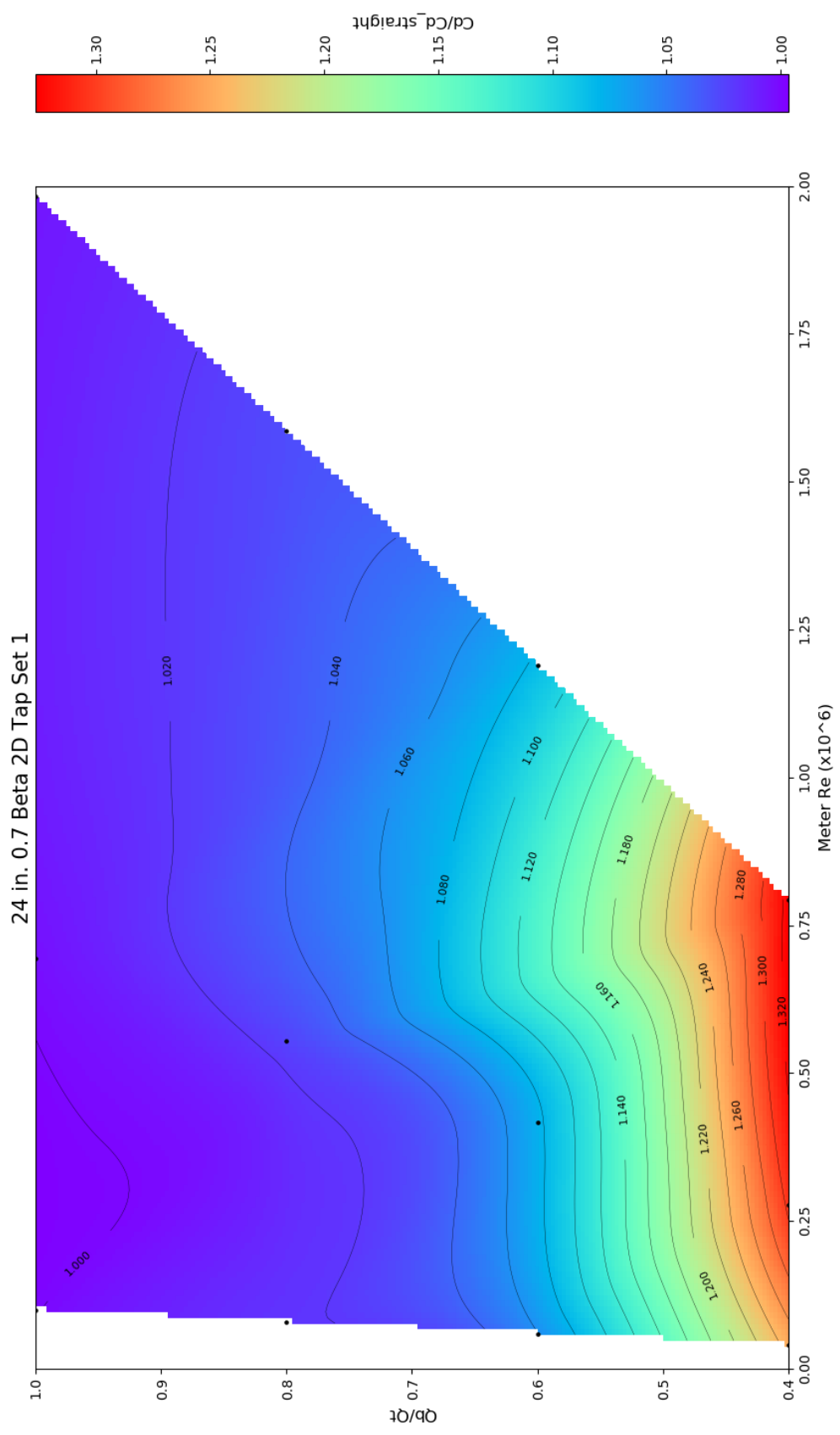


Figure A32. Contour plot for Tap Set 1 of the CFD 24-in. 0.7 beta ratio 2D installation without 20% flow split data.

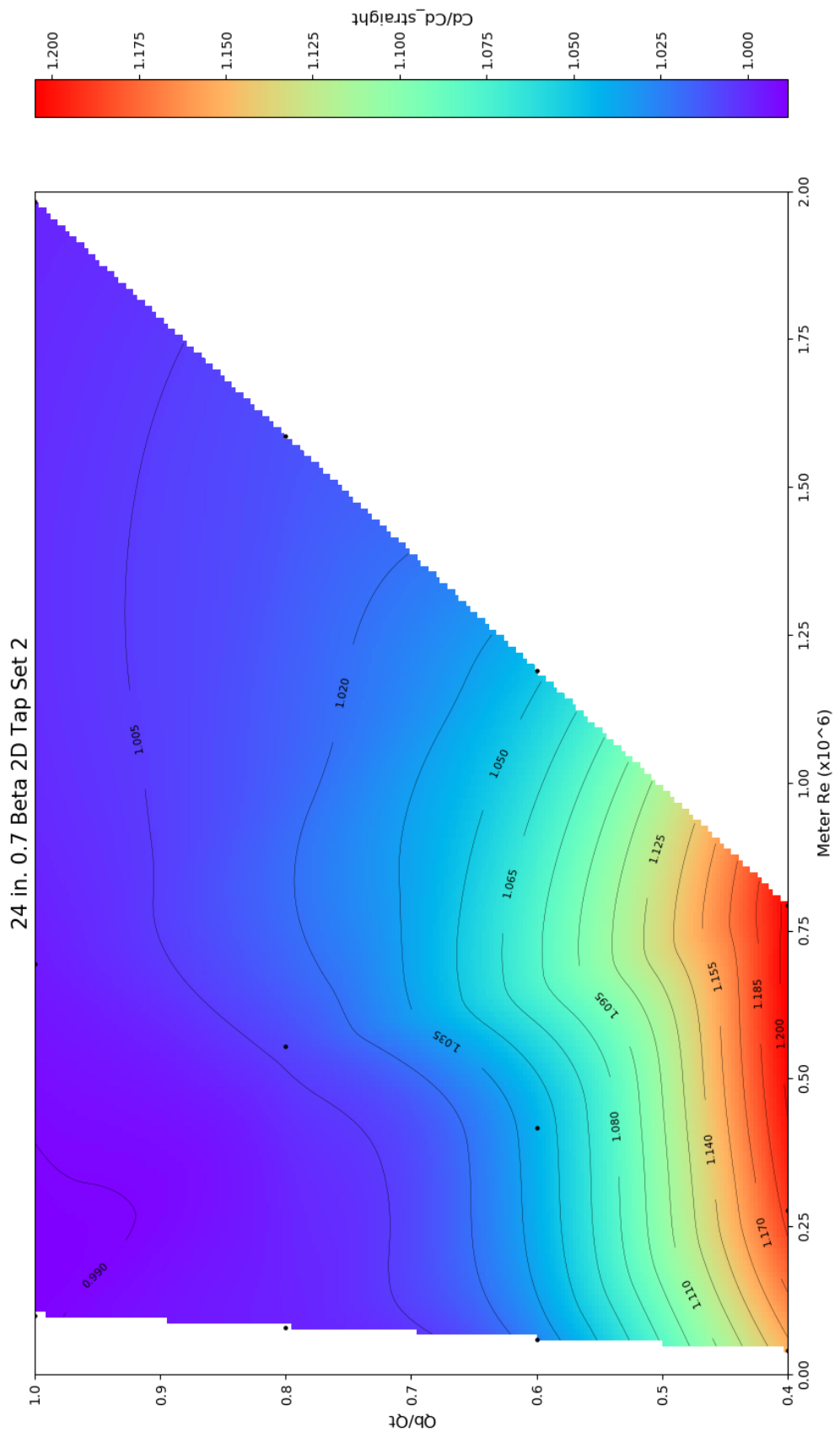


Figure A33. Contour plot for Tap Set 2 of the CFD 24-in. 0.7 beta ratio 2D installation without 20% flow split data.

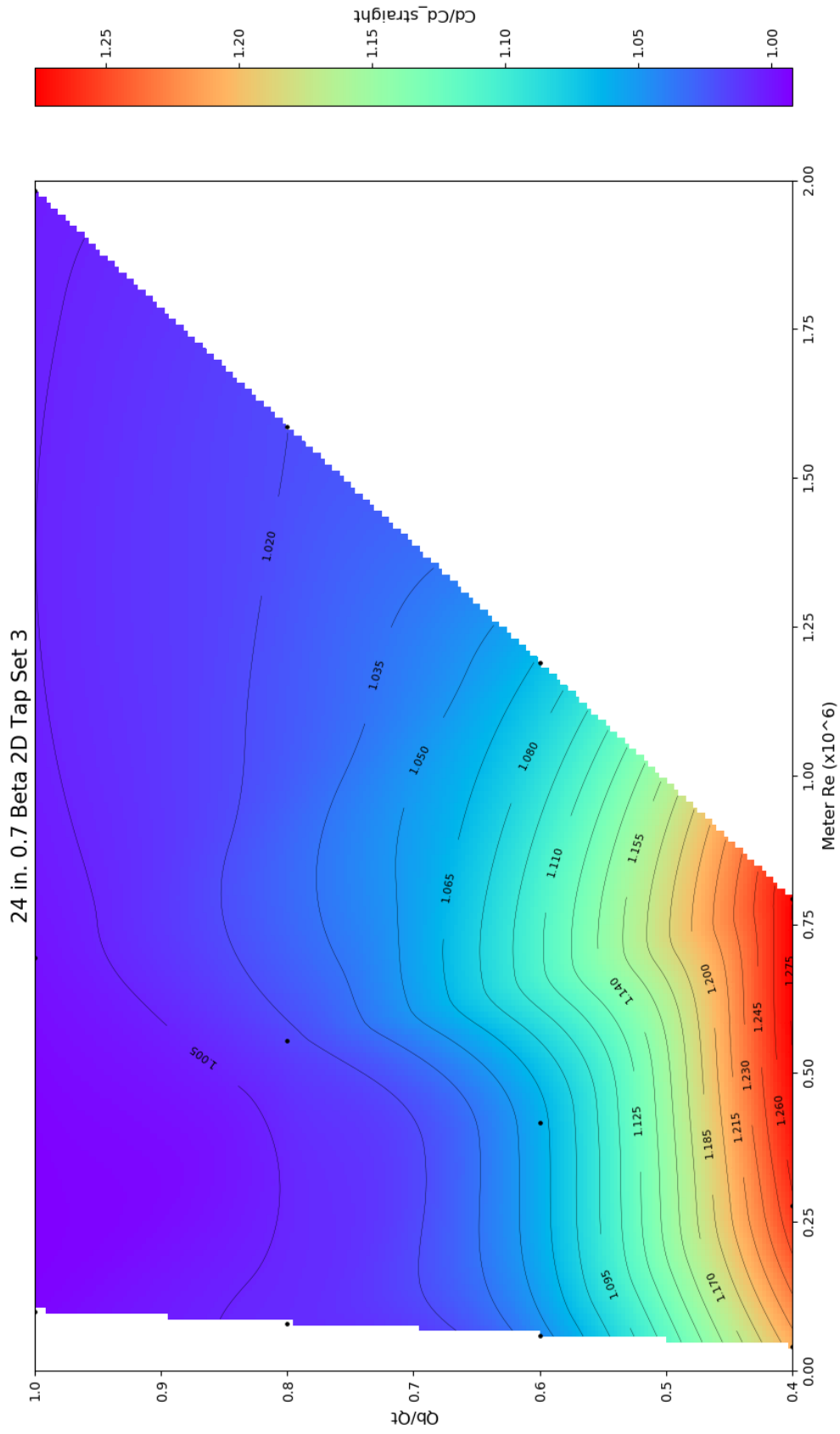


Figure A34. Contour plot for Tap Set 3 of the CFD 24-in. 0.7 beta ratio 2D installation without 20% flow split data.

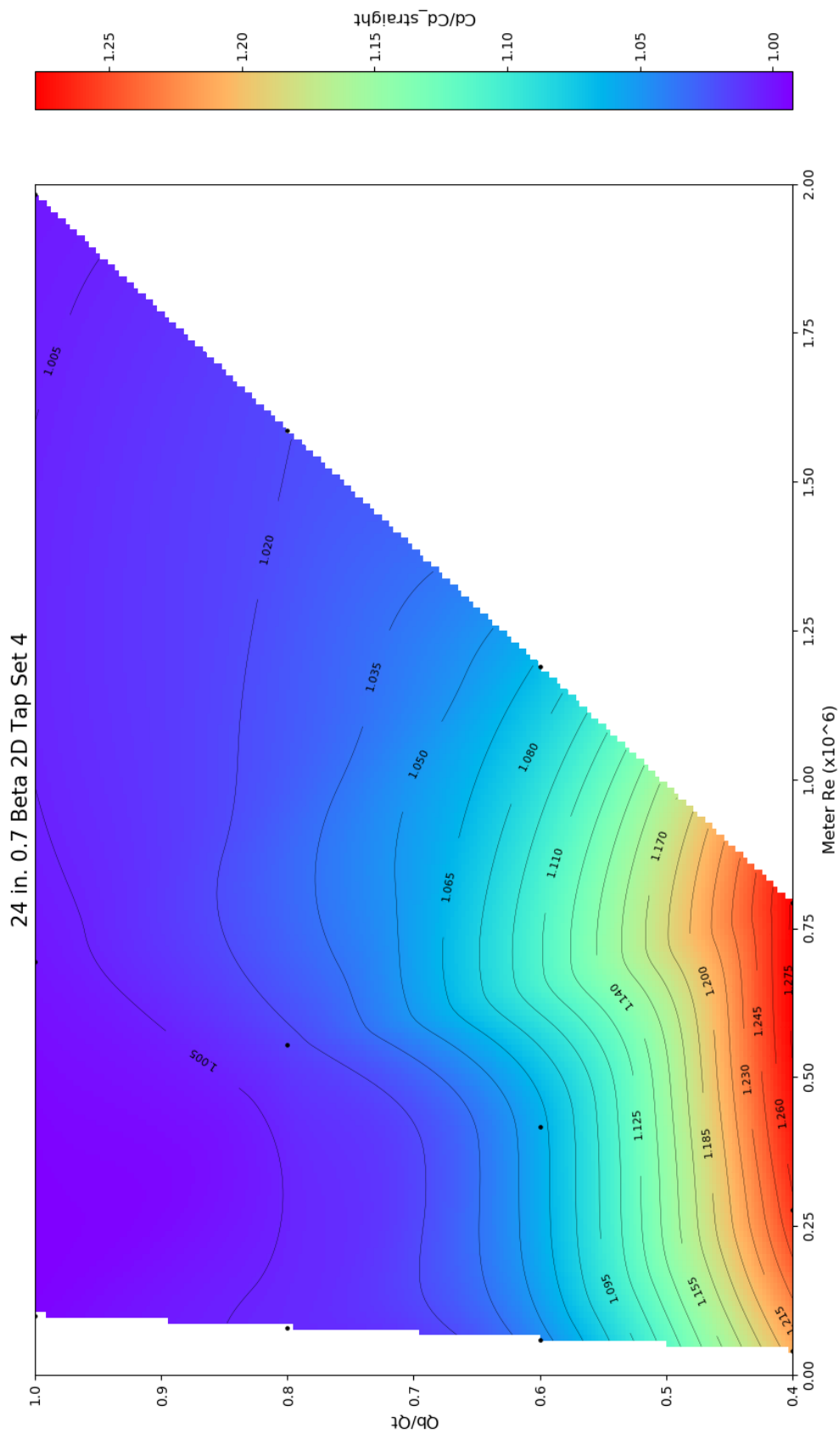


Figure A35. Contour plot for Tap Set 4 of the CFD 24-in. 0.7 beta ratio 2D installation without 20% flow split data.

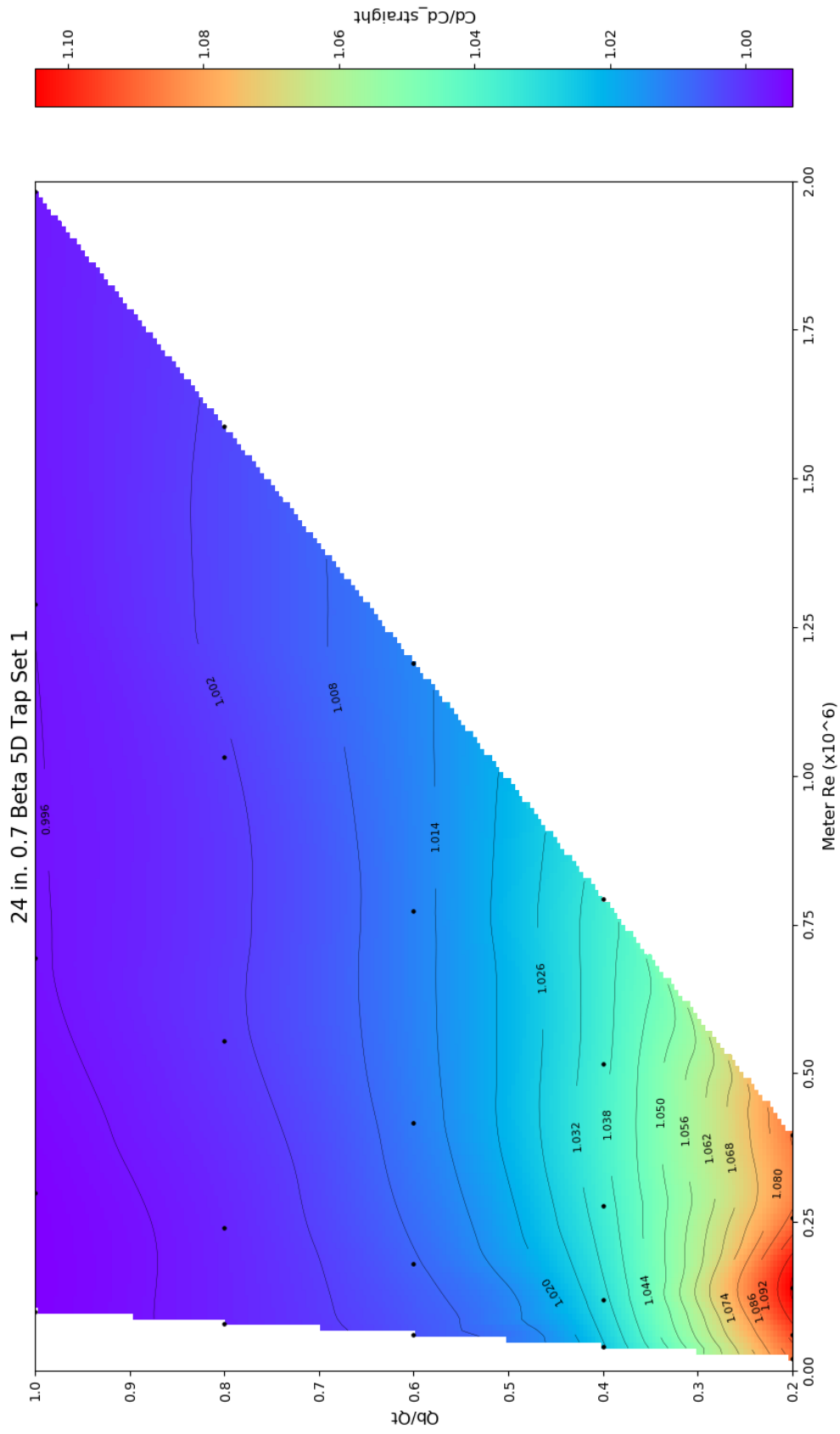


Figure A36. Contour plot for Tap Set 1 of the CFD 24-in. 0.7 beta ratio 5D installation.

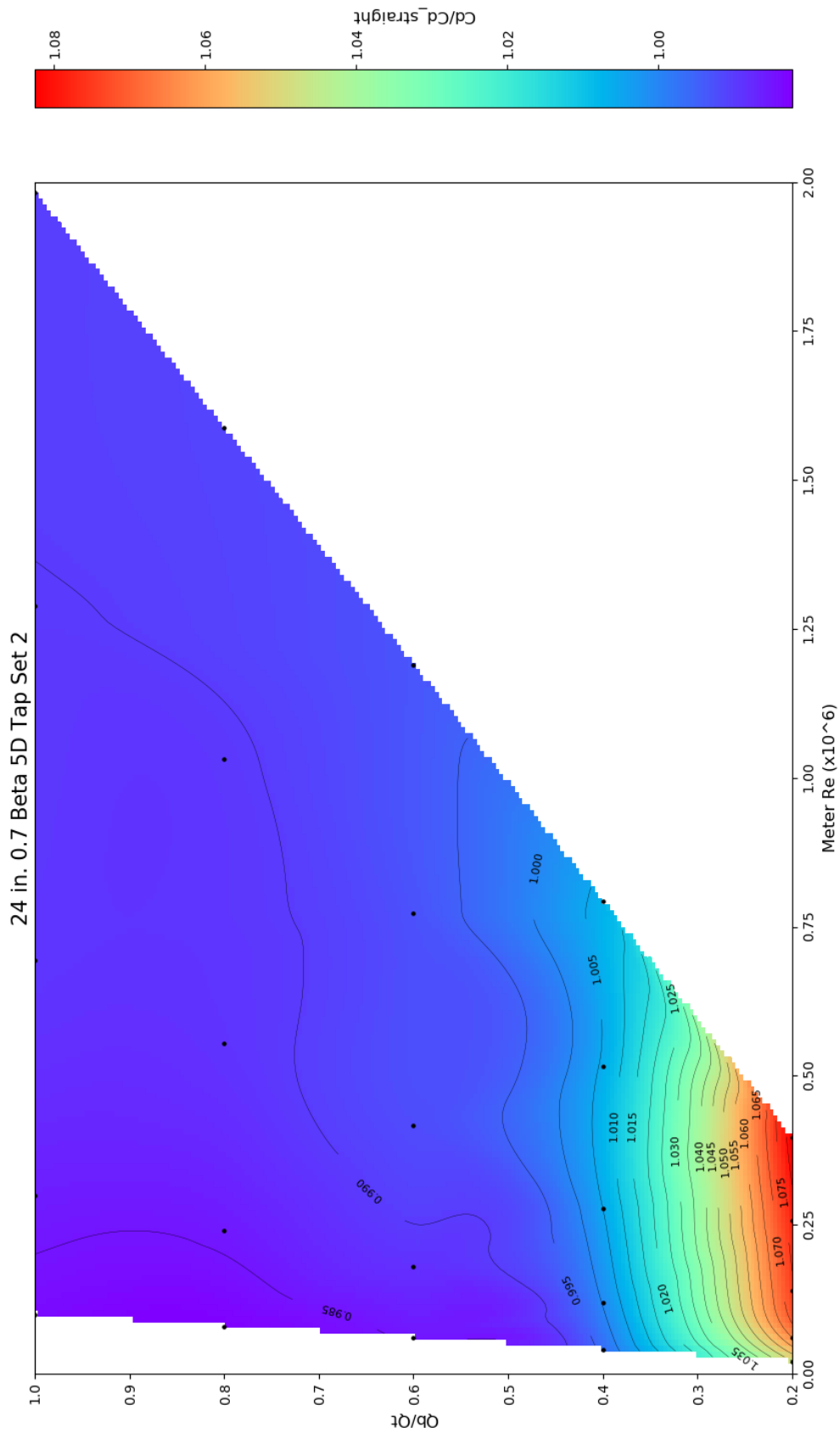


Figure A37. Contour plot for Tap Set 2 of the CFD 24-in. 0.7 beta ratio 5D installation.

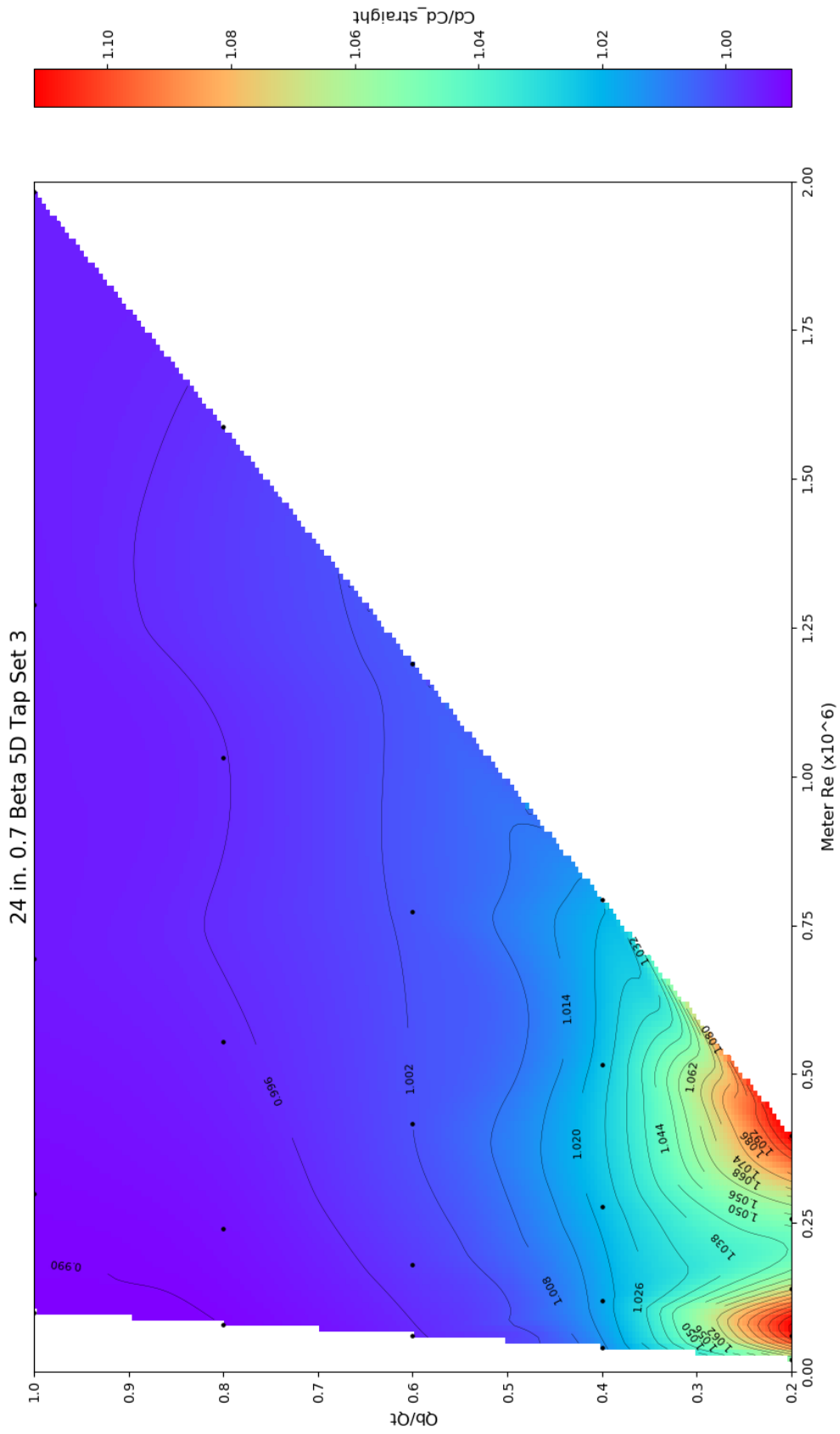


Figure A38. Contour plot for Tap Set 3 of the CFD 24-in. 0.7 beta ratio 5D installation.

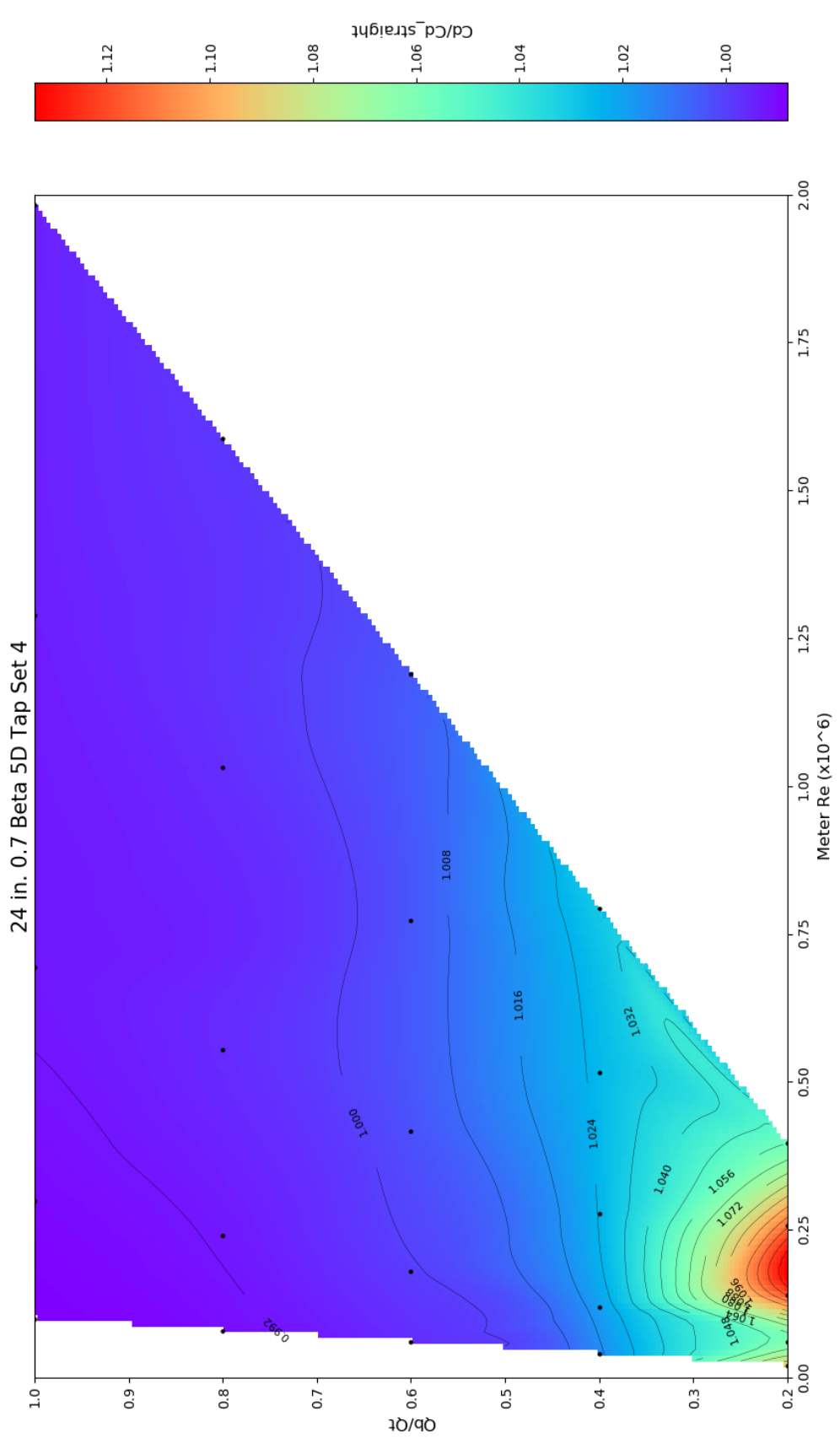


Figure A39. Contour plot for Tap Set 4 of the CFD 24-in. 0.7 beta ratio 5D installation.

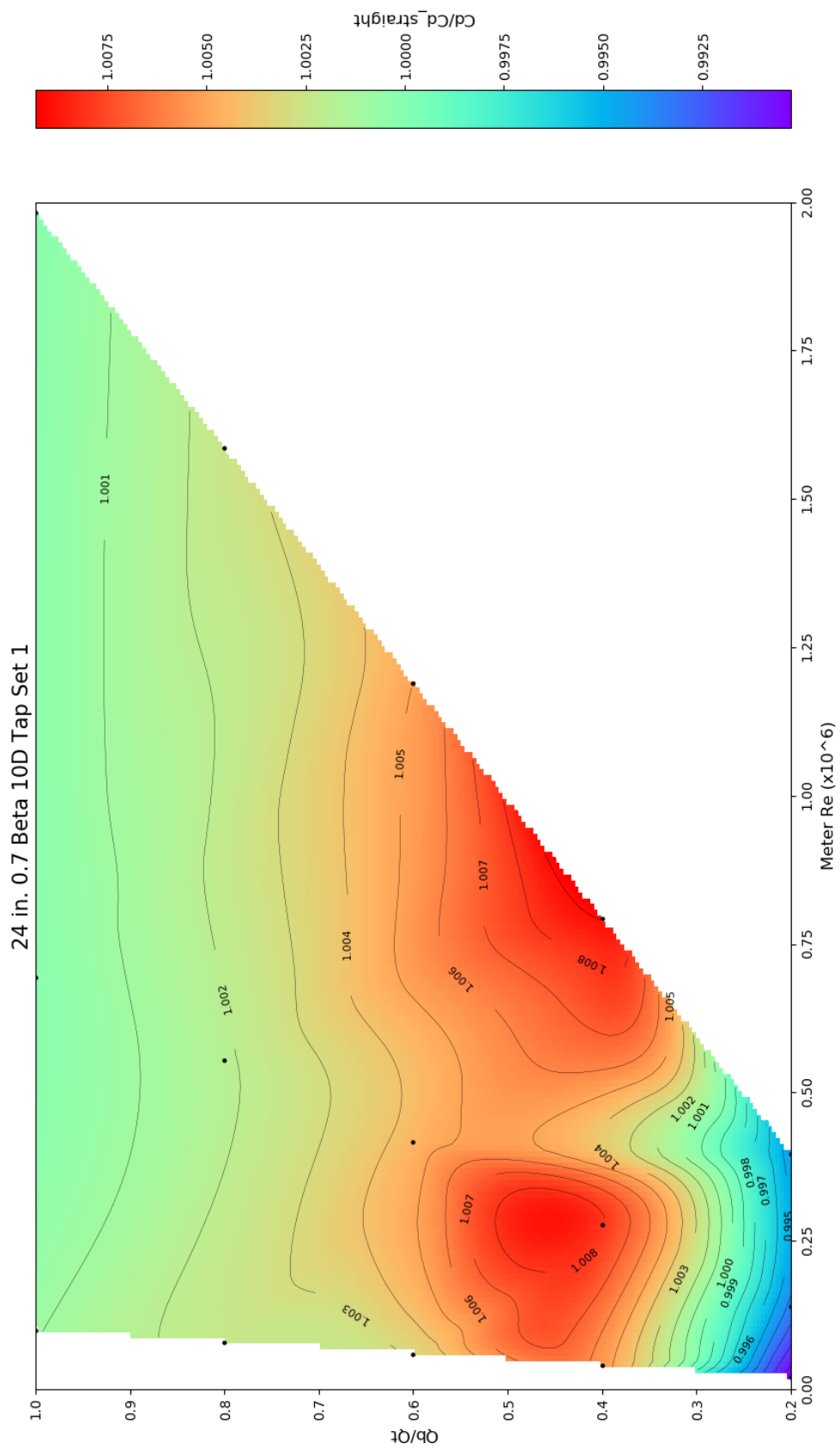


Figure A40. Contour plot for Tap Set 1 of the CFD 24-in. 0.7 beta ratio 10D installation.

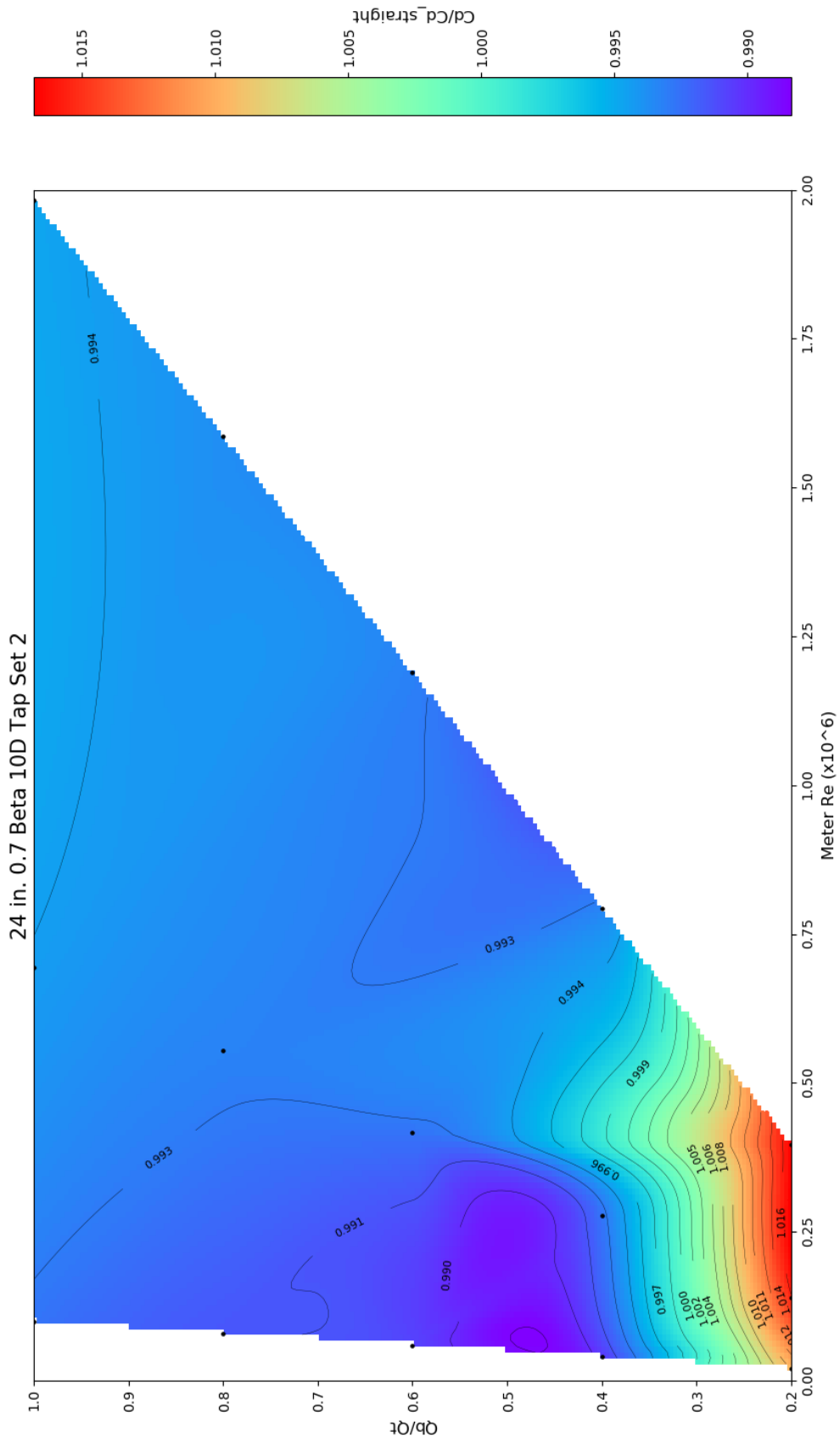


Figure A41. Contour plot for Tap Set 2 of the CFD 24-in. 0.7 beta ratio 10D installation.

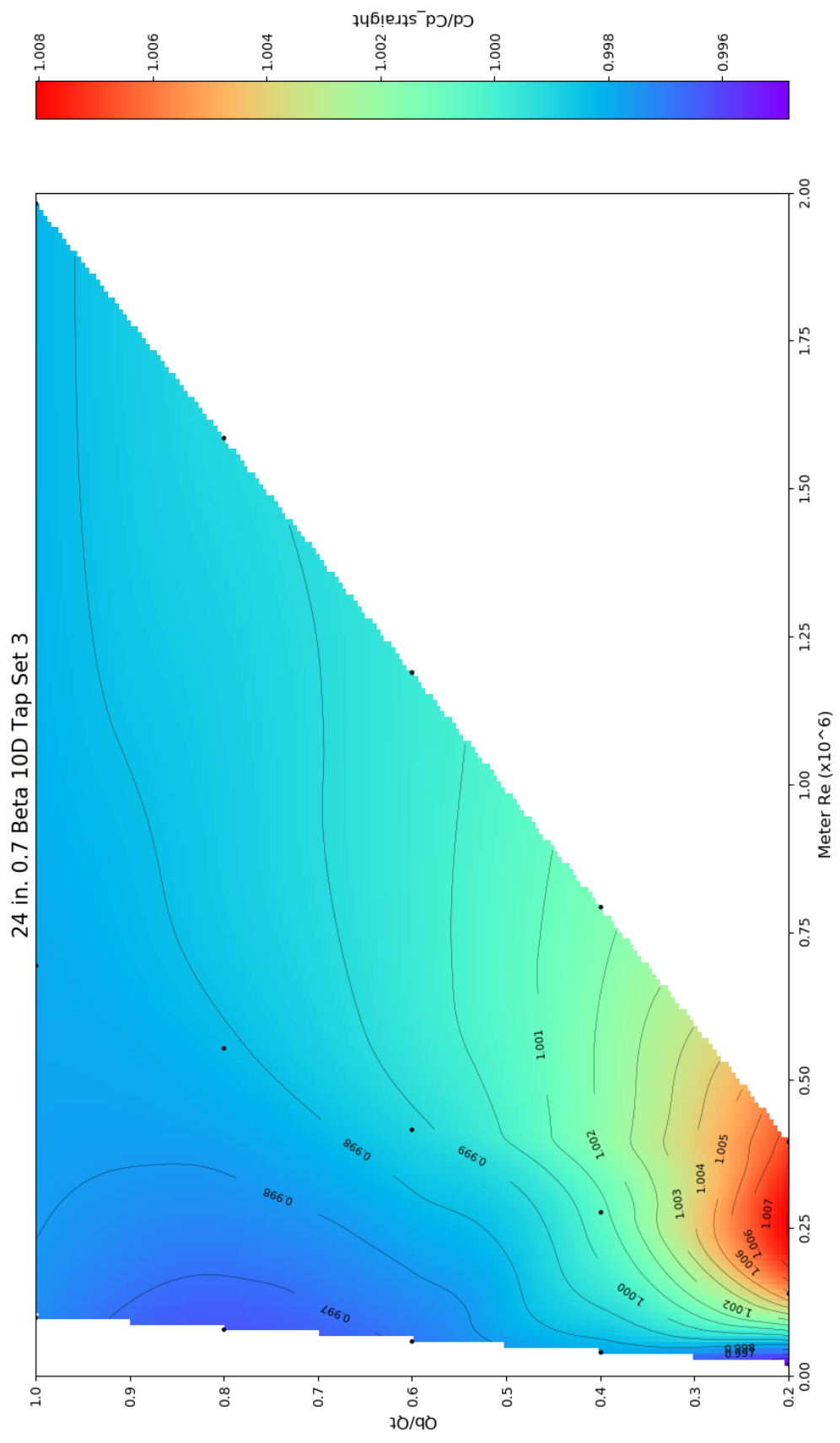


Figure A42. Contour plot for Tap Set 3 of the CFD 24-in. 0.7 beta ratio 10D installation.

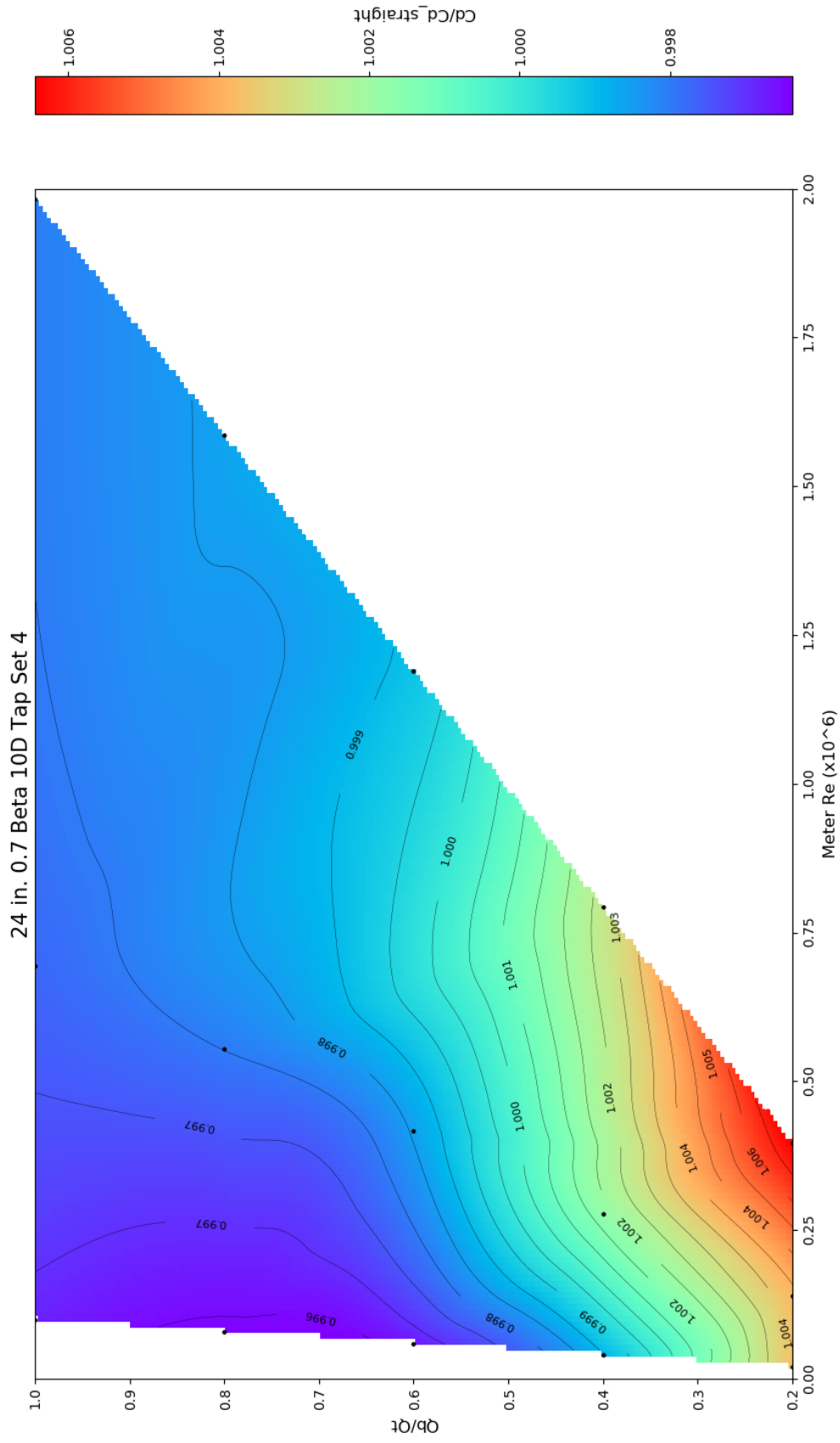


Figure A43. Contour plot for Tap Set 4 of the CFD 24-in. 0.7 beta ratio 10D installation.

APPENDIX B

METHOD FOR DETERMINING GRID INDEPENDENCE

When modeling using CFD, it is important that the mesh base size, hereafter referred to interchangeably as base size or grid, is an appropriate size to minimize simulation run time while producing an answer, like discharge coefficient, that is grid-independent. To find an appropriate base size for the 6- and 24-in. pipe sizes “The Grid Convergence Method” (ASME 2008a) or GCI was used. ASME (2008a) explains that discretization error is estimated by running the same simulation at three different base sizes that are approximately a ratio of 1.3, or more, greater than the finer base size. With this ratio between the three base sizes, the simulation is run and the desired result, such as the discharge coefficient, is input into the GCI as φ_1 , φ_2 , and φ_3 (1 representing the finest base size and 3 the coarsest base size). Next values ε_{32} and ε_{21} are calculated as the difference between the corresponding φ values indicated by the ε subscripts. The ε values are then used to determine a P value that then is used to extrapolate an answer and determine a GCI for the fine base size representing the uncertainty associated with that base size.

Applying the GCI process, 6-in. and 24-in. simulations were run to evaluate grid independence. For the 6-in. base sizes of 0.18, 0.25, 0.35, and 0.49 inches with 40% of the base size volumetric controls in the tee and through the Venturi were used. In STAR-CCM+, volumetric controls are shapes placed in the test geometry where the mesh base size can be larger or smaller, as controlled by a specified base size or percentage of the main base size used for the rest of the geometry. Mesh refinement in challenging areas

produces a better numerical solution of the governing equations because of the high degree of associated turbulence. Because of the volumetric control sections, especially in the Venturi, the GCI represents the uncertainty for the base sizes of 0.072, 0.1, 0.14, and 0.196 inches. Similarly, the same 40% of the base size volumetric control sections were used in the 24-in. pipe. So while the main base sizes were 1.05, 1.45, 2.00, and 2.8 inches, the GCI would be for the uncertainty of base sizes 0.42, 0.58, 0.8, and 1.12 inches.

However, the GCI paper states that: “It should be noted that if either ϵ_{32} and ϵ_{21} is ‘very close’ to zero, the above procedure [speaking of the procedure to calculate P] does not work” (ASME 2008a). After following the GCI procedure for the 6-in. and 24-in. pipe sizes, both sizes had ϵ values of approximately 0.002 or closer to zero. It was decided that 0.002 fits under the definition of “very close” to zero, as no absolute definition was provided in the GCI paper as to what “very close” to zero is defined as. Therefore, the GCI could not be confidently determined by use of the GCI method, because the answers at each base size were very close to each other. Therefore, I had to rely on judgment and laboratory data where possible to validate the CFD simulation.

To show that the model results were grid-independent, the simulations run before a GCI was considered (these simulations were run due to initial confusion about how to determine a grid converged base size) were compared with simulations run after GCI was considered. The simulations used in this comparison were the 0.6 beta 24-in. 2D, 5D, and 10D installations. The initial simulations used a base size of 2.0 inches without a volumetric control through the Venturi; while the later simulations used a base size of 2.0

inches with a volumetric control of 40% of the base size, or 0.8 inches, through the Venturi.

A side by side percent deviation calculation was done to see how the results differed. A histogram of the percent difference for the 2D set up resulted in the greatest percent difference (Figure B1). If the 20% and 40% flow splits are removed (Figure B2), then the percent difference is below 1%. For the other installations of 5D and 10D, only the 20% flow split needed to be dropped from the histograms to see that the percent difference is below 1% for all four tap sets, as can be seen in the histograms of Figure B3- Figure B14.

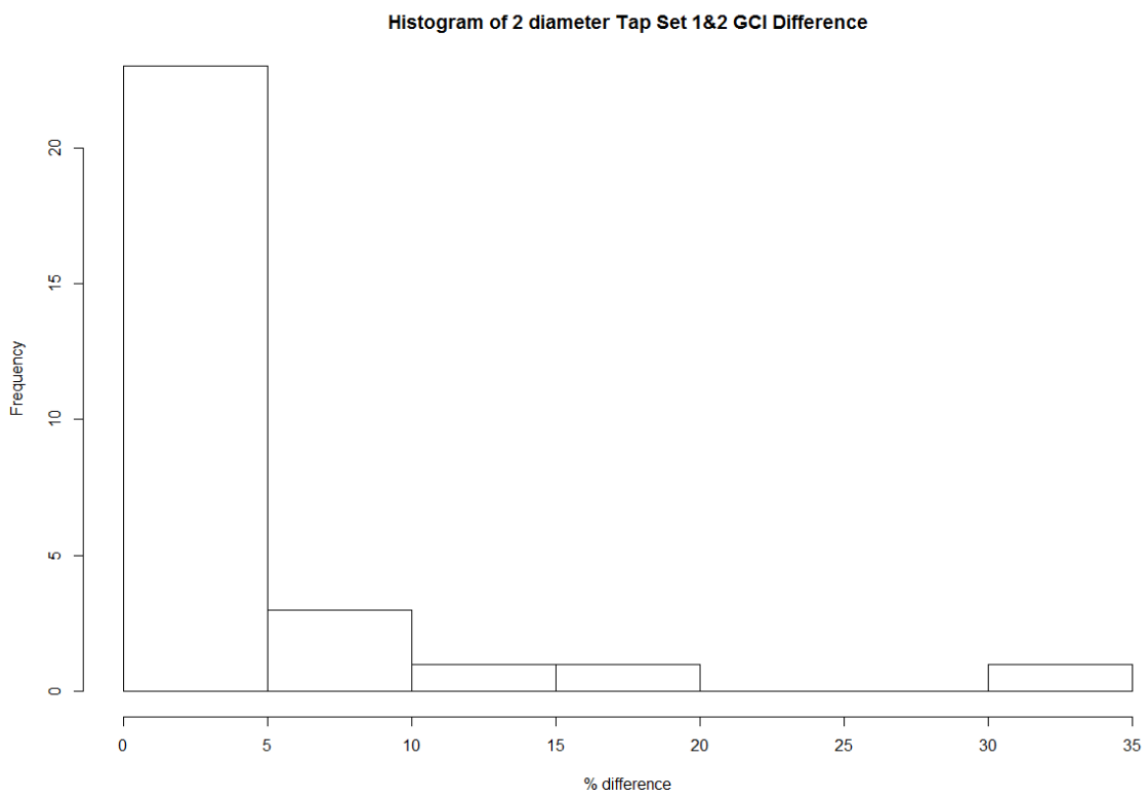


Figure B1. Histogram for the percent difference in the discharge coefficient for the 24-in. 0.6 beta ratio, 2 diameter tee junction installation.

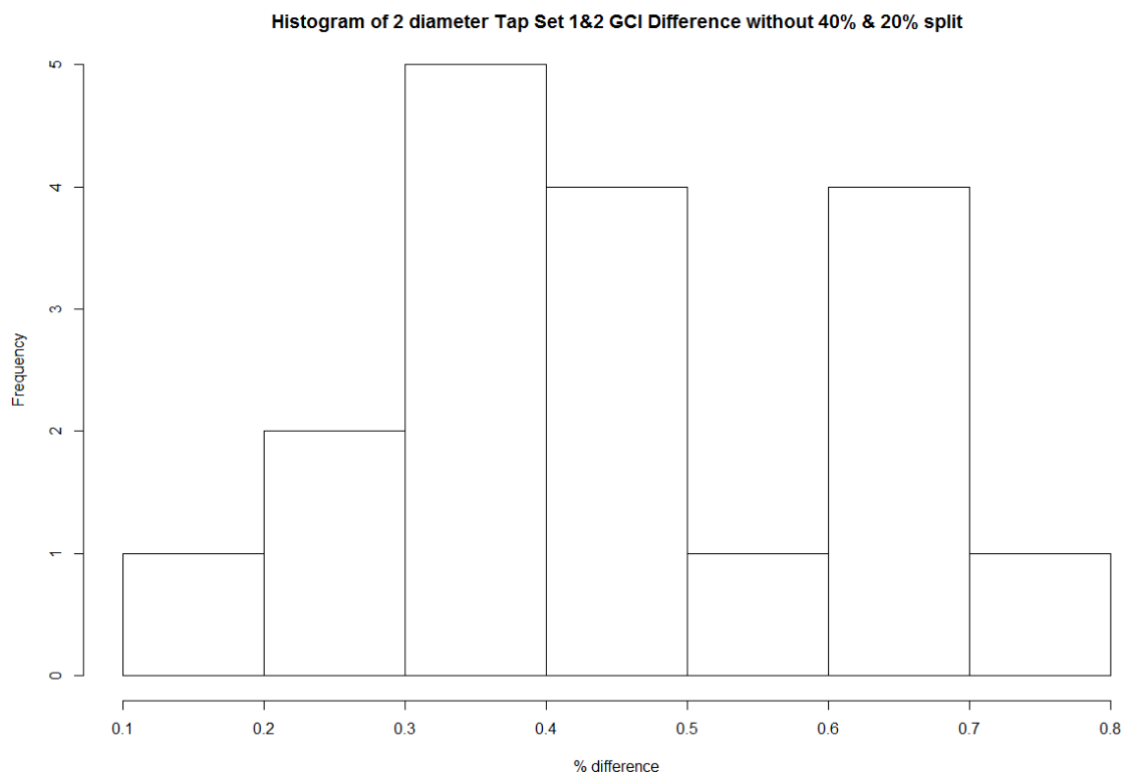


Figure B2. Histogram for the percent difference in the discharge coefficient without the 40% and 20% flow split differences for the 24-in. 0.6 beta ratio, 2D tee junction installation.

Noting that the percent difference in the discharge coefficient typically differs by less than 1% for flow splits above 20%, the 24-in. 0.7 beta ratio classical Venturi simulation results run with a base size of 2.0 in. through the Venturi were not rerun with CFD. Therefore, the CFD results presented are from a base mesh size of 0.35 in. with a volumetric control mesh size of 0.14 in. for the UVT 6-in. Venturi, a base mesh size of 2.0 in. with a volumetric control mesh size of 0.8 in. for the 0.6 beta 24-in. Classical

Venturi, and a base mesh size of 2.0 in. without a volumetric control for the 0.7 beta 24-in. Classical Venturi.

The following are the remaining Histograms for the other installations.

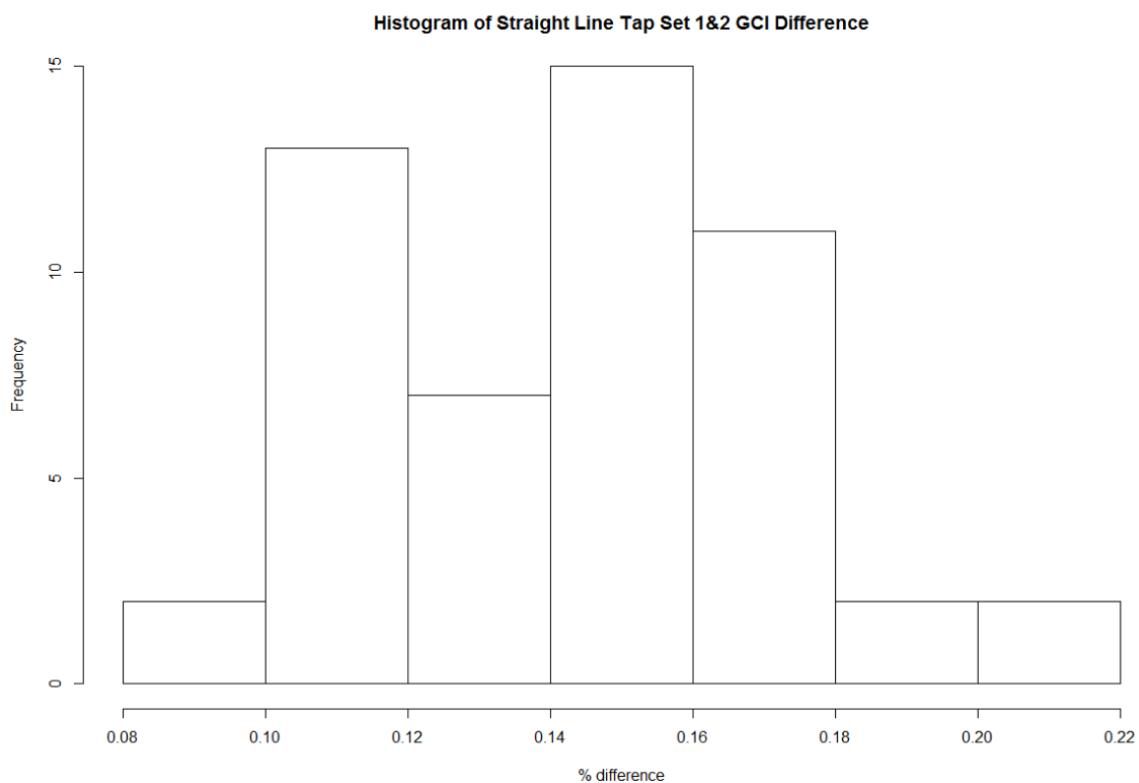


Figure B3. Histogram for Tap Sets 1 and 2 of the percent difference in discharge coefficient between the base size of 2 in. and the base size of 0.8 in. for the 24-in. 0.6 beta ratio, straight-line installation.

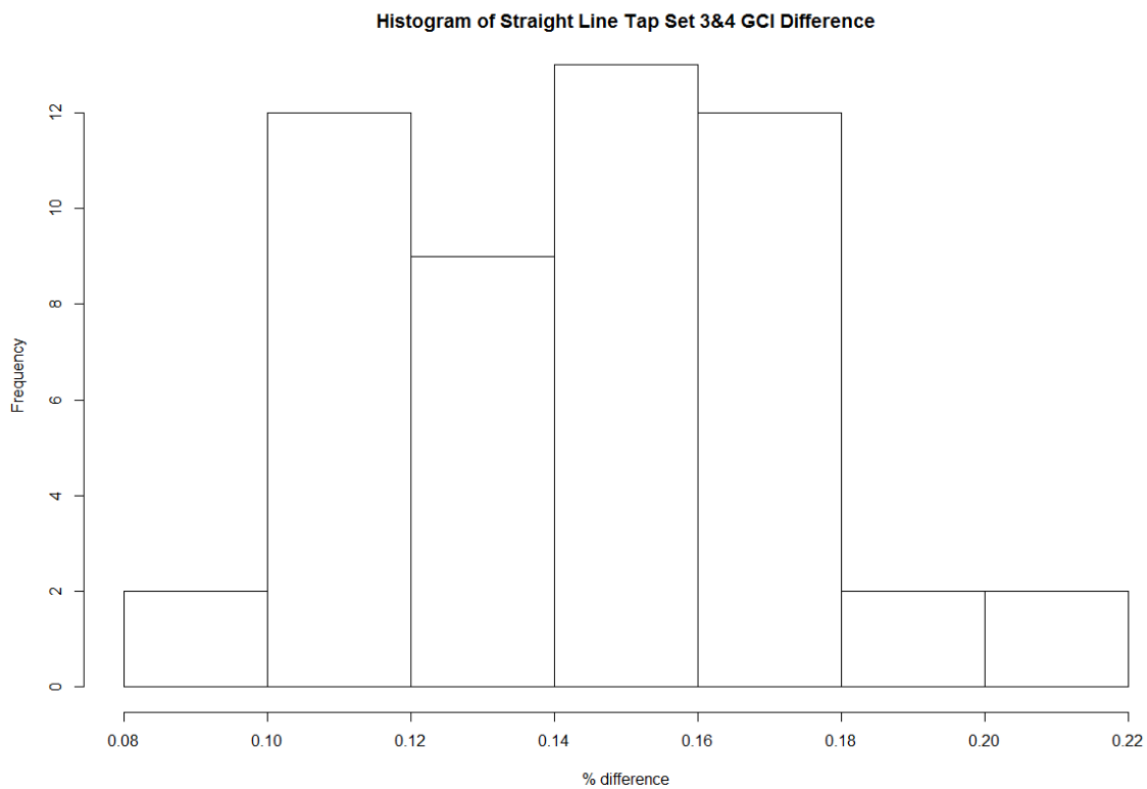


Figure B4. Histogram for Tap Sets 3 and 4 of the percent difference in discharge coefficient between the base size of 2 in. and the base size of 0.8 in. for the 24-in. 0.6 beta ratio, straight-line installation.

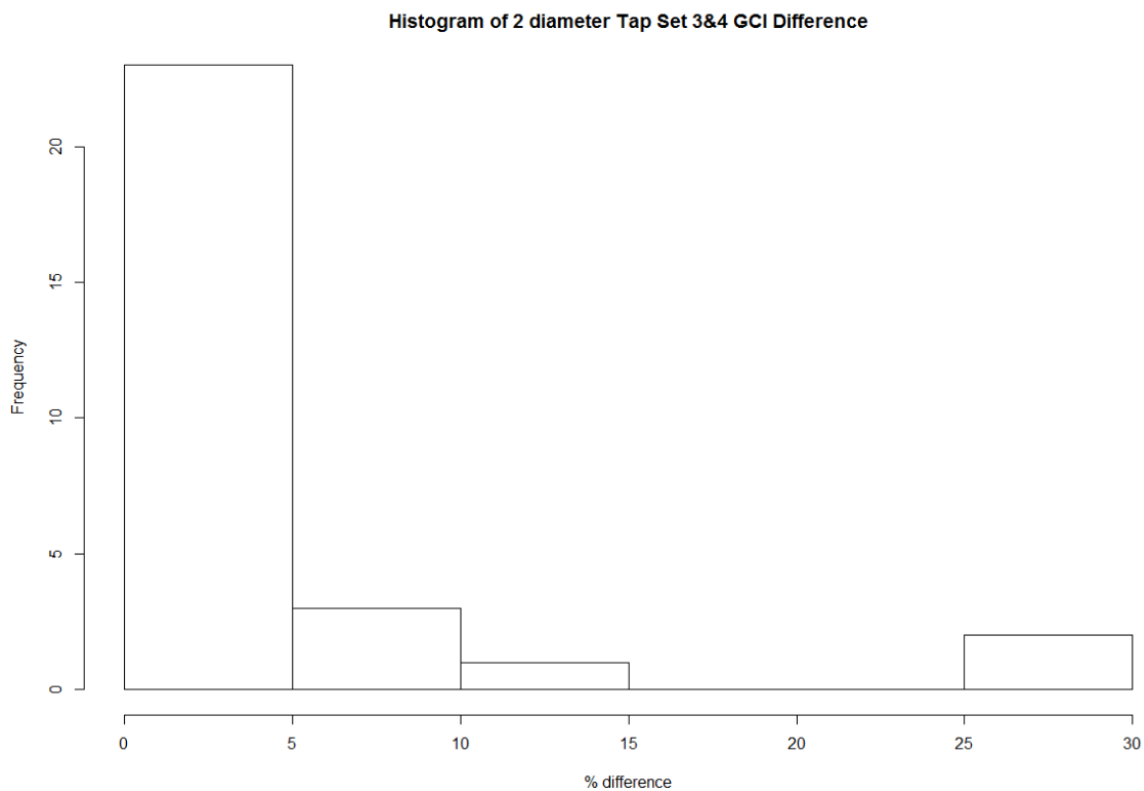


Figure B5. Histogram for Tap Sets 3 and 4 of the percent difference in discharge coefficient between the base size of 2 in. and the base size of 0.8 in. for the 24-in. 0.6 beta ratio, 2D tee junction installation.

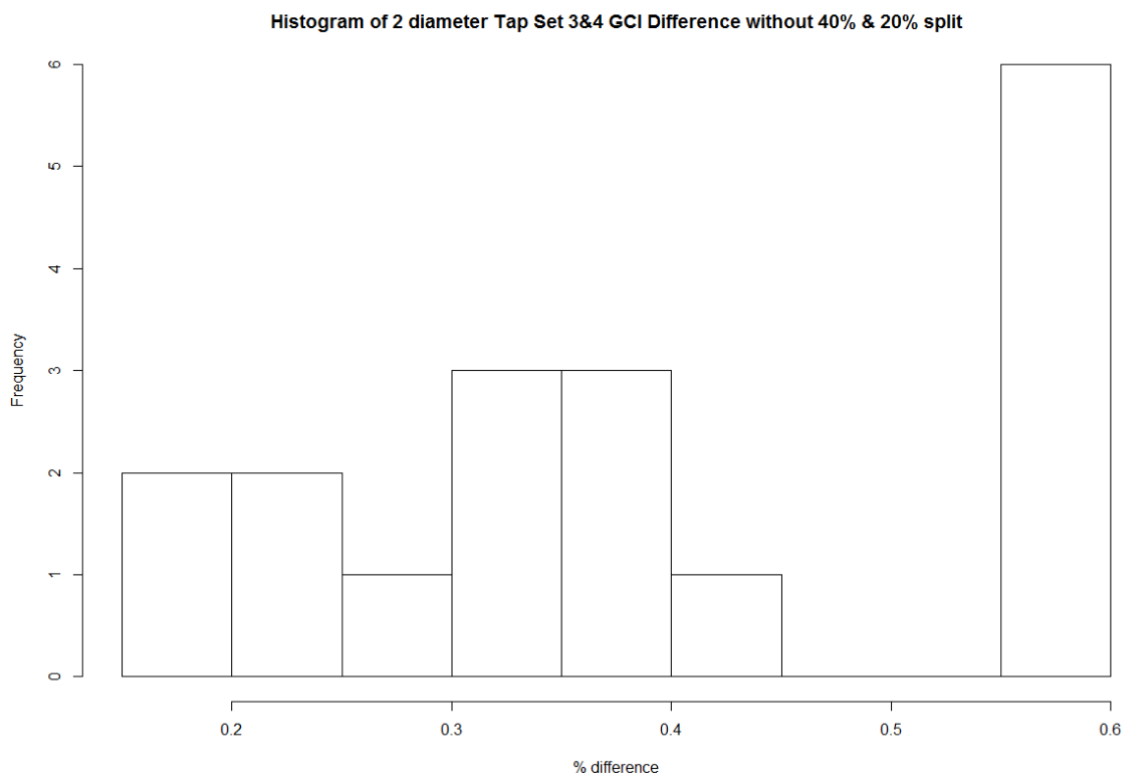


Figure B6. Histogram for Tap Sets 3 and 4 of the percent difference in discharge coefficient between the base size of 2 in. and the base size of 0.8 in. for the 24-in. 0.6 beta ratio, 2D tee junction installation, without the 40% and 20% flow split data.

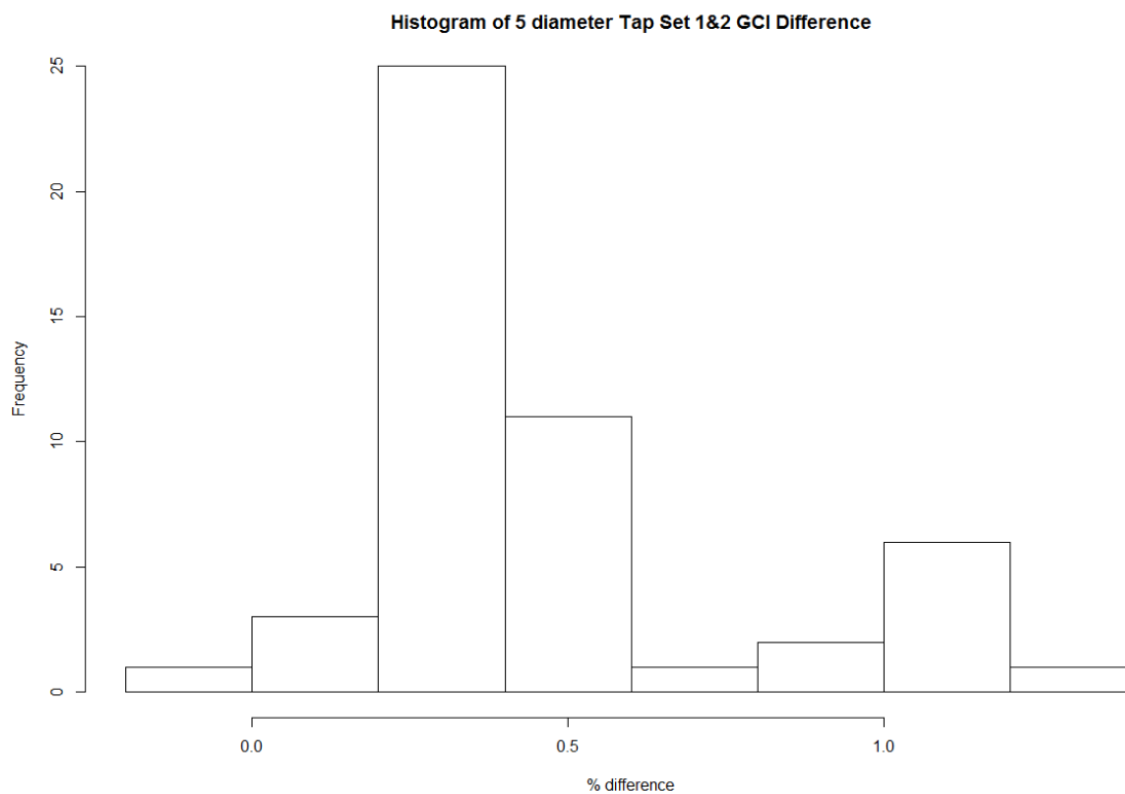


Figure B7. Histogram for Tap Sets 1 and 2 of the percent difference in discharge coefficient between the base size of 2 in. and the base size of 0.8 in. for the 24-in. 0.6 beta ratio, 5D tee junction installation.

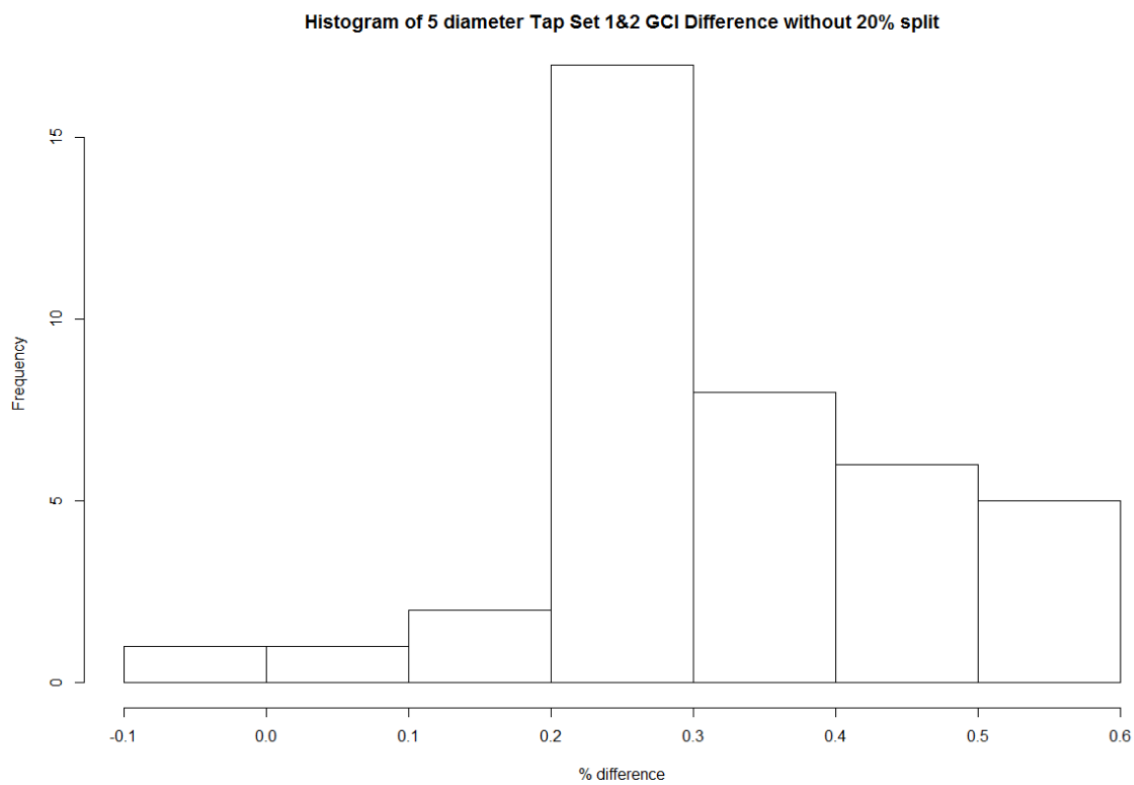


Figure B8. Histogram for Tap Sets 1 and 2 of the percent difference in discharge coefficient between the base size of 2 in. and the base size of 0.8 in. for the 24-in. 0.6 beta ratio, 5D tee junction installation, without the 20% flow split data.

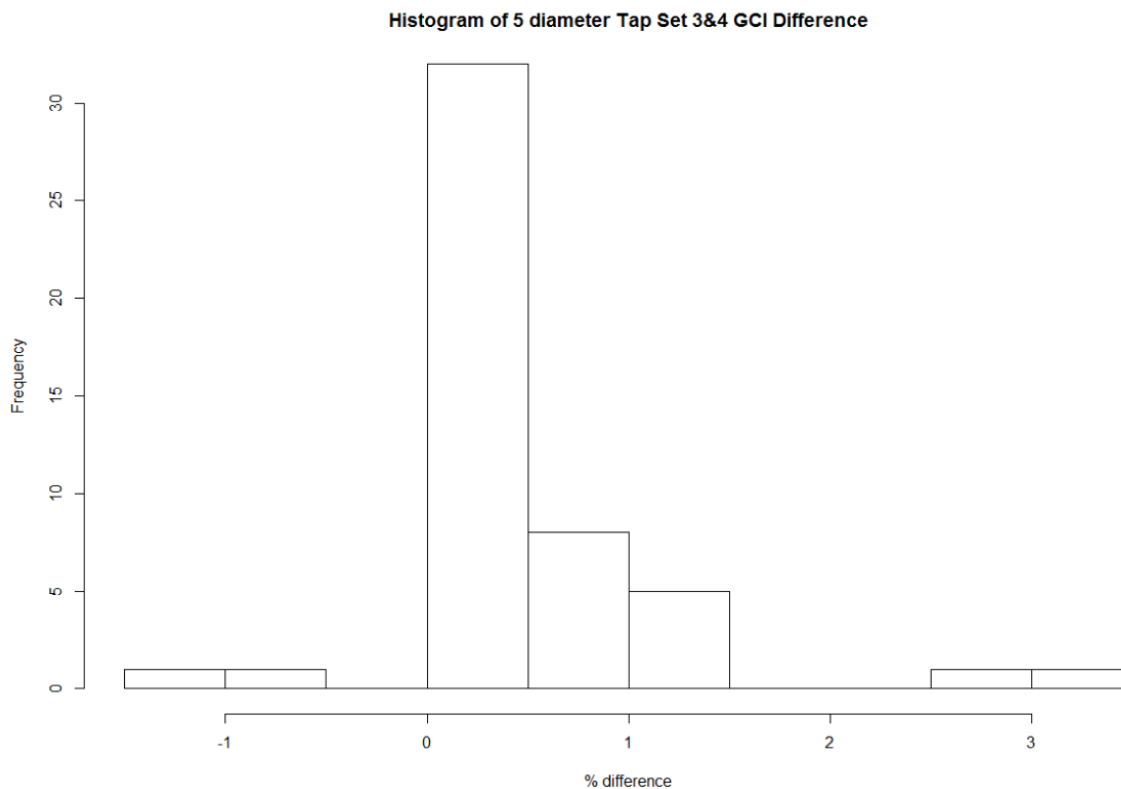


Figure B9. Histogram for Tap Sets 3 and 4 of the percent difference in discharge coefficient between the base size of 2 in. and the base size of 0.8 in. for the 24-in. 0.6 beta ratio, 5D tee junction installation.

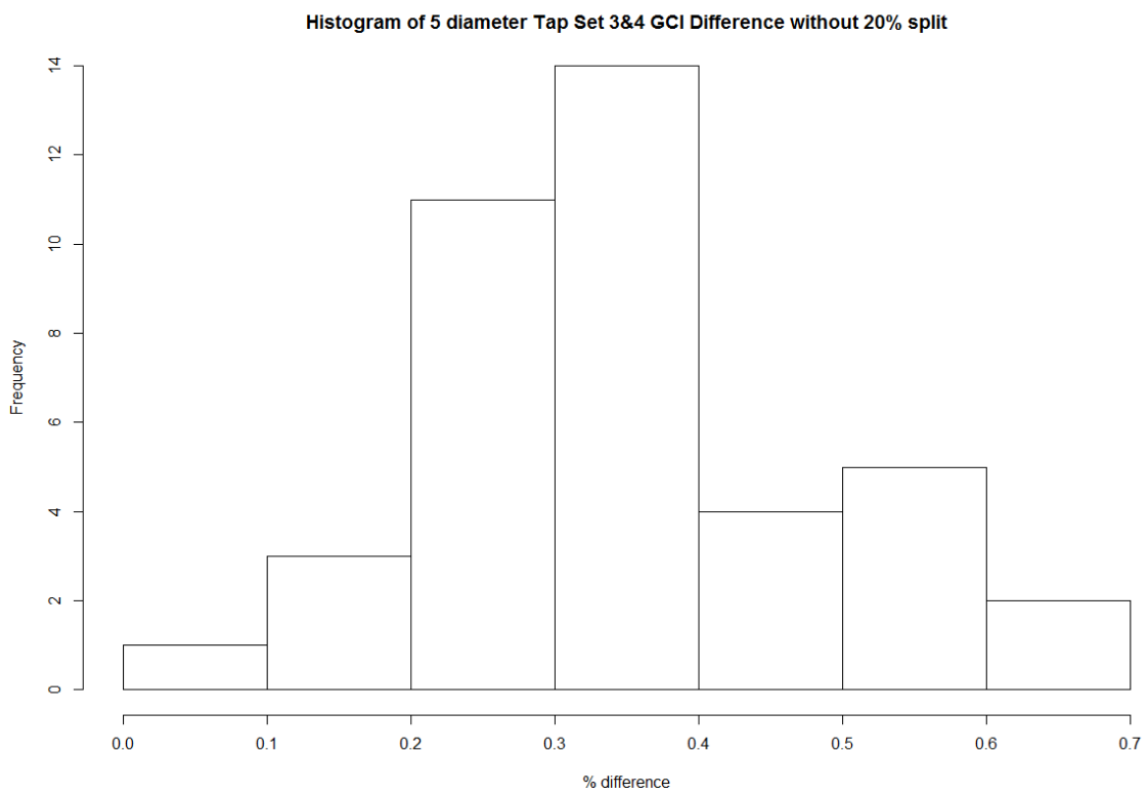


Figure B10. Histogram for Tap Sets 3 and 4 of the percent difference in discharge coefficient between the base size of 2 in. and the base size of 0.8 in. for the 24-in. 0.6 beta ratio, 5D tee junction installation, without the 20% flow split data.

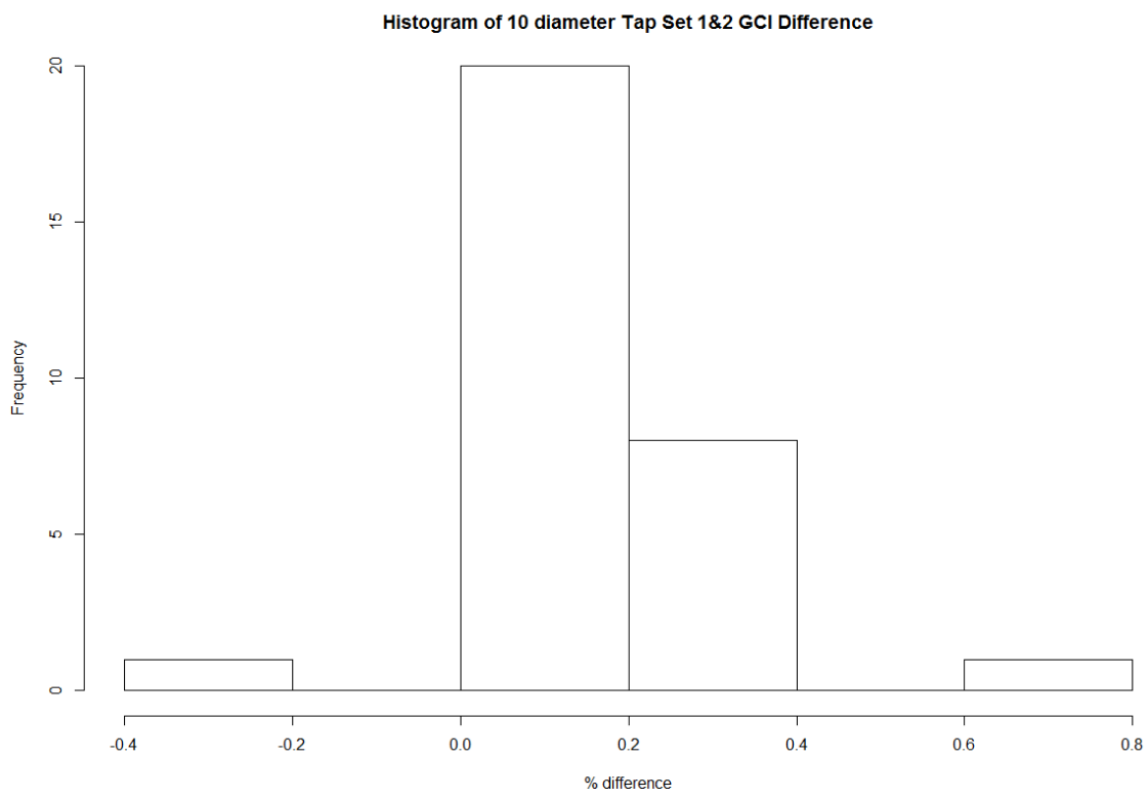


Figure B11. Histogram for Tap Sets 1 and 2 of the percent difference in discharge coefficient between the base size of 2 in. and the base size of 0.8 in. for the 24-in. 0.6 beta ratio, 10D tee junction installation.

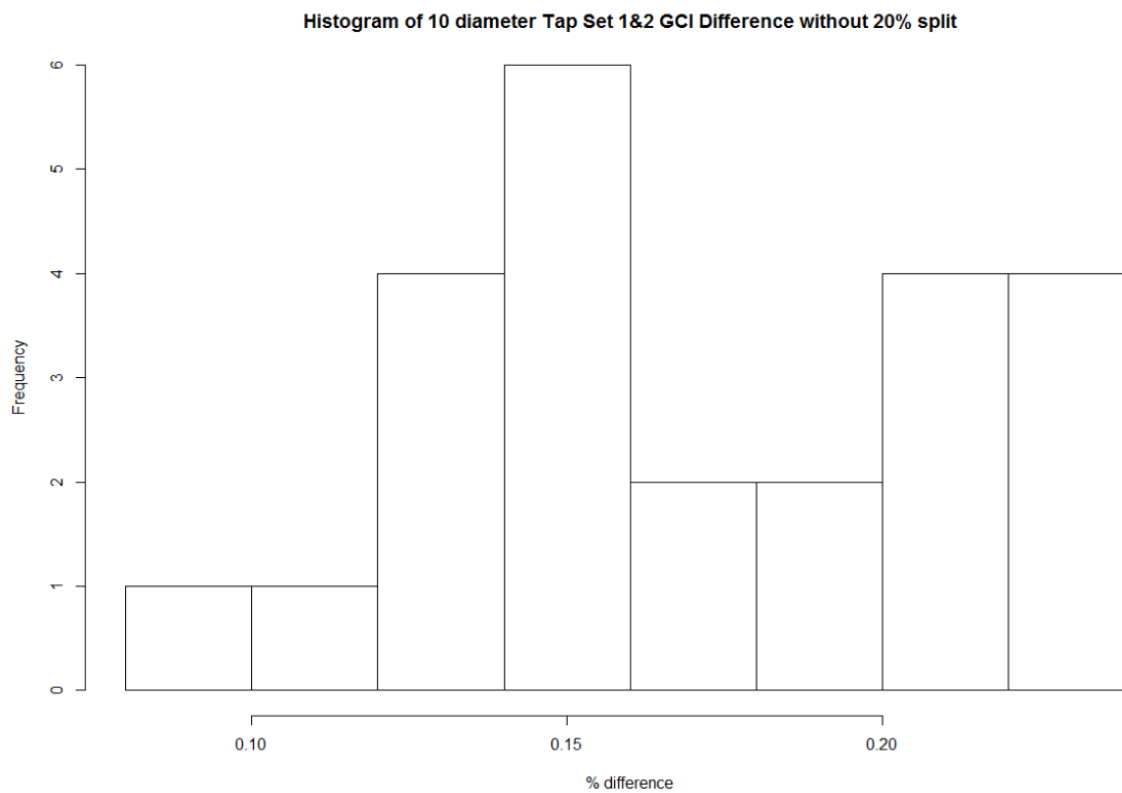


Figure B12. Histogram for Tap Sets 1 and 2 of the percent difference in discharge coefficient between the base size of 2 in. and the base size of 0.8 in. for the 24-in. 0.6 beta ratio, 10D tee junction installation, without the 20% flow split data.

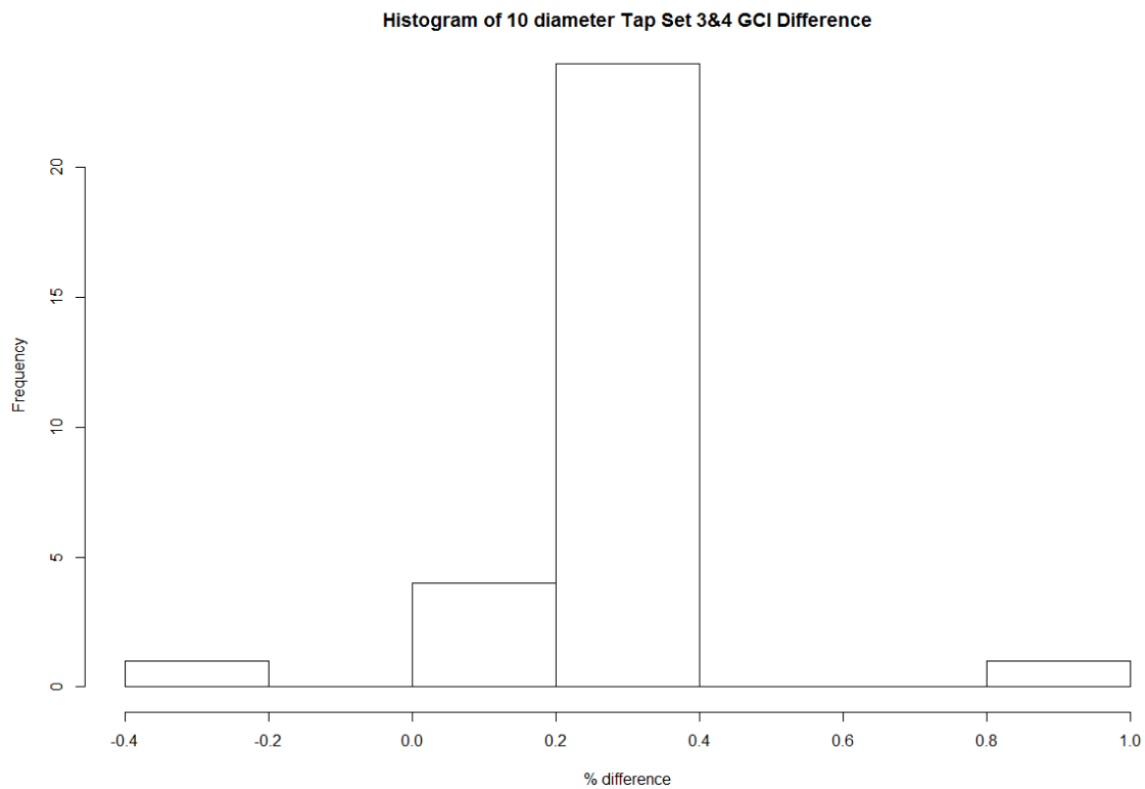


Figure B13. Histogram for Tap Sets 3 and 4 of the percent difference in discharge coefficient between the base size of 2 in. and the base size of 0.8 in. for the 24-in. 0.6 beta ratio, 10D tee junction installation.

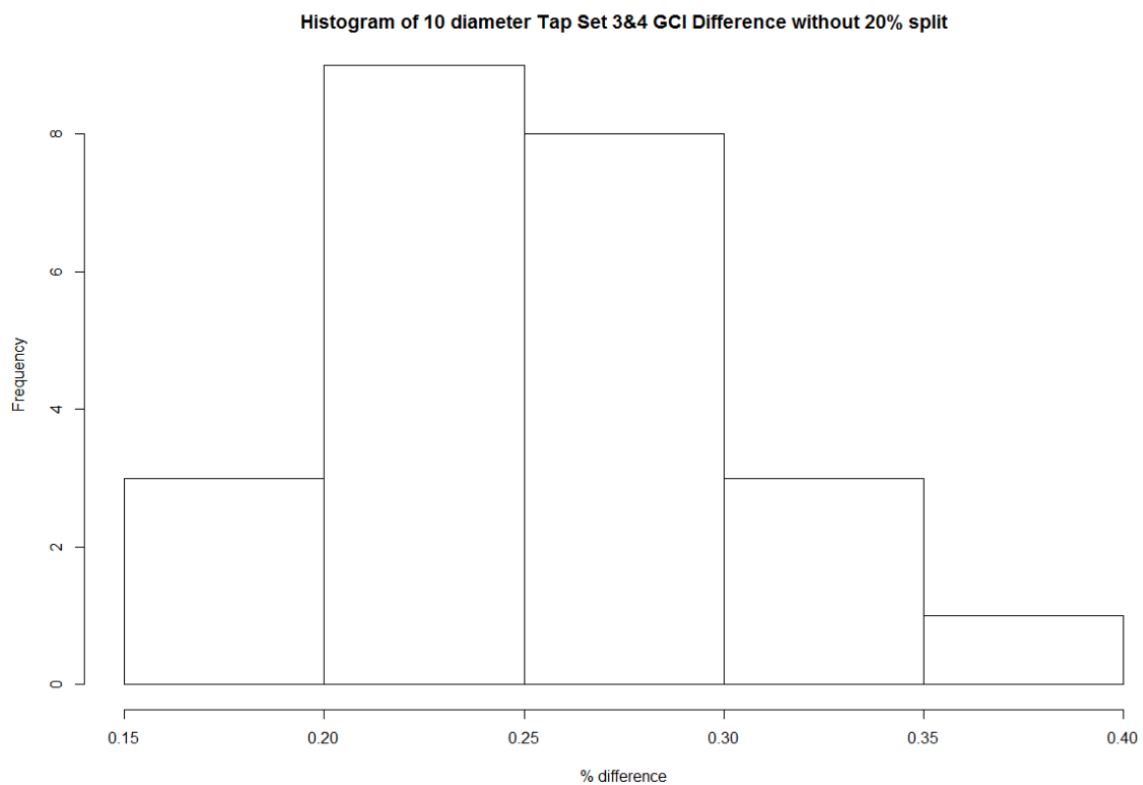


Figure B14. Histogram for Tap Sets 3 and 4 of the percent difference in discharge coefficient between the base size of 2 in. and the base size of 0.8 in. for the 24-in. 0.6 beta ratio, 10D tee junction installation, without the 20% flow split data.

APPENDIX C

METHOD FOR CONTOUR PLOT CREATION

From the CFD model results, differential pressure in psi, the mass flow rate entering the tee and Venturi in lb/s, and mesh throat and inlet area were obtained. These values were used in a spreadsheet to calculate differential pressure in inches of H₂O, discharge coefficients, Reynolds number, percent deviation, etc. Due to the number of simulations and information calculated from the model results, the spreadsheet (also called the original Excel spreadsheet) is cumbersome to query and difficult to make contour plots that guide what ratio to apply to the discharge coefficient in the tee configurations 0D, 2D, 5D and 10D. To make querying and contour plot creation more efficient, a database structure was created and populated. Python code was then written to query the database and create contour plots of discharge coefficient ratios. The database and Python code were created by the author and a colleague, Taylor Vaughn, to fulfill the requirements of a Hydroinformatics course project. Taking the text directly from this project report (Sandberg and Vaughn, 2019) the contour plot creation method will be explained.

“The first step in organizing, automating, and simplifying the process of creating contour plots for the Venturi study was to develop the database. Data from Star CCM+ [differential pressure in psi, the mass flow rate entering the tee and Venturi in lb/s, and mesh throat and inlet area] was input into the original Excel spreadsheet. The original spreadsheet was then converted to a format of columns and column headers [in] a comma-separated values (.csv) file. Using SQLite [DB Browser], a database management

system, a database was created ...” To differentiate the data in the database foreign keys were used. The data were differentiated by the different tee corners, Venturi geometries, pipe sizes, installations (in this section called setups), main Reynolds numbers entering the tee, beta ratios, ways percent deviation was calculated, and water properties. The foreign key ID values and their meanings are shown in Table C1.

“Python code was then written to retrieve the data values from the database and create a pandas dataframe with the selected values. To do this, both Python packages, sqlite3 and pandas (McKinney 2010) must be imported. Using the sqlite3 package, the SQLite database was connected to the Python code. In order to develop the dataframe within the Python code, the ‘read_sql_query’ function from the pandas package was used. This function allows for Python to perform an SQLite query on the database.” The query selects the columns: PipeSizeID, SetupID, TeeID, BetaRatio, MeterRe, FlowSplitRatio, Cd_H(1-4)L(1-4), and CdToCdStraight_(1-4) from the DataValues table. The dataframe produced shows all the values for each column listed. A WHERE statement is used to make the dataframe only show values for a desired setup, beta ratio, and Venturi size.

“The Python code has been [well] commented to explain the procedure for calling only the desired values. The WHERE statement in the query includes conditions for TeeID, MeterID, PipeSizeID, SetupID, BetaRatioID, WPID, and DevID. There are data for different variations of all of these column values, so if the user wishes to analyze data with different parameters they only have to change numbers within the WHERE statement. For example, Table C1 shows the variable, range of values, and description for every WHERE statement value that changes the dataframe. PipeSizeID refers to the inner

diameter of the pipe used for testing. PipeSizeID = 1 refers to a 6-in pipe while PipeSizeID = 2 refers to a 24-in pipe. So, if a user is viewing all the data for a 6-in pipe with a certain setup and would like to see the same data for the 24-in pipe, the user must only change the portion of the SQLite query following WHERE from ‘PipeSizeID = 1’ to ‘PipeSizeID = 2’.”

Table C1. SQLite Query “Where” Statement Variables

VARIABLE	VALUES	DESCRIPTION
TeeID	1 = Sharp corner 2 = Round corner	Type of tee junction used
MeterID	1 = UVT (Universal Venturi Tube) 2 = Classical	Type of Venturi used
PipeSizeID	1 = 6-in pipe 2 = 24-in pipe	Pipe inner diameter
SetupID	1 = SL (Straight-line Condition) 2 = 0 Diameters 3 = 2 Diameters 4 = 5 Diameters 5 = 10 Diameters	Distance Venturi was placed downstream from tee junction
ReMainID	1 = 2,000,000 2 = 1,300,000 3 = 700,000 4 = 300,000 5 = 100,000 6 = Straight-line	Reynolds number at the inlet to the tee junction, except for the straight-line which was a full range of Reynolds numbers
BetaRatioID	1 = 0.6 2 = 0.7	Beta ratio between the Venturi inlet and throat
DevID	1 = From Average 2 = From SL of same Re	The percent deviation either calculated by using the average of all the coefficients or the straight-line coefficient at the same Reynolds number
WPID	1 = 50°F and 1.3072 cP 2 = 46.3°F and 1.3883 cP 3 = 47.5°F and 1.3615 cP	Temperature and viscosity while testing or simulating